Astroglial glutamate transporters are essential for maintenance of respiratory activity in the rhythmic slice preparation

Dissertation
for the award of the degree
Doctor rerum naturalium (Dr. rer. nat.)

Division of Mathematics and Natural Sciences
of the Georg August University Göttingen

submitted by

Christian Schnell
from Arnsberg, Germany

Göttingen, June 2011

Members of the Thesis Committee:

Supervisor/Reviewer:
Prof. Dr. Swen Hülsmann
Department of Neuro- und Sensory Physiology
University Medical Center Göttingen

Reviewer:
Prof. Dr. Gabriele Flügge
Department of Neurobiology
German Primate Center

Prof. Dr. Tobias Moser
Department of Otolaryngology
University Medical Center Göttingen

Oral examination:

Declaration

I hereby declare that my doctoral thesis **'Astroglial glutamate transporters are essential for maintenance of respiratory activity in the rhythmic slice preparation'** has been written independently with no other sources and aids than quoted. This thesis has not been submitted elsewhere for any academic degree.

Göttingen, June 2011

Christian Schnell

Contents

List of abbreviations

$[Ca^{2+}]_{in}$	Intracellular Ca^{2+} concentration
$[K^{+}]_{ex}$	Extracellular K^{+} concentration
ABC transporter	ATP-binding cassette transporter
ACSF	Artificial cerebrospinal fluid
AM	Acetomethylester
$BaCl_2$	Barium chloride
Bic	Bicuculline
BL	Bulk loading
BP	Bandpass
BS	Brainstem
CBX	Carbenoxolone
CCD	Charged-coupled device
CsA	Cyclosporin A
CTRL	Control
Cx30	Connexin 30
Cx43	Connexin 43
DCFS	Divalent cation free solution
DHK	Dihydrokainate
DL-TBOA	DL-threo-b-Benzyloxyaspartic acid
DMSO	Dimethylsulfoxid
EAAT	Excitatory amino acid transport
EGFP	Enhanced green fluorescent protein
Fig.	Figure
GAT	GABA transporter
GFP	Green fluorescent protein
GLT-1	Glial glutamate transporter 1
Glu	Glutamate
GlyT1	Glycine transporter 1
GlyT2	Glycine transporter 2
hGFAP	Human glial fibrillary protein
HIP	Hippocampus
$I_{Resp,A}$	Respiratory-related current recorded from astrocytes
iGluR	Ionotropic glutamate receptors
IP_3	Inositoltriphosphat

LED	Light-emitting diode
LP	Low-pass
MCBL	Multi-cell bolus loading
MDR	Multidrug resistance
MFQ	Mefloquine
mGluR	Metabotropic glutamate receptors
min	Minutes
mRFP	Monomeric red fluorescent protein
n	Number of experiments
n.s.	Not significant
NCX	Na^+/Ca^{2+} exchanger
NMRI	Naval medicine research institute
OGB-1	Oregon Green BAPTA-1
Panx1	Pannexin-1
PBS	Phosphate-buffered saline
PLC	Phospholipase C
PMT	Photomultiplier tube
preBötC	pre-Bötzinger Complex
SCCI	Single-cell calcium imaging
SEM	Standard error of the mean
sIPSC	spontaneous inhibitory postsynaptic currents
SR101	Sulforhodamine 101
Str	Strychnine
TFB-TBOA	(3S)-3-[[3-[[4-(Trifluorome-thyl)benzoyl]amino]phenyl]-methoxy]-L-aspartic acid
V_{Hold}	Holding potential
VRG	Ventral respiratory group

List of Figures

List of Tables

1 Introduction

1.1 Glia

Nervous tissues consist of two major types of cells: neuronal and glial cells. Although glial cell types were already described by Rudolf Virchow in the 19th century (Virchow, 1846), most attention was paid to neurons, which fire action potentials and are the most important cells for detection and processing of information in the brain. The term glia was introduced by Rudolf Virchow according to his assumption, that glia are connective tissue (glia = glue) and do not participate in information processing.

Glial cells are divided into two main groups: Microglia do not originate in the brain and serve as macrophages of the nervous system to detect injuries and damaged cells and to phagocytise invaders. The second group is formed by macroglia which contains schwann cells, oligodendrocytes, NG2 cells, and astrocytes. The macroglia originate from the neural crest and are therefore also named neuroglia. Schwann cells and oligodendrocytes are myelinating cells in the peripheral and central nervous system, respectively. Myelin isolates axons and accelerates the conduction rate of action potentials by decreasing the capacitance of neuronal axons. NG2 cells were supposed to represent oligodendrocyte precursor cells. Recently, it has been shown that they can also generate protoplasmic astrocytes and neurons (for review see Trotter *et al.*, 2010). The major type of glial cells are the astrocytes. The term astrocyte was first used by Michael von Lenhossék. He investigated the glial cells in the vertebrate spinal cord and suggested the name astrocyte due to the star shaped appearance of these cells (van Lenhossék, 1893). Furthermore, there are astroglia-like cells in certain regions of the brain. The Müller cells and the Bergmann glia can be found in the retina and the cerebellum, respectively. The Müller cells are the principal glial cell in the retina and perform tasks similar to that of astrocytes in other brain regions, e.g. K^+ and neurotransmitter clearance (for review see Newman & Reichenbach, 1996). Bergmann glia are one type of astrocytes that is present in the molecular layer of the cerebellar cortex. They guide granule cell migration during development. In adults, different microdomains of bergmann glia locally interact with synapses (for review see Hoogland & Kuhn, 2010).

1.1.1 Astrocytes

The function of astrocytes is very heterogeneous. Differences exist not only between different developmental stages but also between brain regions. In general, astrocytes participate in many processes of the brain. They surround the blood vessels for uptake of nutrients and removal of K^+ (Kettenmann & Ransom, 2005), are important for the supply of neurons with nutrients and energy (Martinez-Hernandez *et al.*, 1977; Hülsmann *et al.*, 2000; Pellerin & Magistretti, 2004), and are also important in the regulation of the extracellular homeostasis (see below). Furthermore, there is an ongoing debate as to whether astrocytes also participate in information processing in the brain. The following sections will focus on the contribution of astrocytes for regulation of the extracellular homeostasis and on recent studies regarding the participation of astrocytes in brain signaling.

Regulation of brain homeostasis

During information processing in the brain, ions and neurotransmitters are released to transmit information between neurons. Most important in this regard is the efflux of K^+ during action potential conductance and the release of glutamate as the most important excitatory neurotransmitter.

Several mechanisms exist in the brain to keep $[K^+]_{ex}$ at approximately 3 mM. One way for removal of K^+ from the extracellular space is explained by the spatial-buffering hypothesis (Orkand *et al.*, 1966). When $[K^+]_{ex}$ is increased, the equilibrium potential for K^+ is shifted to less negativ potentials, causing a net driving force for K^+ influx via K^+ channels (Fig. **??**), presumably via Kir4.1 channels. The following local depolarization of the astroglial membrane potential travels electrotonically through the cell or the glial network and causes a net driving force for K^+ efflux on distant places where $[K^+]_{ex}$ remains unchanged and distributes K^+ to distant sites or to the vascular system (Kofuji & Newman, 2004). The importance of spatial buffering to K^+ removal is still controversial. Two recent studies showed that spatial buffering via Kir channels is rather important for maintaining baseline K^+ concentration than for K^+ buffering after strong neuronal activity (D'Ambrosio *et al.*, 2002; Neusch *et al.*, 2006; Chever *et al.*, 2010). In pathological conditions such as during spreading depression, $[K^+]_{ex}$ can reach levels of 60 mM (Vyskocil *et al.*, 1972).

To remove excess $[K^+]_{ex}$ after strong neuronal activity, K^+ uptake via Na^+/K^+ ATPases might be more important. These transmembrane proteins work as electrogenic transporters for Na^+ and K^+. Driven by ATP hydrolysis, three Na^+ are removed from the cell and two K^+ are transported into the cell. Increase in $[K^+]_{ex}$ results in higher activity of the astroglial isoforms of Na^+/K^+ ATPases (Grisar *et al.*, 1980), causing more K^+ influx into astroglia.

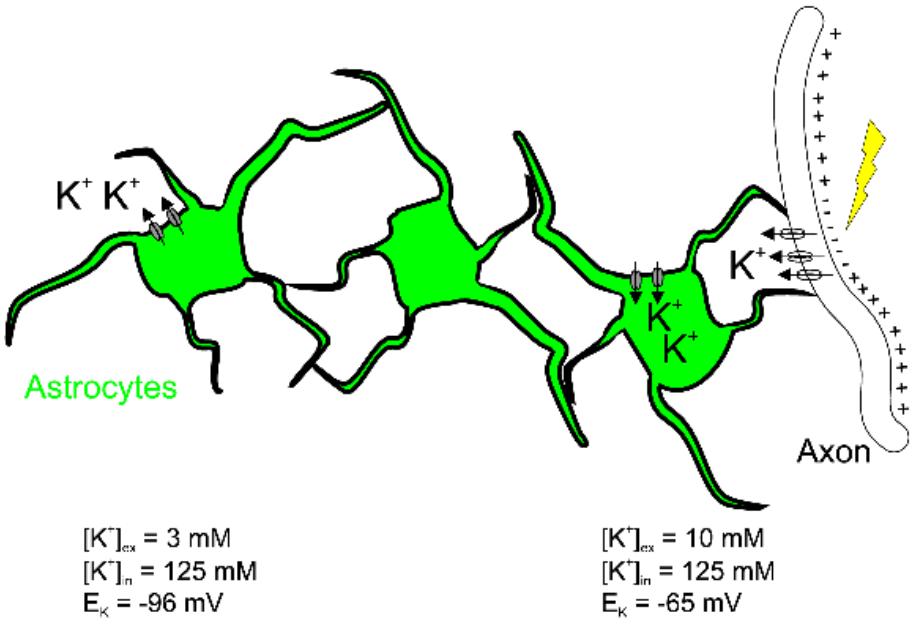

to distant places.]**Spatial buffering serves for removal of K^+ to distant places.** On sites of K^+ release during action potential generation, $[K^+]_{ex}$ increases and causes astroglial depolarization, because the equilibrium potential of K^+ is shifted and K^+ inward fluxes via K^+ channels occur. The depolarization travels electrotonically through the astroglial network and causes release of K^+ in places where $[K^+]_{ex}$ is not increased.

Glutamate is the most abundant excitatory neurotransmitter in the brain. In order to maintain a high signal-to-noise ratio and due to the toxic effects of ongoing glutamate receptor activation, extracellular glutamate levels need to be kept very low. Low extracellular glutamate levels are maintained by different types of transport proteins to protect the brain from excitotoxic effects caused by glutamate (for review see Danbolt, 2001). Glutamate uptake is driven by the electrochemical gradients of Na^+, K^+, and H^+ across the membrane. The five known glutamate transporters (for review see Danbolt, 2001) are named excitatory amino acid transporters (EAAT) 1-5. In case of the most abundant glial glutamate transporters, GLAST (EAAT1) and GLT-1 (EAAT2), one glutamate molecule is electrogenically transported together with three Na^+ and one H^+ in exchange for one K^+ (Levy *et al.*, 1998; Owe *et al.*, 2006, Fig. 1.1). The importance of glial glutamate uptake has been proven on studies with mice lacking GLT-1 or GLAST. In mice lacking GLT-1, glutamate uptake is severly reduced. Furthermore, these mice show seizures and a tendency to die prematurely (Tanaka *et al.*, 1997). The phenotype of GLAST mutant mice is less severe. Neither anatomical changes, nor disturbances of synaptic transmission in the cerebellum were observed. However, a mild phenotype is present, since GLAST mutant mice failed in the quickly rotating rotarod (Watase *et al.*, 1998). Although neurons also express glutamate transporters, the glial glutamate transporters GLAST and GLT-1 account for the major part of glutamate uptake (Rothstein *et al.*, 1996).

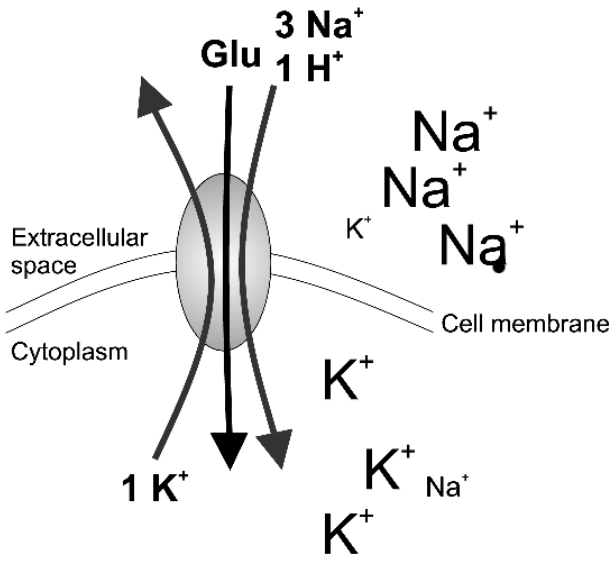

Fig. 1.1: **Glutamate uptake is driven by K^+ and Na^+ gradients over the membrane.** The two glial glutamate transporters GLAST and GLT-1 use the electrochemical gradient of K^+ and Na^+ for uptake of glutamate. Together with one glutamate, three Na^+ and one H^+ is exchanged against one K^+, resulting in a net uptake of two positive charges.

Astrocytes also express transporters for the uptake of inhibitory neurotransmitters. GABA is taken up by four different GABA transporters (GAT). Depending on the brain region, the transporters can be localized on neurons and astrocytes (Schousboe, 2000). Glycine is taken up by two glycine transporters. Glycine transporter 2 (GlyT2) is localized on neurons (Liu *et al.*, 1993; Zafra *et al.*, 1995; Gomeza *et al.*, 2003a), while the glycine transporter 1 (GlyT1) is mainly expressed by glial cells (Zafra *et al.*, 1995; Szoke *et al.*, 2006). GlyT1 knockout mice show a respiratory deficiency, causing the premature death of GlyT1 knockout mice 6-14 hr after birth (Gomeza *et al.*, 2003b).

Participation of astroglia in information processing

After the first description of neurotransmitter receptor expression in cultured astrocytes (Bowman & Kimelberg, 1984; Kettenmann *et al.*, 1984), ionotropic (Jabs *et al.*, 1994; Steinhäuser *et al.*, 1994) and metabotropic (Petralia *et al.*, 1996) glutamate receptors as well as other neurotransmitter receptors were found on astroglia in many regions of the brain. The expression of neurotransmitter receptors enables astrocytes to detect activity of neighbouring, transmitter-releasing cells. Many receptors reported to be expressed in astrocytes are metabotropic receptors. Their activation can trigger Ca^{2+} signaling via the IP_3/PLC pathway, a key step of several cellular functions. In the recent years, several studies have shown astroglial Ca^{2+} signaling upon synaptic activity triggered by several

signaling molecules (for review see Agulhon *et al.*, 2008). Elevations of $[Ca^{2+}]_{in}$ can induce the release of many different molecules from astrocytes, that may act as gliotransmitters to affect neighbouring neurons or astrocytes. The gliotransmitters released by astrocytes include ATP (Coco *et al.*, 2003), D-serine (Mothet *et al.*, 2005), and glutamate (Parpura *et al.*, 1994). While it is generally accepted that astrocytes release gliotransmitters, the mechanism of astroglial transmitter release is still controversial. Ca^{2+}-dependent release via vesicle exocytosis (for review see Parpura & Zorec, 2010) or lysosome exocytosis (Li *et al.*, 2008) as well as Ca^{2+}-independent release through hemichannels (Ye *et al.*, 2003) or reversed transporter modus (Szatkowski *et al.*, 1990) have been published.

The publications showing close astroglial monitoring of synaptic activity and release of gliotransmitters affecting synaptic efficacy, revealed new possibilities of neuron-glia interaction and led to the concept of the tripartite synapse (Araque *et al.*, 1999). This concept refers to recent findings, that synapse-associated glia are not only passive listeners of synaptic activity, but can also release glutamate in a Ca^{2+}-dependent manner and modulate neuronal activity in the hippocampus (Bezzi *et al.*, 1998). In the tripartite synapse concept it is emphasized that a synapse consists not only of a pre- and a postsynaptic terminal, but is closely ensheathed by associated glia cells which are able to modulate activity of the neurons. For a better understanding of synaptic function it might therefore be necessary to regard the glial cells as active participants in synaptic function (Fig. 1.2).

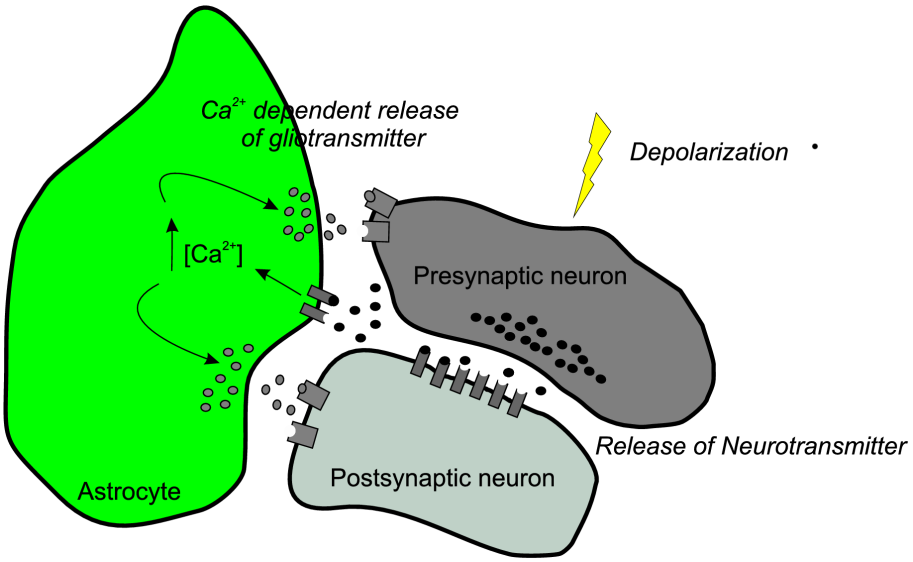

Fig. 1.2: **Astrocytes actively participate in synaptic transmission processes.** Depolarization of a presynaptic neuron causes neurotransmitter release and activation of postsynaptic receptors as well as receptors on astrocytes that surround the synapse. Activation of astroglial receptors can induce Ca^{2+}-dependent release of gliotransmitter, which can modulate activity of the pre- and postsynaptic neuron or transmit information via intercellular Ca^{2+} waves to more distant cells.

1.1.2 Methods to identify astrocytes

For a long time, direct investigation and understanding of the physiological role of astrocytes has been hampered by the lack of reliable astrocyte markers for living tissues. Until recently, brain slices had to be fixed after the experiment and stained immunohistochemically for example for GFAP, a protein that is widely used as an astrocyte specific marker. The major drawback of this method is that identification is only possible after the physiological experiment and is very time-consuming. Therefore, the introduction of transgenic mouse lines with fluorescently labeled astrocytes (Zhuo *et al.*, 1997; Nolte *et al.*, 2001; Hirrlinger *et al.*, 2005b), made research on glia much easier. Still, the use of transgenic mouse lines is not always possible or desirable. For this reason, other methods of astrocyte identification are used: (1) low-K^+ induced Ca^{2+} oscillations and (2) labeling with Sulforhodamine 101 (SR101).

The so-called low-K^+ method (Dallwig *et al.*, 2000) is based on astroglia specific intracellular Ca^{2+} oscillations in rodents that are induced by lowering $[K^+]_{ex}$ below 1 mM. The mechanism is not completeley understood yet, but it was hypothesized that Kir4.1 channels are responsible for the low-K^+ induced Ca^{2+} oscillations (Härtel *et al.*, 2007).

The second method makes use of the fluorescent dye SR101, that was shown to selectively label astrocytes in the neocortex (Nimmerjahn *et al.*, 2004) and the hippocampus (Langer & Rose, 2009) of rodents.

1.2 The respiratory network

Gas exchange is a necessary condition for living animals to supply the cells of a body with oxygen and remove carbon dioxide (CO_2). In vertebrates, this gas exchange takes place in the lungs during breathing. Several muscles are involved in the process of breathing to control inspiration and expiration. These muscles, for example the diaphragm and intercostal muscles, are innervated by motoneurons located in the spinal cord, which are themselves innervated by rhythmically active neurons in the brainstem (for review see (Richter & Spyer, 2001)). Vital, rhythmically active neurons are located in a region of the ventral medulla within the ventral respiratory group (VRG)), which is called the pre-Bötzinger Complex (preBötC, Fig. 1.3, (Smith *et al.*, 1991; Feldman *et al.*, 2003)) and can be isolated in coronal brainstem slices with ongoing rhythmic activity. Ramirez *et al.* (1996) adapted this preparation for mice, enabling *in vitro* studies in a defined surrounding and at a cellular level in the preBötC.

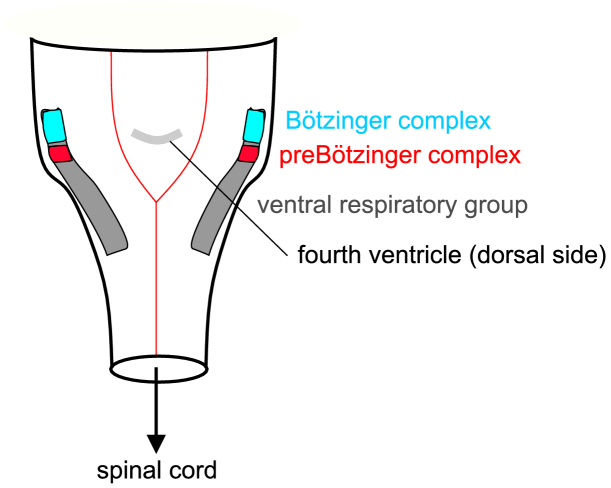

Fig. 1.3: **The preBötC is located in the VRG in the brainstem.** Schematic drawing of the ventral surface of the brainstem. The preBötC lies rostral of the BötC and both are located within the VRG. The fourth ventricle is located on the dorsal side of the brainstem and serves together with the inferior olive as orientation marks for cutting the rhythmic slice.

In the rhythmic slice preparation, major parts of respiratory activity are caused by rhyhmically active, glutamatergic inspiratory neurons that fire synchronously (Greer *et al.*, 1991; Pace *et al.*, 2007). The concerted action of inspiratory neurons can be recorded with extracellular field potential electrodes placed on the surface of the slice in the region of the preBötC, and is caused by increases of extracellular K^+ (Brockhaus *et al.*, 1993) and glutamate concentrations. In the following years, properties of the neuronal network were investigated to clarify changes in the respiratory network during development (Ramirez *et al.*, 1996; Manzke *et al.*, 2008)) and also the importance of synaptic inhibition within the respiratory network (Shao & Feldman, 1997; Winter *et al.*, 2009). Furthermore, the effect of several neurotransmitters on respiratory neurons has been examined, for example serotonin (Richter *et al.*, 2003), and norepinephrine (Viemari & Ramirez, 2006).

1.2.1 Properties of astrocytes in the respiratory network

Despite many publications regarding the function of neurons in the respiratory network, no attention has been paid to the role and function of glia within this network for a long time. Only since the late 1990s, the contribution of astrocytes for maintenance of the network was investigated. To investigate the metabolic coupling between astrocytes and neurons, Hülsmann *et al.* (2000) blocked the glial Krebs cycle and the glutamate-glutamine cycle and observed a blockade of respiratory activity in the rhythmic slice preparation. Another discovery was the importance of the function of the astroglial glycine transporter 1 (GlyT1), that was investigated by (Gomeza *et al.*, 2003b; Szoke *et al.*, 2006). This transporter is responsible for the uptake of synaptically released glycine and its knockout causes severe respiratory defects and finally leads to the early death of these mice during the first postnatal day (Gomeza *et al.*, 2003b).

Grass *et al.* (2004) defined three populations of astrocytes in the respiratory network of TgN(hGFAP-EGFP) mice, that can be distinguished by K^+ currents and glutamate transporter expression. Especially the astrocytes with a high K^+ conductance and expression of glutamate transporters (passive and intermediate astrocytes), may serve to maintain extracellular homeostasis and network stability (Grass *et al.*, 2004).

The contribution of the astroglial Kir4.1 channels to K^+ conductance of preBötC astrocytes and for maintenance of respiratory activity was investigated by Neusch *et al.*, 2006. Kir4.1 is supposed to play a major role in spatial K^+ buffering. Therefore it was suprising, that knockout of these K^+ channels did not cause major respiratory problems, even though the K^+ levels in the respiratory network has been shown to increase during synchronous firing of respiratory neurons (Brockhaus *et al.*, 1993). Although the animals died during the second postnatal week, the results of that study indicate that spatial buffering via Kir4.1 channels is not the major way of K^+ removal (see also D'Ambrosio *et al.*, 2002).

Besides these studies regarding participation of astroglia in maintaining the extracellular homeostasis, other studies investigated the expression of neurotransmitter receptors on astrocytes in the respiratory network. Astroglial expression of receptors for substance P, 5-HT, TRH (Härtel *et al.*, 2009), and ATP (Huxtable *et al.*, 2009) was confirmed by immunohistochemistry and by widefield Ca^{2+} imaging. In other brain regions, neurotransmitter-triggered Ca^{2+} transients in astrocytes have been shown to be involved in several processes like release of gliotransmitters, activation of Ca^{2+} waves and other cellular processes in astrocytes as desribed above and may provide a mechanism for modulation and stabilization of respiratory activity in the rhythmic slice preparation.

1.3 Aims of this study

1.3.1 Identification of astrocytes

The first part of this thesis summarizes data of the currently available methods for the identification of astrocytes in acute slices. In the first section it was tested to apply the method of SR101 labeling. This method has already been shown to work in mouse hippocampal slices and would be a valuable tool for identification of astroglia also in the brainstem.
In the second section, the involvement of the NCX in low-K^+ induced Ca^{2+} oscillations was investigated. Since contribution of Kir4.1 channels to the astroglial Ca^{2+} oscillations in low-K^+ solution has been shown (Härtel *et al.*, 2007), it was tested using widefield Ca^{2+} imaging, if $[Na^+]_{in}$ might be increased by anomalous gating of Kir4.1 causing Na^+ influx, followed by reverse-mode action of the NCX and subsequent increase of $[Ca^{2+}]_{in}$.

1.3.2 Detection and modulation of respiratory activity

Previous studies have shown, that astrocytes in the preBötC region express Kir4.1 channels as the major K^+ conductor and glutamate transporters for glutamate uptake. These proteins are necessary to maintain extracellular homeostasis in the brain and may be of special importance in the preBötC, because of the concerted activity of respiratory neurons. Therefore it was examined, if the rhythmic fluctuations of extracellular K^+ and glutamate concentrations during respiratory activity are detected by astrocytes. Since preBötC astrocytes also express neurotransmitter receptors, we tested for respiratory-related Ca^{2+} transients in astrocytes with two-photon imaging. Since intracellular Ca^{2+} signals have been shown to trigger the release of gliotransmitters and modulation of synaptic activity, it was tested if they also provide a mechanism for astroglial modulation of respiratory activity.

2 Materials and methods

2.1 Animals

All mice (Table 2.1) were obtained from the animal facility of the Center for Physiology and Pathophysiology or from the animal facility of the Max-Planck-Institute of experimental medicine in Göttingen. The animals were treated in accordance with the guidelines of the German Physiological Society, the regulations of the State of Lower Saxony and the Federal Republic of Germany.
TgN(hGFAP-EGFP) and TgN(hGFAP-mRFP) mice express fluorescent proteins under the control of the human glial fibrillary protein (hGFAP) promotor: in case of TgN(hGFAP-EGFP) an enhanced version of the green fluorescent protein, the EGFP protein, and in case of TgN(hGFAP-mRFP) line, a monomeric Red Fluorescent Protein is expressed, respectively. Since expression of both proteins is under the control of an astroglia specific promotor, these mouse lines were used to identify astrocytes by fluorescence. In TgN(GlyT2-EGFP) mouse line, EGFP was expressed under control of the neuronal glycine transporter 2 (GlyT2), enabling the identification of glycinergic neurons. By crossbreeding mice of this line with mice of the TgN(hGFAP-mRFP) line, astrocytes and glycinergic neurons were identified by their red and green fluorescence, respectively (see Figure 2.1). Some experiments were also performed with mice originating from the Naval Medicine Research Institute (NMRI, see also http://www.criver.com/fr-FR/ProdServ/ByType/ResModOver/ResMod/Pages/NMRI_Mouse.aspx).

[1] http://www.criver.com/fr-FR/ProdServ/ByType/ResModOver/ResMod/Pages/NMRI_Mouse.aspx

Table 2.1: Mouse lines

Line	**Reference**
TgN(hGFAP-EGFP)	Nolte *et al.* (2001)
TgN(hGFAP-mRFP)	Hirrlinger *et al.* (2005b)
TgN(GlyT2-EGFP)	Zeilhofer *et al.* (2005)
TgN(GlyT2-EGFP/hGFAP-mRFP)	crossbreeding started in the laboratory
NMRI	Charles River Lab. Intern. (Willmington, MA) [1]

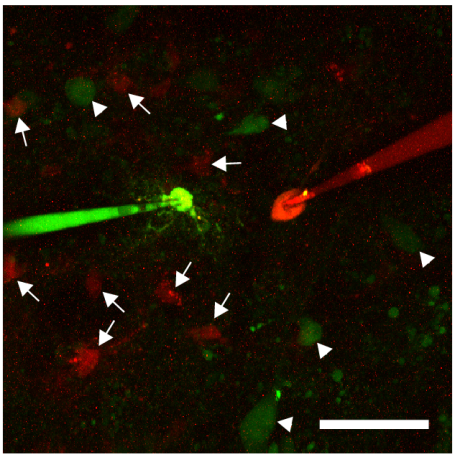

Fig. 2.1: **Maximum intensity projection of a photomultiplier recording of two patched cells of a GlyT2-EGFP/hGFAP-mRFP mouse brain slice**
The image shows two patched cells. The cell on the left is a mRFP-expressing astrocyte that was patched with an OGB-1 filled electrode. Soma and processes are filled with OGB-1 and therefore labeled in green. The cell on the right side is an GlyT2-EGFP expressing neuron. Since the patch electrode is filled with Calcium Orange, electrode and cell appear in red. Other mRFP-expressing astrocytes and GlyT2-EGFP-expressing neurons are indicated by arrows and arrowheads, respectively. Scale bar: 40 µm

2.2 Solutions & Drugs

2.2.1 Solutions

During preparation of acute slices and throughout the experiments, *Artificial Cerebrospinal Fluid* (ACSF, for composition see Table 2.2) was used as a bath solution. The composition of ACSF is based on the cerebrospinal fluid.
For non-transgenic mice, the low-K^+ method allowed the identification of astrocytes by decreasing the extracellular K^+ concentration ($[K^+]_{ex}$) from 3.0 mM to 0.2 mM (low-K^+ solution, table 2.2). Dallwig *et al.* (2000) and Härtel *et al.* (2007) showed that astrocytes exclusively show intracellular Ca^{2+} oscillations in response to this solution. This method enabled us to identify astrocytes via Ca^{2+} imaging in non-fluorescent mice.
In experiments with rhythmic slices, $[K^+]_{ex}$ was increased to 8 mM to stabilize and maintain activity of the respiratory network.
All solutions were bubbled with a gas mixture composed of 95 % O_2 and 5 % CO_2 to set pH to 7.4 and ensure proper tissue oxygenization. Gassing of solutions was started at least 20 minutes prior to use.

Table 2.2: Composition of bath solution in mmol/l

Compound	**ACSF**	**low K^+**	**DCFS**
NaCl	118.0	120.8	118.0
$NaHCO_3$	25.0	25.0	25.0
NaH_2PO_4	1.0	1.0	1.0
$MgCl_2 \cdot 6\ H_2O$	1.0	1.0	–
KCl	3.0	0.2	3.0
$CaCl_2$	1.5	1.5	–
Glucose	30.0	30.0	30.0

2.2.2 Intracellular solutions

Two different intracellular solutions were used for patch clamp experiments. The first intracellular solution was used only for electrophysiological recordings (in mM: 140 KCl, 1 $CaCl_2$, 2 $MgCl_2$, 4 Na_2ATP, 10 HEPES, 10 EGTA, pH 7.2). The electrodes were filled with sterile filtered (pore size 0.2 µm; Nalge Nunc, Rochester, NY) solution using a Microloader (Eppendorf, Hamburg).
The second intracellular solution (in mM: 160 KCl, 2.2 $MgCl_2$, 11 HEPES, 4.4 Mg_2ATP, pH 7.2) was used for single-cell Ca^{2+}-imaging experiments to fill cells with Ca^{2+} indicator dyes via the patch pipette. The fluorescence indicator was first dissolved in H_2O and used at a final concentration of 50 to 200 µM diluting the intracellular solution by 10 %. This technique enabled the simultaneous recording of electrophysiological and fluorescence imaging data.

2.2.3 Drugs

Drugs were stored as stock solutions in Aqua dest. at −20 °C. Substances that were not soluble in water were dissvolved in DMSO, Hepes-Ringer or NaOH. All drugs were diluted in ACSF and applied via the bath perfusion system. In case of DMSO as the solvent, the calculated final DMSO concentration never exceeded 0.1 %. For an overview of the used drugs, see Table 2.3.

Table 2.3: Drugs

Drug (Abbreviation)	**Concentration**	**Solvent**	**Supplier**
Barium Chloride ($BaCl_2$)	100 µM	H_2O	Sigma-Aldrich (Schnelldorf, Germany)
Bicuculline (Bic)	10 µM	H_2O	Sigma-Aldrich
Carbenoxolone (Cbx)	100 µM	H_2O	Sigma-Aldrich
7-(hydroxyimino)cyclopropan[b]chromen-1a-carboxylate ethyl ester (CPCCOEt)	100 µM	DMSO	Tocris (Bristol, UK)
Cyclosporin A (CsA)	50-200 µM	DMSO	Tocris
Dihydrokainate (DHK)	300 µM	NaOH	Tocris
DL-threo-b-Benzyloxyaspartic acid (DL-TBOA)	100 µM	DMSO	Tocris
Glutamate (Glu)	1 mM	Hepes-Ringer	Sigma-Aldrich
KB-R7943 mesylate (KB-R7943)	20 µM	DMSO	Tocris
Mefloquine (MFQ)	0.1-1 µM	DMSO	Bioblocks (San Diego, CA)
MK-571 sodium salt (MK-571)	50-200 µM	H_2O	Enzo Life Sciences (Lörrach, Germany)
SN-6	10 µM	DMSO	Tocris
Strychnine (Str)	10 µM	H_2O	Sigma-Aldrich
(3S)-3-[[3-[[4-(Trifluoromethyl)benzoyl]amino]phenyl]-methoxy]-L-aspartic acid (TFB-TBOA)	1 µM	DMSO	Tocris

2.3 Preparation of acute brain slices

In this work, acute slices of neonatal mice (P0-P12) were used. Either rhythmic slices (650 µm thick) or thinner slices (200-300 µm) containing the preBötzinger complex (preBötC) (Smith *et al.*, 1991) were prepared from the brainstem. Preparation of these slices was performed with minor changes according to the protocol of Winter *et al.* (2009). In detail, after decapitation the brain was quickly removed from the skull and placed in ice-cold ACSF. By cutting through the tectum, the cerebrum was separated from the brainstem together with the cerebellum. Afterwards, the brainstem was separated from the cerebellum and glued with the dorsal side onto an agar block that was trimmed before to an angle of approximately 20° to keep projections of the preBötC in the rhythmic slice. Then, the tissue was transferred to a vibrabtome (VT1000S, Leica, Bensheim) and coronal slices were cut in rostro-caudal direction until the widest opening of the fourth ventricle was reached. A 200-250 µm slice was cut to reach the level of the inferior olive. Afterwards, a rhythmic slice of 650 µm or 3-4 thin slices (200-300 µm) containing the preBötC were cut. The slices were kept at least for 1 h at room temperature in carbogenated ACSF before being transferred to the recording chamber.
Preparation of hippocampal slices was performed following the same protocol until the dissection of the cerebrum from the brainstem and cerebellum. After this step, the cerebrum was mounted onto an agar block and coronal slices were cut from rostral to caudal, until the hippocampus was reached. Depending on the age of the animal, 3-4 250 µm slices containing the hippocampus were cut and incubated for 1 h in ACSF at room temperature before start of the experiment or staining procedure (2.5.4).

2.4 Electrophysiology

2.4.1 Field potential recordings

In the rhythmic slice preparation as described in section 2.3, the respiratory activity of the preBötC was preserved and could be measured using an extracellular field potential electrode for several hours after preparation. The slice was fixed in the recording chamber with a platinum grid to keep the slice submerged and stable for recordings (Edwards *et al.*, 1989). To activate and maintain rhythmic activity, $[K^+]_{ex}$ was increased to 8 mM (Smith *et al.*, 1991; Ramirez *et al.*, 1996). To record the activity of the respiratory network, the field potential electrode was placed on the surface of the slice in the region of the preBötC. The signal passed the preamplifier which was also connected to the bath and was then band-pass filtered (0.25-1.5 kHz) and amplified (5000-10000 times). The A/D converter digitized this analog signal with an acquisition rate of 1 kHz. Additionally, the signal was integrated with a custom-built integrator (Paynter Filter, time constant 50-100 ms).

Recording and storage were performed with Clampex 9.2 software (Molecular Devices, Sunnyvale, CA).

Ag-AgCl electrodes from Science Products (Hofheim, Germany) were used as reference electrodes.

2.4.2 Whole-cell voltage-clamp recordings

Whole-cell voltage-clamp recordings were performed on acute slices with epifluorescence illumination to identify fluorescently labeled astrocytes (for details see 2.5). Recordings were performed with a Multiclamp 700A amplifier controlled by pClamp 9.2 and an A/D converter (Molecular Devices) to digitize analog data. Signals were filtered (3 kHz, Bessel filter) and stored with an aquisition rate of 10 kHz.
Electrodes were made from borosilicate capillaries (Biomedical Instruments, Zöllnitz, Germany) that were pulled by a programmable, horizontal puller (Zeitz-Instrumente, Munich, Germany). The electrode when filled with one of the intracellular solutions (see 2.2.2) had a resistance of 3-6 MΩ. The electrode was plugged into a custom-built electrode holder and fixed in the micromanipulator (MM3A-LS, Kleindiek Nanotechnik GmbH, Reutlingen, Germany). Positive pressure was applied to ensure a continued outflow of electrode solution in order to keep the tip of the electrode clean and prevent it from clogging. Following pipette potential offset correction, the tip of the electrode was brought towards the cell, before capacitance correction was performed. Afterwards, the electrode was moved closer to the cell until electrode resistance increased. At this moment, the pressure was released and it was observed if a high-resistance connection between cell membrane and electrode (GΩ seal or gigaseal) was established. If not, gentle suction was applied until formation of the gigaseal connection and establishment of cell-attached mode. With a short suction or a short voltage pulse (1 V, 100 µs), the cell membrane under the electrode was disrupted and the whole-cell voltage-clamp mode established. The membrane potential was clamped to −70 mV and a voltage-step protocol ranging from potentials of −160 mV to +20 mV (19 steps with Δ10 mV increments, 200 ms duration of each voltage step) was carried out to further characterize the patched cell (Fig. 2.2). In agreement with Grass *et al.* (2004), bright fluorescent astrocytes in TgN(hGFAP-EGFP) mice showed a passive current-voltage relation, as well as mRFP-expressing astrocytes in TgN(hGFAP-mRFP) mice. However, 2 of 26 patched mRFP-expressing astrocytes showed a current-voltage relation that was characteristic for outward rectifying astrocytes and another 2 were of the intermediate type (see Grass *et al.*, 2004).

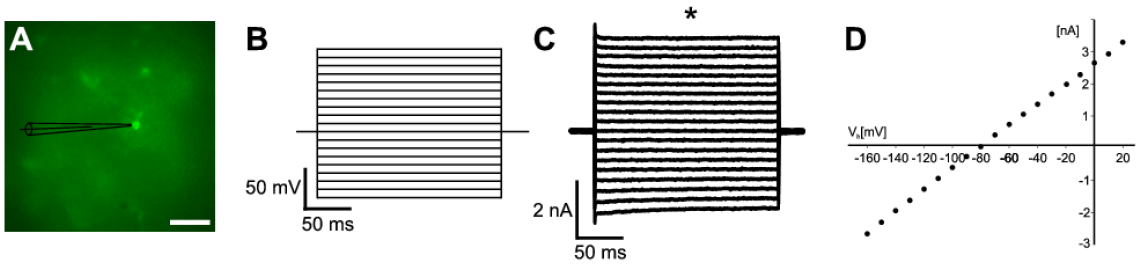

Fig. 2.2: **Characterization of patched astrocytes**
A Example of a bright, EGFP+ patched astrocyte. Scale bar: 40 µm **B** Voltage step protocol to clamp cells for 200 ms to different membrane potentials ranging from −160 mV to +20 mV in 10 mV steps allows the characterization of the patched cells. **C** Almost symmetrically in- and outward components of the cell from (A) as response to the voltage step protocol. Asterisk marks the time the current is measured for the IV-curve. **D** Linear IV-curve of the recording confirms passive character of this cell.

2.4.3 Electrical stimulation

Electrical stimulation experiments were performed to test if strong synchronized neuronal activity can trigger Ca^{2+} signals in preBötC astrocytes. To achieve this, patch electrodes filled with ACSF were placed at the border of the preBötC. Trains of 200 pulses (100 Hz, 200 µs pulse duration, 20-150 V) were applied every 20 s using a Digitimer stimulator (Type 3072, Digitimer, Hertfordshire, UK) that was triggered by a programmable pulse generator (Master 8, A.M.P.I., Jerusalem, Israel).

2.5 Fluorescence imaging

2.5.1 Widefield Ca^{2+} imaging

Different sources of light and techniques can be used for the excitation of fluorophores. For patch clamp experiments and widefield Ca^{2+} imaging, either a light-emitting diode (LED) or a monochromator was used to excite EGFP or mRFP for the identification of astrocytes or the Ca^{2+} indicator dye. Though brightness, intensity and lifetime of a LED is much better than a monochromator, in terms of different excitation wavelengths, a monochromator is more flexible.

The widefield imaging setup was based on an Axiscope FS (Zeiss, Oberkochen, Germany). The filter set consisted of a dicroic mirror (505 nm) and a band-pass emission filter 545/50 nm) for Ca^{2+} imaging with Oregon Green BAPTA-1 (OGB-1). Fluorescence was detected with an Andor Ixon 885 EM CCD camera (T.I.L.L. Photonics, Gräfelfing, Germany). For recording and control of the camera as well as the monochromator, Imag-

ing Workbench software (Indec BioSystems, Santa Clara, CA) was used. This setup was equipped with two objectives: 5x (0.12 NA) and 40x (0.8 NA), both from Zeiss.

2.5.2 Two-photon imaging

Most of the Ca^{2+} imaging experiments were perfomed at the two-photon laser setup which was combined with a commercial scanhead (TriM Scope, LaVision Biotech, Bielefeld). Two-photon imaging, introduced by Denk *et al.* (1990), makes use of the probability of a dye molecule to absorb two photons simultaneously and thus combine their energy and bring the molecule to its excited state. The probability of two-photon absorption decreases outside the focal plane because of the quadratic dependence of the two-photon absorption on the spatial distribution of the excitation intensity (Denk *et al.*, 1990). The advantage of this technique is that bleaching as well as photo damage outside of the focal plane is reduced. Due to the small volume of two-photon excitation, no pinhole as a spatial filter is required and all light emitted by fluorophores can be detected by a detector. Another advantage of two-photon excitation is the use of near-infrared light for excitation, which has longer wavelengths, thus enabling imaging in deeper regions, because tissue is more transparent for light with longer wavelengths.

The setup used here is based on a fixed-stage, upright microscope (Axiscope FS2, Zeiss, Oberkochen, Germany). Two-photon excitation was achieved by using a pulsed infrared titanium sapphire laser (#1 in Figure 2.3, MaiTai BB, Spectra Physics, Darmstadt, Germany). The laser beam was coupled into a commercial scanhead (#2, TriM Scope, LaVision Biotec) that can split the laser beam in a line of up to 64 foci (Nielsen *et al.*, 2001). This increases the amount of emitted light per time without increasing photo damage and also enabling fast Ca^{2+} imaging measurements. Upron reflection off a dicroic mirror (#3), the laser beam passes the water immersion objective (#4, 40x (0.8 NA) or 20x (1.0 NA), both from Zeiss). The objective was connected to a piezo-focus (#8) (Physik Instrumente, Karlsruhe, Germany) to allow accurate recording of z-stacks. Afterwards, the beam excited the dye molecules of the probe. The emitted light of the fluorophores passed the dicroic mirror (680 LP) and was filtered by appropriate emission filters (#5) before being detected either by a CCD camera (#6, Ixon 885 or Clara, Andor Technology) or by two photomultiplier tubes (PMT, Hamamatsu Photonics, Hamamatsu, Japan). For wide-field Ca^{2+} illumination (#7) LEDs (KSL 70 with 470 or 530 nm, Rapp OptoElectronic, Hamburg, Germany) or a monochromator (Polychrom II, T.I.L.L. Photonics, Gräfelfing, Germany)) were used. The dicroic mirror was 495 LP for EGFP and a 485/555 dualband mirror for mRFP. All filters were obtained from AHF Analysentechnik (Tübingen, Germany).

One inlet and one outlet at the recording chamber ensured proper supply of the tissue with heated (30 °C if not stated otherwise) and carbogenated ACSF. A pump (Watson-

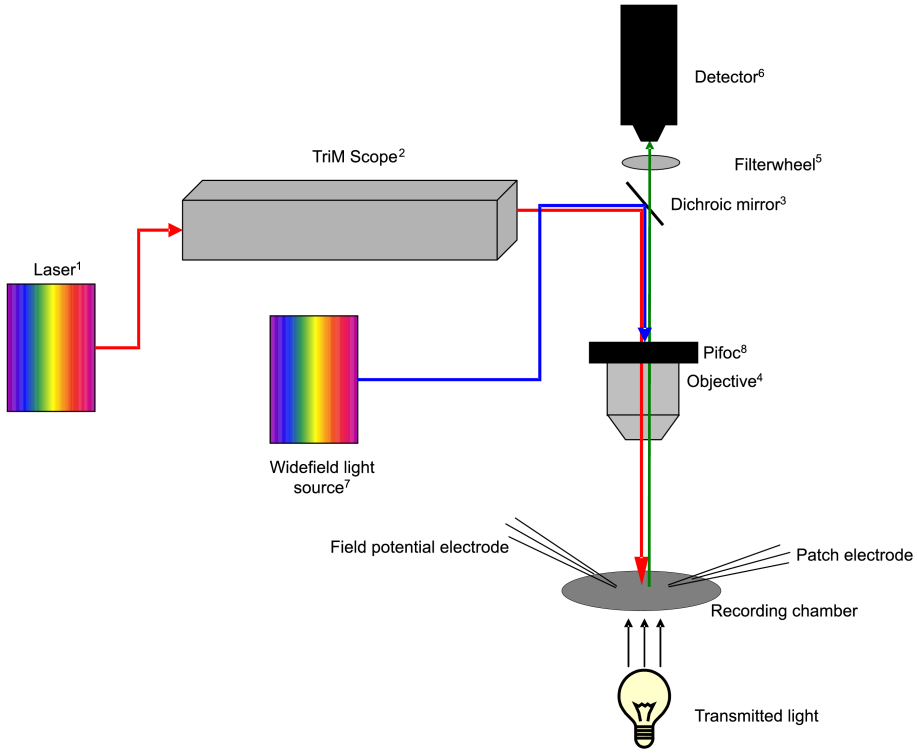

Fig. 2.3: **Description of the two-photon setup**
This scheme illustrates the construction of the two-photon setup consisting of light sources like Laser or widefield illumination (#1, #7), the TriM Scope (#2) for splitting up the laser beam and optical parts like dicroic mirror (#3), objective (#4), emission filter (#5) and CCD or PMT detectors (#6). Additionally, a piezo-focus (#8) was used for recording of z-stacks. For detailed description see text of this section.

Marlow 205S, Watson-Marlow, Cornwall, UK) served for a continuous flow rate of ~6 mL per minute.

2.5.3 Fluorescent dyes

Most of the Ca^{2+}-imaging experiments were performed with OGB-1 in its cell permeable form as acetomethylester (AM) or for whole-cell voltage-clamp recordings as cell impermeant hexapotassium salt (Invitrogen, Karlsruhe, Germany). This Ca^{2+} indicator is well established, its fluorescence could be well separated from fluorescence of EGFP-labeled astrocytes (Winter *et al.*, 2009) and its staining was more effective and bright in the brainstem compared to other Ca^{2+} indicator dyes. Other dyes that were used for single cell Ca^{2+} imaging were Calcium Orange hexapotassium salt (Invitrogen) and Quest Fluo 8L (Biomol, Hamburg, Germany). For more details see Table 2.4.

Table 2.4: **Properties of used fluorescent dyes**. The second column shows the excitation wavelengths (λ_{ex}) and emission wavelenghts (λ_{em}), while the third column shows the wavelengths used for two-photon excitation ($\lambda_{ex,\ 2P}$). Column four shows the dye concentrations used for single cell Ca^{2+} imaging (SCCI), multi-cell bolus loading (MCBL) or bulk loading (BL). The dissociation constant (K_d) for Ca^{2+} indicator dyes is shown in the last column.

Fluorescent dye	$\lambda_{ex}/\lambda_{em}$ **[nm]**	$\lambda_{ex,\ 2P}$ **[nm]**	**Concentration**	K_d **[μM]**
OGB-1	493/523	800	50-200 μM (SCCI), 0.3-0.8 mM (MCBL), 5 μM (BL)	0.17
Calcium Orange	550/574	800	50-200 μM (SCCI)	0.19
Quest Fluo-8L	490/514	800	50-200 μM (SCCI)	1.9
EGFP	489/ 509	900		-
mRFP	554/ 585	720		-
SR101	578/593	800	1 μM (BL)	-

To investigate activity-dependent dye uptake in neurons of amphibians and rodents, several groups used the red fluorescent dye Sulforhodamine 101 (SR101). Recently, Nimmerjahn *et al.* (2004) showed that SR101 specifically labels astrocytes in the neocortex. Since then, SR101 is used as an astroglial specific marker for *in vivo* identification of astrocytes in the neocortex (Nimmerjahn *et al.*, 2004) or *in vitro* in the hippocampus (Langer & Rose, 2009). SR101 was obtained from Sigma Aldrich and used at a concentration of 1 μM.

2.5.4 Staining procedures

To detect changes in the intracellular Ca^{2+} concentration ($[Ca^{2+}]_{in}$), cells were loaded with a fluorescent dye. Depending on cell type and experimental design, different protocols are available to fill the cells with fluorescent Ca^{2+} indicator dyes. The protocols used in this thesis are as follow:

Filling of single cells via patch pipettes

To fill only single, selected cells with fluorescent dyes, the dye was dissovled as described in 2.2.2 and loaded into the patch pipette. A few minutes after establishing the whole-cell mode, the dye diffused and had spread even into distant branches, hereby enabling Ca^{2+} imaging with a low background staining. Simultaneous electrophysiological recordings were possible. The main advantage of this method is that changes of fluorescence can be clearly assigned to the patched cell, because other cells are not labeled with the fluorescent dye.

Multi-cell bolus loading

To load cells in a distinct area of the acute slice, the multi-cell bolus loading method was used (adapted from Stosiek *et al.*, 2003). The estherized form of the Ca^{2+} indicator dye was dissolved in DMSO with 20 % pluronic acid and stored as aliquots of 8 mM at -20 °C. This stock was diluted in MCBL solution (in mM: 50 NaCl, 2.5 KCl, 10 Hepes, pH 7.4) to reach a final concentration of 0.3 to 0.8 mM. A few µl of this solution were filled into an electrode (resistance ∼1 MΩ). This electrode was placed beneath the surface of the slice before pressure injection (1-2 bar) was started for 1 to 2 min. After 45 min, during which the dye was taken up by cells and the remaining dye was washed out, the experiments were started.

Bulk loading

To broadly label superficial cells of the slice, the slices were incubated for 1 h at 34 °C in ACSF to allow recovery from the preparation. Afterwards, slices were put into a custom-built staining chamber for 45-60 minutes at 30 °C, which was filled with Ca^{2+} indicator dyes (between 4 and 8 µM) dissolved in ACSF with pluronic acid. This was followed by a 30 minutes wash out step in ACSF before experiments were started.
Unless stated otherwise, this method was also used for SR101 labeling of cells, but with shorter incubation times. Staining was allowed in ACSF (1 µM SR101) for 20 minutes at 34 °C, following 10 minutes to wash out excessive dye at 34 °C. If slices were not directly transferred to the recording chamber, they were kept in ACSF at room temperature until the start of the recording.

2.6 Immunohistochemistry

For immunohistochemical analysis of astroglial protein expression, TgN(hGFAP-EGFP) mice were used. Brain slices were prepared in the same way as for experiments with acute slices until dissection of the brainstem from the cerebellum. The whole brainstem was fixed with Paraformaldehyde (4 %) for 48 h and kept in PBS (in mM: NaCl 137, KCl 2.7, Na_2HPO_4 8.1, KH_2PO_4 1.4) supplemented with NaN_3 until cutting of slices using the Leica vibratome (VT1000S). 50 µm thick slices containing parts of the preBötC were cut.

2.6.1 Antibodies

Primary antibodies

Immunohistochemical stainings were performed with antibodies against group I metabotropic glutamate receptors (mGluR I) and against Pannexin-1 (Panx1). The group I mGluR antibody was purchased from Abcam (Cambridge, UK): ab51314 (polyclonal from rabbit against mGluR1). For immunohistochemical detection of Panx1 expression,

we used an antibody, which was raised in chicken (Aves Labs, Tigard, OR, also see Locovei *et al.*, 2006) and kindly provided by Eliana Scemes (Rose F. Kennedy Center, Albert Einstein College of Medicine, NY).

Secondary antibodies

mGluR expression was detected with Cy3-conjugated anti-rabbit antibody 111-165-144 from Dianova (Hamburg, Germany) raised in donkey. Cy3-conjugated anti-chicken antibody raised in donkey, for the detection of Panx1 expression was kindly provided by Till Manzke (Department of Neuro- and Sensory Physiology, University Medical Center Göttingen).

2.6.2 Staining protocols

Fixed slices were transferred to a 4-well plate to perform the immunolabeling as described below.

mGluR I staining with antibody ab51314

- 3 x 10 minutes washes in PBS
- 2 h permeabilization and blocking in 0.1 % Triton X-100 and 10 % goat serum in PBS
- primary antibody 1:250 in PBS, 4 °C over night
- 3 x 10 minutes washes in PBS
- secondary antibody 1:500 or 1:1000 in PBS, room temperatur, 2 h
- 3 x 10 minutes washes in PBS

Pannexin-1 staining

- 3 x 10 minutes washes in PBS
- 2 h permeabilization 0.1 % Triton X-100 in PBS
- primary antibody 1:500 in PBS, 4 °C, 48 h
- 3 x 10 minutes washes in PBS
- secondary antibody 1:300 in PBS, room temperatur, 2 h
- 3 x 10 minutes washes in PBS

As the last step, slices were transferred onto microscope slides and mounted in Fluomount Mounting Medium (Dako Industries, Carpinteria, CA).

2.7 Data recording

2.7.1 Software for data recording and processing

Electrophysiological data were recorded with pClamp 9 in combination with Multiclamp 700A Commander (Molecular Devices). Fluorescence measurement data were recorded with Imaging Workbench 6.0 software (INDEC Biosystems) at the widefield-imaging setup. The two-photon setup was controlled by the ImSpector software (LaVision BioTec) of different versions as supplied by the manufacturer. Immunohistochemical data were recorded with LSM 510 software from Zeiss at the confocal laser-scanning microscope. For analysis of electrophysiological data, Clampfit 10.1 (Molecular Devices) and Igor Pro 3.16 (WaveMetrics, Lake Oswego, OR) were used.

2.7.2 Processing of Ca^{2+} imaging data

Analysis of Ca^{2+} imaging data was performed with ImageJ using plugins of the Wright Cell Imaging Facility (www.uhnres.utoronto.ca/facilities/wcif/download.php), for which recorded raw data were converted to tiff format. In the next step, background subtraction was performed using the ImageJ macro. Regions of interest (ROIs) were defined and fluorescence was averaged within each ROI for every image of a timeseries recording. The resulting traces of fluorescence changes over time were copied to Igor Pro in order to perform ΔF calculation with a custom-written macro. For this, the first $\sim$10 data points of each recording were defined as baseline fluorescence (F_0) and averaged. Changes of fluorescence are displayed as changes over F_0 according to this equation:

$$\Delta F/F_0 = \frac{F - F_0}{F_0}$$

2.7.3 Cycle-triggered averaging

In order to increase signal-to-noise ratio of the small astroglial rhythmic currents and to further analyze these currents as well as Ca^{2+} signals, in some experiments cycle-triggered averaging was performed. For averaging of electrophysiological recordings, Yoshitaka Oku (Department of Physiology, Hyogo College of Medicine, Nishinomiya, Japan) provided a routine written in MATLAB© (Mathworks, Natick, MA). Briefly, the integrated field-potential recorded by the extracellular field-potential electrode was used to perform a peak detection. Time windows surrounding the peak were defined, for example 1 s before and 2 s after the peak. Both signals, membrane currents of astrocytes and the integrated field potential were averaged to provide averaged signals for further analysis (Fig. 2.4).

The routine was adapted by writing a similar script to average Ca^{2+} imaging data in order to test for rhythmic Ca^{2+} signals in phase with respiratory bursts. Although respiratory bursts were also used as a trigger, they were not detected automatically. To correlate field-potential recordings with optical recordings, for every image a trigger pulse was recorded simultaneously with the field-potential recording. By this, each peak of the respiratory burst trace could be assigned to an image of the Ca^{2+} imaging recording. A defined number of images before and after this image were used for averaging, similar to the time windows described above.

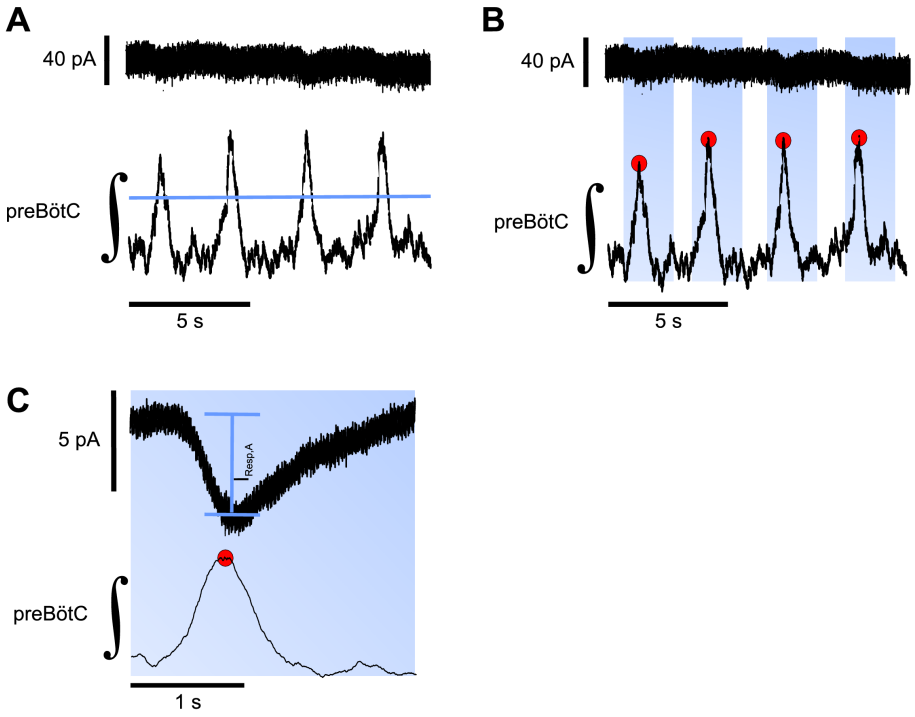

Fig. 2.4: **Cycle-triggered averaging increases signal-to-noise ratio.** Cycle-triggered averaging was performed to average the recorded data using the respiratory bursts as triggers. **A** Integrated field-potential activity (lower trace) and the membrane current of a rhythmic astrocyte (upper trace); $V_m = -70$ mV. A threshold line (blue) is set to detect respiratory bursts. **B** Peaks of respiratory bursts are labeled with red dots and time windows (blue boxes) are defined, which are used to average the traces (in this figure 1 s before and 2 s after the respiratory burst are used for averaging). **C** Averaged signal of both traces. Signal-to-noise ratio is increased and allows determination of parameters like amplitude ($I_{Resp,A}$) of the respiratory-related membrane current fluctuations.

2.7.4 Recording and analysis of SR101 experiments

The SR101-labeling experiments were performed at the two-photon setup to record 40 µm z-stacks consisting of 20 images. Since ImSpector software allowed precise adjustment of exposure time, laser power, number of foci and depth of recording, the recordings were performed under very similar conditions every time. λ_{ex} was always set to 800 nm and filter settings were 531/40 bandpass for EGFP detection and 645/75 bandpass for SR101 detection. This resulted in one EGFP and one SR101 stack. To analyze the intensity of SR101 labeling, first Autoquant (Media Cybernetics, Bethesda, MD) was used for deconvolution of 3D stacks. The results were imported to Imaris (Bitplane, Zürich, CH) in order to spot EGFP-expressing astrocytes and SR101+ cells independent from each other. The spots had a diameter of 6 µm and were aligned on each cell by hand. Bitplanes center function was used to center the spot on each cell. If the center function was not able to center the spot, the cell was discarded from further analysis. By this measures, the number of labeled cells and median intensities could be exported as *.csv files for statistical analysis.

2.8 Statistical analysis

The results are presented as mean values ± standard error of the mean (SEM) if not stated otherwise. Data were displayed as boxplots to check for homogeneity of variance and a normal distribution. Both conditions need to be fulfilled to perform a t-test or paired t-test for analysis of statistical significance. If data were not Gaussian distributed, a rank-sum test was performed. If p-values were smaller than 0.05, the differences were considered to be significant and the results are marked with asterisk. The software used for statistical analysis was SigmaStat 3.1 (Systat Software, Chicago, IL).

3 Results

3.1 Identification of astrocytes via different imaging methods

The introduction of transgenic mouse lines with astrocytes expressing fluorescent proteins (Zhuo *et al.*, 1997; Nolte *et al.*, 2001; Hirrlinger *et al.*, 2005b), made the identification of astroglia quicker and easier. Since the use of transgenic mouse lines is not always desirable and possible, there is still a need for other methods to identify astrocytes in living tissues. In the last decade, different groups introduced two methods that are currently used: (1) Labeling of astrocytes with Sulforhodamine 101 (SR101) and (2) lowering $[K^+]_{ex}$ below 0.2 mM to elicit Ca^{2+} oscillations selectively in astrocytes (low-K^+ method).

3.1.1 Identification of astrocytes via Sulforhodamine 101 labeling

SR101 is a Texas Red-based red dye that was shown to selectively label astrocytes in the neocortex *in vivo* (Nimmerjahn *et al.*, 2004) and in hippocampus slices of mice (Langer & Rose, 2009). Here, it was investigated, whether this method is also applicable for identification of astrocytes in the brainstem.

SR101 labeling in the brainstem is not sufficient for identification of astrocytes

The first SR101 stainings in the brainstem were performed according to the protocol of Langer & Rose (2009) (1 µM SR101 at 34 °C for 20 min) of NMRI mice (P2 to P10). This staining protocol resulted in very few and weakly stained cells that partly had a large soma and did not resemble astrocytes (Fig. 3.1 D-F). Additionally, some blood vessels were stained with SR101. The same protocol was also applied to hippocampal slices of mice of the same age of the TgN(hGFAP-EGFP) line, to have an additional astrocyte marker (Fig. 3.1). It is clearly evident that SR101 strongly labeled astrocytes in the hippocampus (Fig. 3.1 B), but only very weakly in the brainstem (Fig. 3.1 E and H). Astrocytes in the brainstem are labeled to some extend with SR101. This was, however, only evident after increasing the gain of the ima.ps Fig. 3.2 summarizes the results of SR101 stainings. The intensity of SR101 labeling in the CA1/CA3 region of the hippocampus was significantly higher compared to the intensity of SR101 labeling in the brainstem (66.0 ± 18.7 a.u. vs. 21.2 ± 3.5 a.u.; Mann-Whitney Rank Sum Test; $n = 5$ slices; $p < 0.05$), while

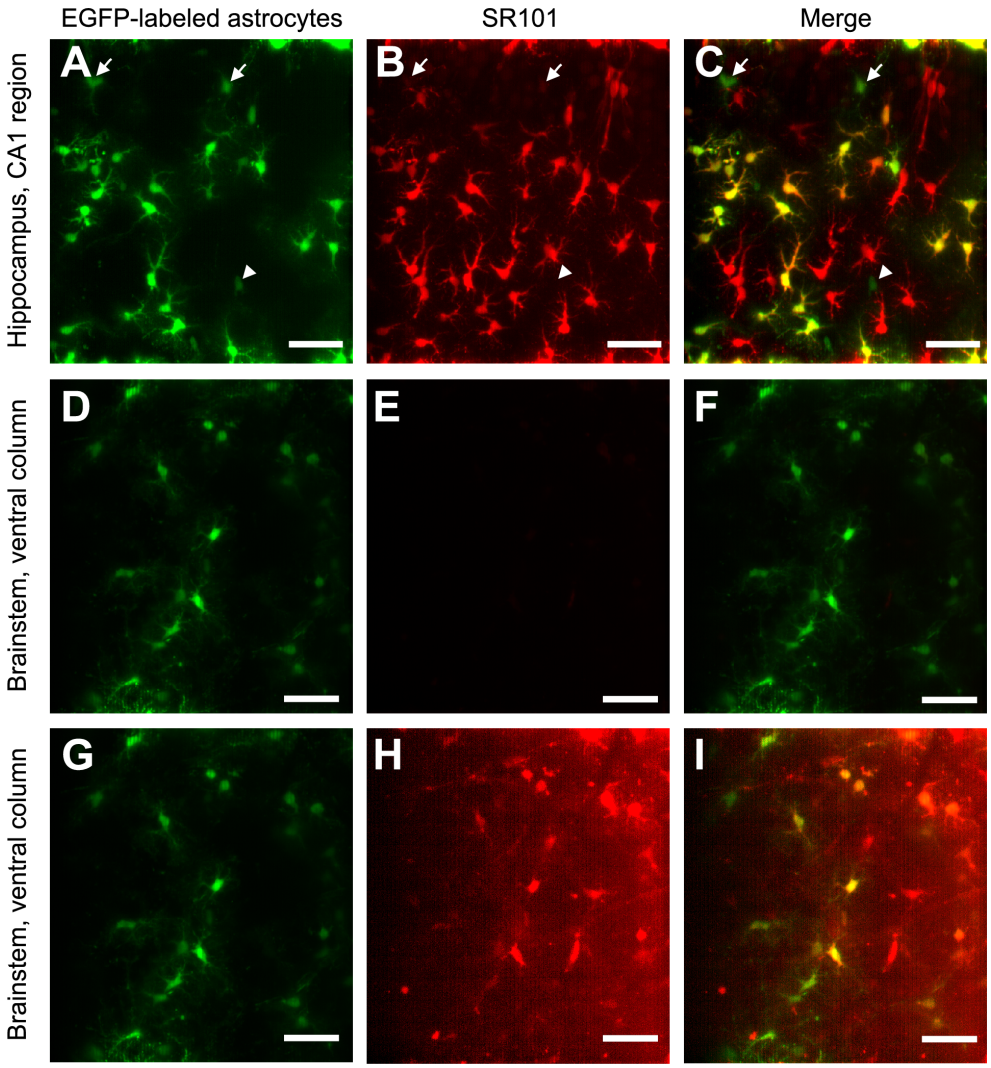

Fig. 3.1: **SR101-labeling is different between hippocampus and brainstem in CTRL conditions.**
Maximum intensity projections (40 µm stack) of SR101 labeling (red) of EGFP-expressing astrocytes (green) in the hippocampus (upper row) and the brainstem (lower rows).**A, D, G** EGFP-expressing astrocytes in the CA1 region of the hippocampus (A) and the ventral column in the brainstem (D, G). **B, E** After incubation in SR101, staining is very prominent in hippocampal astrocytes (B), but not detectable in the brainstem (E) with the same recording settings and brightness as in (B). **C** Merge of EGFP (green) and SR101 (red) labeling proves that except one cell (marked by arrowhead), all hippocampal EGFP-expressing astrocytes are also SR101+ (yellow cells), although two cells are labeled very weak (arrows). **G-I** The same recording as in the row above, but the gain in (H) was adjusted to display the weak labeling of astrocytes. **I** Merge of (G) and (H) confirms overlap of EGFP and SR101 fluorescence. Scale bars: 40 µm.

the fraction of SR101+ astrocytes was comparable in both regions (Fig. 3.2). In the hippocampus, $71.6 \pm 6.8\,\%$ of EGFP-expressing astrocytes were also SR101+ and in the brainstem $55.8 \pm 14.4\,\%$ of astrocytes were also filled with SR101 (t-test, n.s.).

Although the astroglial-specific SR101 staining in the hippocampus was confirmed, it turned out that SR101 staining in the brainstem is not sufficient for a reliable identification of astroglia in the brainstem. But what is the reason for this difference?

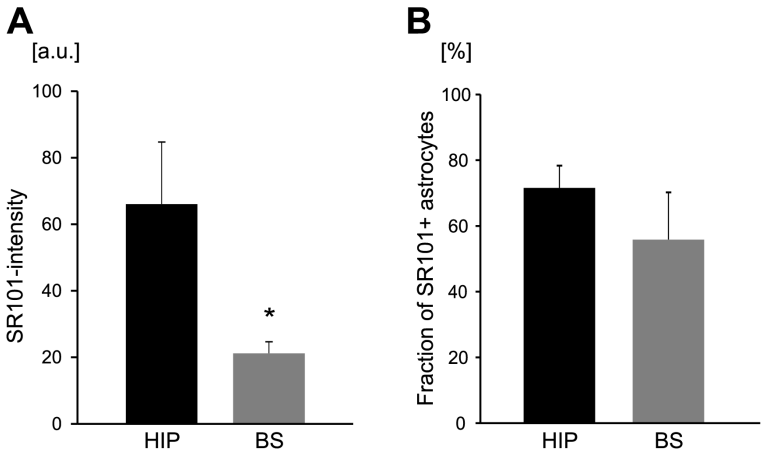

Fig. 3.2: **SR101-labeling of hippocampal astrocytes is significantly stronger than that of brainstem astrocytes.**
A Mean intensity of SR101 labeling in the CA1/CA3 region of the hippocampus (HIP) and the ventral column of the brainstem (BS). SR101 labeling in the hippocampus is significantly higher compared to the brainstem (66.0 ± 18.7 a.u. vs. 21.2 ± 3.5 a.u.; Mann-Whitney Rank Sum Test; $n = 5$ slices; $p < 0.05$). **B** The fraction of SR101+ astrocytes in each stack showed no significant difference between hippocampus and brainstem ($71.6 \pm 6.8\,\%$ vs. $55.8 \pm 14.4\,\%$) (n.s.; t-test; $n = 5$ slices).

Carbenoxolone decreased SR101 labeling in hippocampal astrocytes

Nimmerjahn *et al.* (2004) observed a spread of SR101 after local application and suggested involvement of gap junctions, because Carbenoxolone (CBX), which blocks gap junctions and hemichannels (Davidson *et al.*, 1986), suppressed SR101 labeling. Thus, either different hemichannel expression or regulation could be causal for the different SR101 uptake in hippocampal and brainstem astrocytes. Functional expression of gap junctions (Dermietzel *et al.*, 1989) and hemichannels (Ye *et al.*, 2003) in astrocytes has already been shown for different regions, and dye coupling of preBötC astrocytes was also observed (Szoke *et al.*, 2006). Thus, it was tested if blockade of hemichannels in the brainstem could reduce dye uptake and SR101 labeling. First, CBX ($100\,\mu M$) was applied in the hippocampus to test if CBX blocks the labeling with SR101 also in slices. Indeed, CBX reduced SR101-

labeling intensity significantly (Fig. 3.3 A, B, C; 50.61 ± 8.8 a.u. vs. 18.34 ± 0.88 a.u.; Mann-Whitney Rank Sum Test; $p < 0.05$; $n = 6$ slices), while the fraction of SR101+ astrocytes was similar (Fig. 3.3 D; 70.5 ± 5.7 % vs. 53.4 ± 8.9 % of EGFP-expressing astrocytes; n.s.; t-test; $n = 6$ slices).

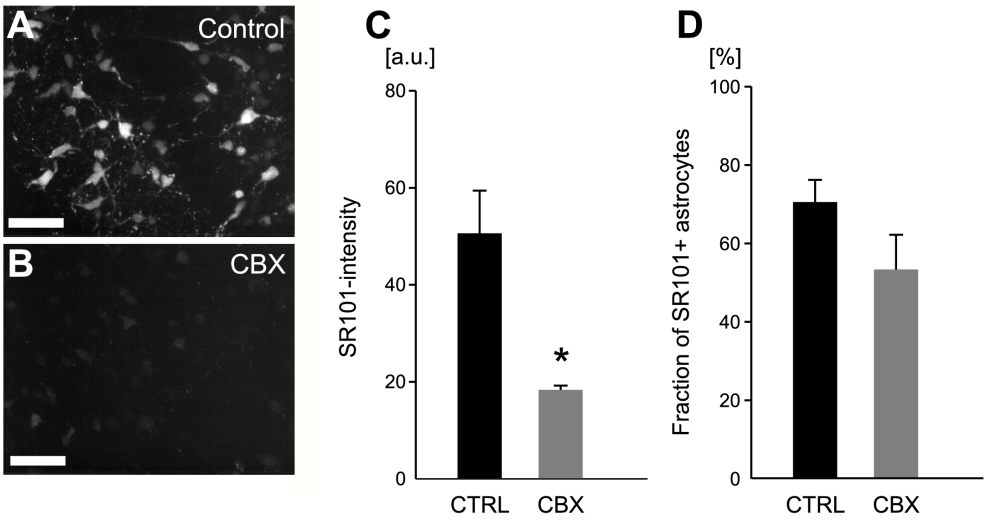

Fig. 3.3: **CBX reduced SR101 labeling in the hippocampus.**
A Maximum intensity projection of SR101+ cells in the hippocampus under CTRL conditions (scale bar: 40 µm). **B** The same staining protocol but with CBX (100 µM) during staining with SR101 significantly reduced intensity of SR101 labeling as well as the number of stained cells (scale bar: 40 µm). **C** Intensity of SR101 staining in presence of CBX was significantly lower compared to stainings without CBX (50.61 ± 8.8 a.u. vs. 18.34 ± 0.88 a.u.; Mann-Whitney Rank Sum Test; $p < 0.05$; $n = 6$ slices). **D** The fraction of SR101-labeled astrocytes was not changed by CBX (70.5 ± 5.7 % vs. 53.4 ± 8.9 % of EGFP-expressing astrocytes; t-test; $p < 0.05$; $n = 6$ slices).

Panx1 hemichannels do not account for SR101-labeling differences

Hemichannels are most widely regarded as being composed of connexins. However, since a publication from Panchin *et al.* (2000), the innexin homologues pannexins gained attention. Later, Panx1 was reported to be expressed in astrocytes (Bruzzone *et al.*, 2003) and to form hemichannels (Bruzzone *et al.*, 2003; Huang *et al.*, 2007). Panx1 forms hemichannels that are permeable for dyes (Silverman *et al.*, 2008). Since Panx1 expression in the brainstem has not been investigated yet, it was tested here, if different expression of Panx1 or differences in the open probability of these hemichannels can explain the SR101-labeling differences between hippocampus and brainstem. In order to investigate the involvement

of Panx1 hemichannels in SR101 uptake, immunohistochemical stainings against Panx1 were performed as well as pharmacological blockade of Panx1 during SR101 staining.

Representative confocal images of Panx1 immunostained brain slices are shown in Fig. 3.4. Panx1 is widely expressed in the hippocampus (Fig. 3.4 A) as well as in the brainstem (Fig. 3.4 B) of EGFP-expressing astrocytes and other cell types. In both regions, the Panx1 labeling showed a ring-like pattern around the soma and was also detected on some processes. Staining in the hippocampus appeared to be more intense than in the brainstem. Additionally, while the cytosol was only weakly labeled in the brainstem, a stronger Panx1 labeling in the cytosol was observed in the hippocampus.

Since immunohistochemical analysis of Panx1 expression did not reveal substantial differences between hippocampus and brainstem, we tested if Panx1 contributes to SR101 uptake in the hippocampus. Panx1 hemichannels were blocked with Mefloquine (MFQ, 0.1-1 µM, Iglesias *et al.*, 2008, 2009) during SR101 incubation to block its uptake (Fig. 3.5) Obviously, MFQ did not prevent SR101 uptake in hippocampal astrocytes. Higher concentrations of MFQ also showed no effect of SR101 uptake (1 µM, $n = 3$ slices, Fig. 3.5 D, F).

Taken together, the immunohistochemical analysis revealed no substantial differences in Panx1 expression between brainstem and hippocampus. Incubation in MFQ failed to block SR101 uptake in hippocampus astrocytes. The results indicate that Panx1 hemichannels are not involved in SR101 uptake.

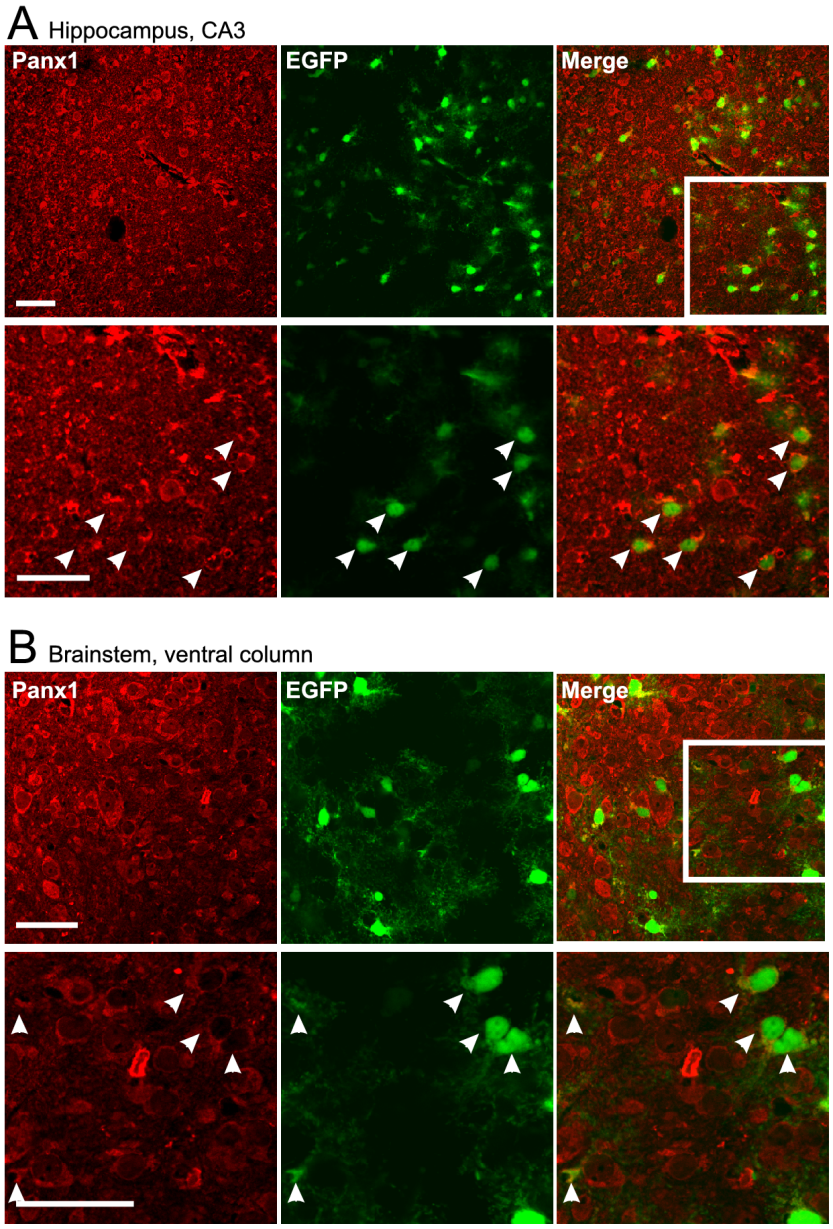

Fig. 3.4: **Panx1 expression in the hippocampus and the brainstem was similar.** **A** Upper row: Overview of immunohistochemical labeling of Panx1 (red) in the CA3 region of the hippocampus of a TgN(hGFAP-EGFP) mouse (age P5). Staining was performed as described in Methods (2.6.2) and shows a broad expression of Panx1 in the hippocampus. Lower row: Higher magnification of the region indicated by the white box (upper row, merged image) reveals Panx1 expression on EGFP-expressing astrocytes (green, arrowheads) as well as on other cells. **B** Overview of Panx1 expression in the brainstem from the same mouse as in (A). Upper row: Overview shows strong Panx1 expression on several cell types (red). Lower row: the magnified region from the white box (merged image of the upper row) shows strong Panx1 expression in the membrane and weak labeling of the cytosol of EGFP-expressing astrocytes (green, arrowheads). Scale bars: 40 µm.

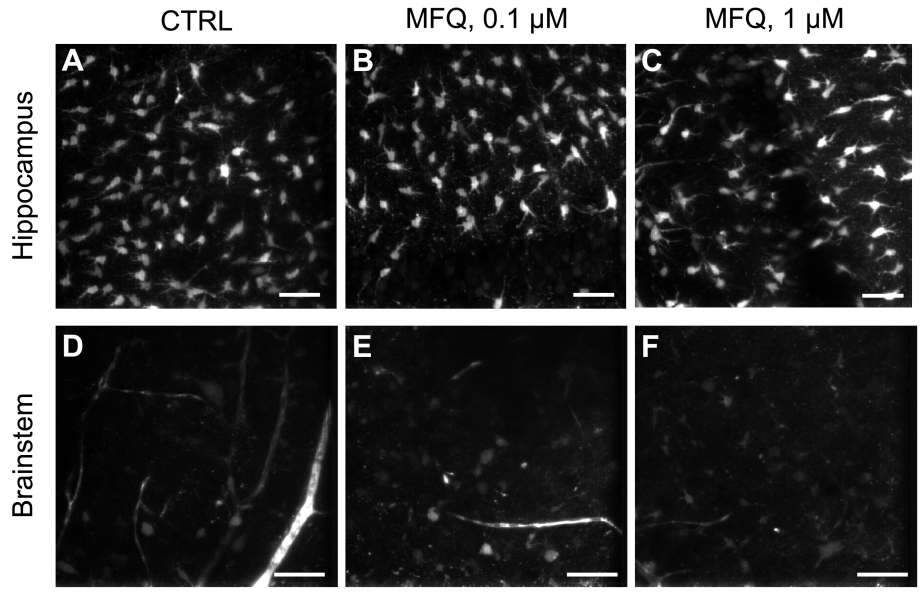

Fig. 3.5: **MFQ did not block SR101 labeling.**
A Astrocytes in the hippocampus (CA3 region) labeled by SR101 following the standard staining protocol. **B** Same staining conditions as (A), but with Panx1 blocker MFQ (100 nM) present in the staining solution. Obviously, blockade of Panx1 hemichannels did not affect staining efficiency of SR101 in the hippocampus. **C** Higher concentrations of MFQ also (1 µM) showed no effect on SR101 uptake. **D** CTRL staining of brainstem astrocytes shows weak labeling of astrocytes and strong labeling of blood vessels. **E** MFQ (0.1 µM) had no obvious effect on SR101 labeling. **F** Higher MFQ concentrations (1 µM) did not change the SR101 labeling. Scale bars: 40 µm.

Gap junction hemichannels do also not account for SR101-labeling differences

CBX inhibited SR101 uptake in the hippocampus and blocks also gap junction hemichannels, which are blocked by extracellular divalent cations. Therefore, next SR101 stainings were performed in divalent cation free solution (DCFS). DCFS is of the same composition as ACSF but lacks the divalent cations Mg^{2+} and Ca^{2+} and is commonly used to open gap junctions (for example DeVries & Schwartz, 1992; Valiunas, 2002; Ye *et al.*, 2003). Here, SR101 staining was performed in DCFS instead of ACSF to open gap junction hemichannels in the brainstem to try to enhance SR101 uptake. However, this measure did not result in improved SR101 labeling of brainstem astrocytes (Fig. 3.6). SR101 intensity showed no significant change in the hippocampus (Fig. 3.6 B, C 98.47 ± 29.17 a.u. (CTRL) vs. 69.24 ± 17.38 a.u. in DCFS (n.s.; t-test; $n = 4$ slices), and the number of stained cells did not change as well (Fig. 3.6 D; 73.7 ± 9.4 % vs. 67.7 ± 3.4 % of EGFP-expressing astrocytes; n.s.; t-test). The SR101 intensity in the brainstem was also not changed (Fig. 3.6 F, G) (24.1 ± 4.1 a.u. vs. 23.1 ± 3.5 a.u.; n.s.; t-test; $n = 3$ slices), but the number of SR101+ cells in the brainstem tended to be reduced. However, the reduction was not significant.

(Fig. 3.6 H; $63.6 \pm 11.5\,\%$ vs. $36.8 \pm 21.8\,\%$ of EGFP-expressing astrocytes; n.s; t-test; $n = 3$ slices).

To exclude that SR101 in the brainstem leaks out from the astrocytes through open hemichannels during washout, CBX (100 µM) was added to the washout solution to close gap junction hemichannels in absence of SR101. This did not improve SR101 staining of brainstem astrocytes compared to DCFS alone (Fig. 3.7, lower row). SR101 labeling in the brainstem remained non-selective for astrocytes as seen from the experiments above. In contrast, most of the hippocampal EGFP-expressing astrocytes were also SR101+ positive and the EGFP-/SR101+ cells resembled EGFP-expressing astrocytes (Fig. 3.7, upper row).

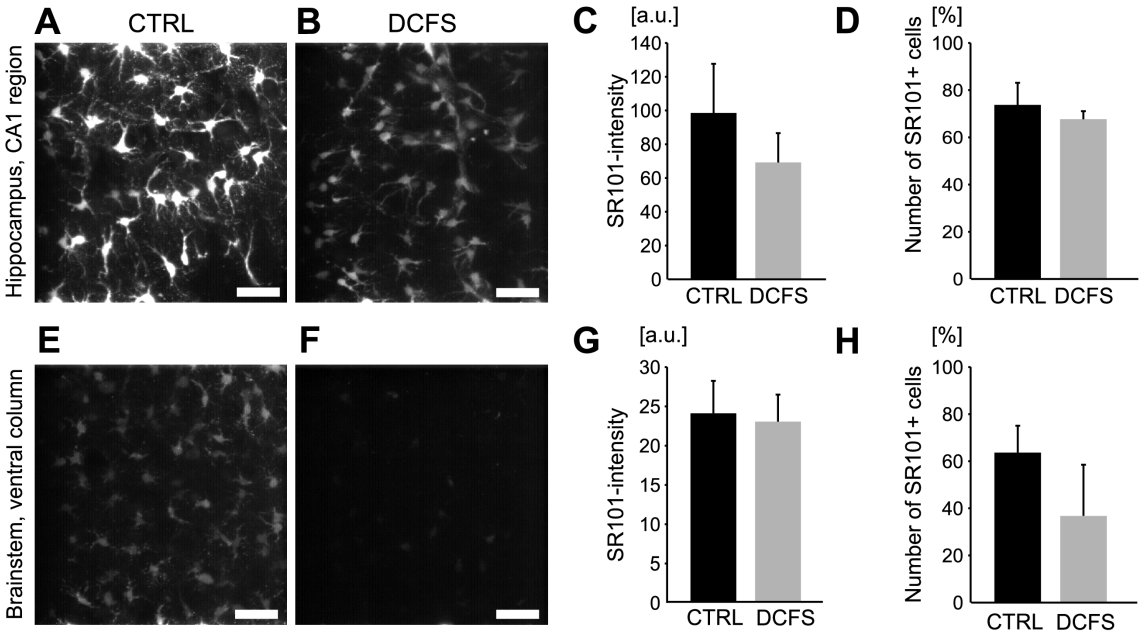

Fig. 3.6: **SR101 staining in divalent cation free solution is not significantly changed.** **A** SR101-staining in the hippocampus (CTRL). **B** SR101 intensity is decreased when staining is performed in DCFS instead of normal ACSF. **C** No significant change of SR101 intensity in the hippocampus between CTRL (98.47 ± 29.17 a.u.) and DCFS (69.24 ± 17.38 a.u.; n.s.; t-test; n=4 slices). **D** Number of stained cells is not changed compared to CTRL ($73.7 \pm 9.4\,\%$ vs. $67.7 \pm 3.4\,\%$). **E** CTRL SR101-staining in the brainstem. **F** SR101 intensity is slightly decreased when staining is performed in DCFS instead of normal ACSF. **G** No significant reduction of SR101 intensity in DCFS (24.1 ± 4.1 a.u. in CTRL vs. 23.1 ± 3.5 a.u. in DCFS (n.s.; t-test; $n = 3$). **H** The number of SR101+ cells is not significantly reduced ($63.6 \pm 11.5\,\%$ vs. $36.8 \pm 21.8\,\%$ of EGFP-expressing astrocytes; n.s; t-test; $n = 3$ slices).

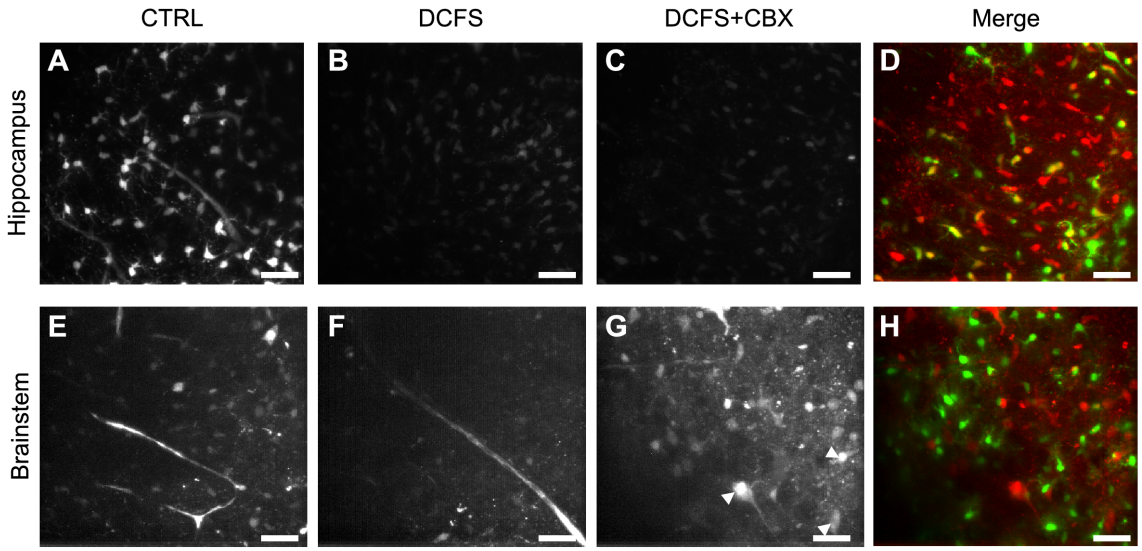

Fig. 3.7: **SR101 staining of brainstem and hippocampal astrocytes in DCFS alone and with additional CBX to prevent leakout of SR101 did not improve astroglial SR101 labeling.**
A CTRL SR101-staining in the hippocampus. **B** SR101 intensity is decreased when staining is performed in DCFS. **C** No increase of SR101 labeling after staining in DCFS and with CBX in the washout solution. **D** Merge of (C) with EGFP recording of this stack. Gain was increased to show that number of SR101+ cells is not decreased compared to CTRL. **E** CTRL SR101 staining in the brainstem. **F** The SR101 intensity is decreased when staining is performed in DCFS, with a few SR101+ astrocytes visible. **G** General SR101 intensity is increased, when CBX was present in the washout solution after staining in SR101. However, the staining is more promiment in cells that do not resemble astrocytes (white arrowheads). **H** Merge of (G) with EGFP recording shows that there is no overlap between EGFP-expressing astrocytes (green) and SR101+ cells (red).

Blockade of SR101 staining by CBX suggested involvement of gap junctions or hemichannels in SR101 staining, but different expression of Panx1 and opening of hemichannels with DCFS was not able to improve astroglial SR101 staining in the brainstem.

Time-lapse SR101 staining under two-photon observation confirms non-selective SR101 uptake in the brainstem

The results presented so far indicate on one hand the involvement of gap junction hemichannels in SR101 labeling, but on the other hand could not prove the uptake via hemichannels, because CBX might interfere with other mechanisms and not only block gap junction hemichannels. Furthermore, opening of these hemichannels did not improve SR101 labeling in the hippocampus and the brainstem.

To elucidate, if different uptake mechanisms or removal of SR101 from brainstem astrocytes might cause the alterations, SR101 staining was recorded using two-photon time-lapse imaging. For this, the first 40 µm z-stack was recorded in ACSF. After that, 1 µM SR101 was added to the bath solution for 20 min. During SR101 incubation (20 min at 34 °C) and its washout (40 min at 34 °C), a new z-stack was recorded every 2 min to observe staining as well as washout of SR101. Time-lapse recording of SR101 staining in the brainstem revealed that SR101 was indeed taken up by several cells types, but fluorescence of SR101+ cells overlapped only weakly with EGFP fluorescence from astrocytes (Fig. 3.8 A). Furthermore, most of the SR101+ cells were larger and did not resemble astrocytes in size or shape. These large cells accumulated more SR101 than EGFP-expressing astrocytes. After 40 min of start of of washout, SR101 was rapidly removed from both cell types and reached almost CTRL level (Fig. 3.8 B).

The same experiment was performed with hippocampus slices (Fig. 3.9). 20 min after addition of SR101 to the bath solution (Fig. 3.9 A), almost all EGFP-expressing astrocytes were filled with SR101 as well as many EGFP-negative cells. In contrast to the brainstem, these cells resembled astrocytes in size and shape. 40 min after washout of SR101 was started, nonselective SR101-labeling and background fluorescence has disappeared. The intensity profile of a neuron and an astrocyte (Fig. 3.9 B) reveal that SR101 was quickly removed from non-astrocytes after washout, but remained in EGFP-expressing astrocytes.

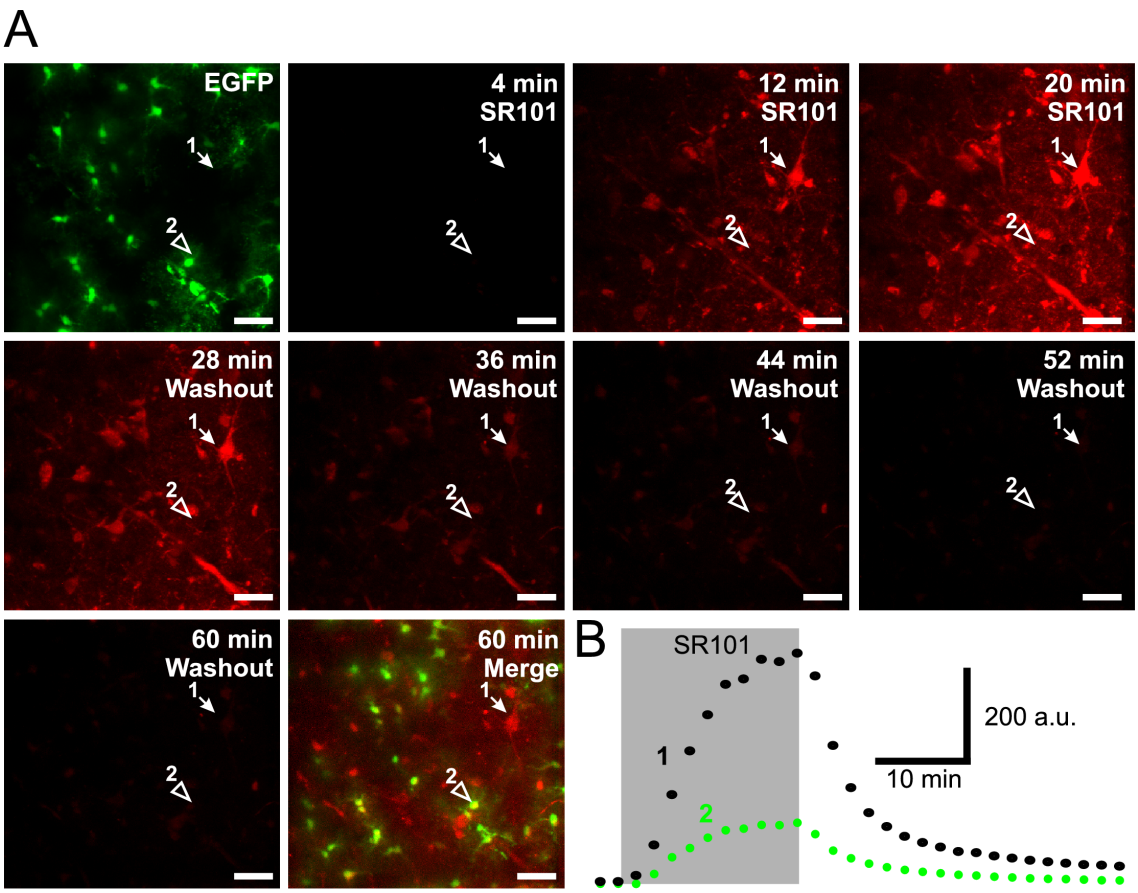

Fig. 3.8: **Time-lapse recording of SR101 staining in the brainstem using two-photon imaging reveals SR101 uptake.**
Maximum intensity projections of SR101 labeling in the brainstem of a TgN(hGFAP-EGFP) mouse. **A** Upper row: First image from left is a recording of EGFP-expressing astrocytes. The second to fourth images show increase of SR101-labeling after addition of SR101 to the bath solution. Middle row: After 22 min, SR101 was washed out and SR101 staining decreased. Lower row: The last image shows a merge of SR101 fluorescence (red, with increased gain) and EGFP fluorescence (green) of astrocytes to show weak astroglial SR101 labeling after 40 min. The white arrow (1) points presumably to a neuron that was filled with SR101, the open arrowhead (2) points to an EGFP-expressing astrocyte. **B** Intensity profile of SR101 fluorescence shows strong fluorescence increase of non-EGFP (cell 1) and weaker SR101 increase of astrocytic SR101-labeling (cell 2, corresponding cells from A). In both cells, SR101 fluorescence decreased rapidly to baseline level after washout of SR101. Scale bars: 40 µm.

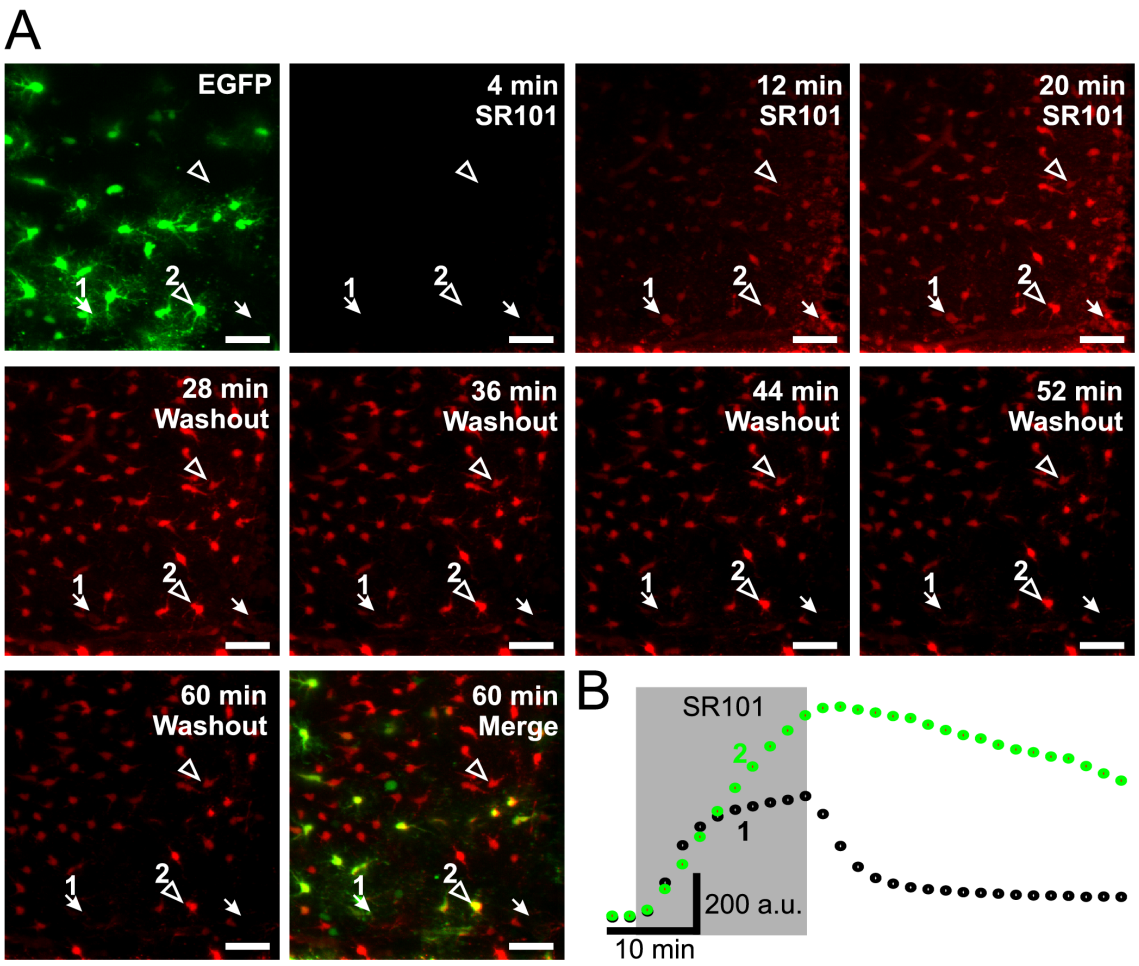

Fig. 3.9: **Time-lapse recording of SR101 staining in the hippocampus using two-photon imaging reveals SR101 uptake.**
Maximum intensity projections of SR101 labeling in the hippocampus of a TgN(hGFAP-EGFP) mouse. **A** Upper row: First image from left is a recording of EGFP-expressing astrocytes. The second to fourth images show increased SR101-labeling after addition of SR101 to the bath solution. After 22 min, SR101 was washed out and SR101 background staining decreased. The last images shows a merge of SR101 fluorescence (red) and EGFP fluorescence of astrocytes (green) to show strong astroglial SR101 labeling after 60 min. The white arrows point presumably to neurons, the open arrowheads point to EGFP-expressing astrocytes. **B** Intensity profile of SR101 fluorescence shows strong fluorescence increase of a non-EGFP cell (1) and an astrocyte (2). In both cells, SR101 fluorescence decreased after washout of SR101, but staining in the astrocyte remained stronger than in the non-EGFP cell (90.4 % vs. 10.2 % higher compared to CTRL at the beginning). Scale bars: 40 µm.

Involvement of multi-drug resistance transporters

Next it was tested, if SR101 is actively removed from the astrocytes in the brainstem and therefore did not accumulate sufficiently inside the astrocytes. Potential candidates are multidrug resistance (MDR) transporters, which are known to remove xenobiotics from cells. Manzini *et al.* (2008) improved labeling of neurons with fluorescent dyes by blocking MDR transporters with MK-571. The addition of MK-571 (200 µM) to the staining solution resulted in an increase of the labeling intensity in cells of the brainstem (Fig. 3.10). The result is very similar to the maximum staining of the time-lapse staining experiments. In the presence of MK-571, cells were labeled with SR101, but they differed in size and shape from astrocytes and are presumably neurons. Almost no overlap between SR101 and EGFP fluorescence could be observed. Interestingly, for the hippocampus the result was different. MK-571 completely blocked SR101 labeling of hippocampal astrocytes, when it was present in the staining solution (Fig. 3.11). In contrast to this, MK-571 only in the washout solution did not prevent SR101 staining.

An additional set of experiments was performed with another MDR-inhibitor. Cyclosporin A (CsA) (CsA, 10 µM) present in the washout phase increased SR101 labeling. However, the SR101 labeling was still not sufficient for reliable identification of astrocytes in the brainstem. Due to poor solubility of CsA, higher concentrations could not be tested (see also Hirrlinger *et al.* (2001)).

Taken together, inhibitors of MDR transporters did not significantly improve SR101 labeling in the brainstem. Since time-lapse staining experiments using two-photon microscopy did not reveal astrocytic SR101 staining, it is unlikely that the weak SR101 labeling is due to faster removal of SR101 from brainstem astrocytes compared to hippocampal astrocytes.

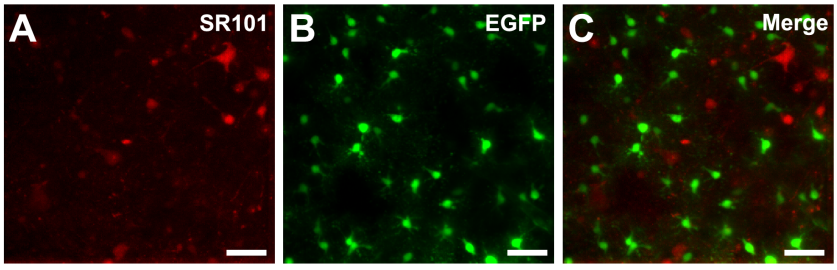

Fig. 3.10: **Brainstem: In the presence MRP1-blocker MK-571, SR101 labeled more cells than under CTRL conditions.**
A In the presence of MK-571 in the staining solution, more cells became labeled with SR101 in the brainstem than without MK-571. **B** EGFP-expressing astrocytes. **C** Merge of images A and B shows that SR101 and EGFP fluorescence does not co-localize. Scale bars: 40 µm.

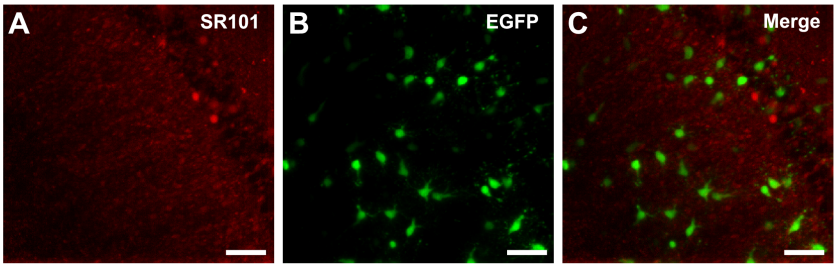

Fig. 3.11: **Hippocampus: The presence of MRP1-blocker MK-571 inhibited SR101 staining.**
A In the presence of MK-571 in the staining solution, no cells were filled with SR101. **B** EGFP-expressing astrocytes **C** Merge of images A and B shows that no co-localisation overlap of SR101 and EGFP fluorescence. Scale bars: 40 µm.

3.1.2 Astroglia specific Ca^{2+} signals in low-K^+ solution

Lowering the extracellular potassium concentration $[K^+]_{ex}$ triggers Ca^{2+} oscillations selectively in astrocytes of rats (Dallwig *et al.* (2000) and mice (Härtel *et al.* (2007)). The low-K^+ induced Ca^{2+} response is mediated via Kir4.1 channels, which were proposed to become permeable to divalent cations in low-K^+ solution (Härtel *et al.* (2007)). Another possible mechanism also involves the Na^+/Ca^2 exchanger (NCX). This exchanger uses the Na^+ gradient over the membrane to transport Ca^{2+} out of the cell. Under conditions of Na^+ accumulation in the cell, the exchanger can also operate in the reversed mode, transporting Na^+ out and Ca^{2+} in. By blocking NCX it was tested here, if low-K^+ solution causes Na^+ influx via Kir channels, leading to increased $[Na^+]_{in}$ and finally triggering Ca^{2+} entry via reversed mode action of the NCX. To test for this, NCX blockers KB-R7943 (1-20 µM) and SN-6 (10 µM) were used to block NCX during low-K^+ application.

Brainstem slices of neonatal mice (P2-P9) were loaded with the calcium indicator dye Oregon Green BAPTA-1 (OGB-1). After 3 min of imaging at 1 Hz, the bath solution was changed to low K^+ for 2 min, followed by washing in ACSF again. At the end of the low-K^+ induced Ca^{2+} response, imaging was stopped to prevent bleaching of OGB-1. After 14 min of incubation with SN-6 or KB-R7943, imaging was restarted and low K^+ applied again, this time in combination with the respective NCX blocker. CTRL experiments were performed without NCX blockers during the incubation time or the second low-K^+ application. For analysis, calcium traces of astrocytes responding to the first low-K^+ application were extracted and compared with those astrocytes that also showed a low-K^+ response in presence of the NCX blocker. This number was compared with the results of experiments with two low-K^+ applications without any blocker (CTRL). Only those astrocytes were considered for analysis that showed a Ca^{2+} transient after application of 1 mM glutamate at the end of the recording as a test for viability.

A representative recording of these experiments is shown in Figure 3.12. Three of four cells showed Ca^{2+} oscillations characteristic for low-K^+ solution also in presence of SN-6. Even under CTRL conditions, only 76.6 ± 6.5 % (n=6 slices) of astrocytes that responded to the first low-K^+ application, also responded to the second application, the reduction of responding astrocytes in presence of KB-R7943 (84.1 ± 9.7 %; n.s.; t-test; n=4 slices) or SN-6 (80.7 ± 2.4 %; n.s.; t-test; n=4 slices) was not significant. This was also true for the amplitudes of low-K^+ induced Ca^{2+} oscillations (Fig. 3.12 D).

These results indicate that the NCX does not contribute to low-K^+ induced Ca^{2+} elevations in astrocytes.

In order to establish the SR101 labeling in our lab, it was planned to perform these experiments also with SR101-labeled astrocytes in hippocampus slices of NMRI mice. However, due to the spontaneous activity of hippocmapal astrocytes, this was not possible. In contrast to brainstem astrocytes identified by fluorescence or low-K^+ response, astrocytes in the hippocampus displayed a lot of spontaneous Ca^{2+} transients with high amplitude and frequency, making reliable identification of astrocytes by low-K^+ induced Ca^{2+} responses impossible (Figure 3.13).

Others have reported similar data from cortex astrocytes at room temperature. After increasing temperature of the bath solution to 37 °C, spontaneous activity in the astrocyte population was no more observable (Schipke *et al.*, 2008b). In contrast, increase of temperature from 30 °C to 37 °C did not reduce spontaneous activity in our experiments (Fig. 3.13).

Taken together, the results from this section have shown that (1) NCX are probably not involved in the generation of low-K^+ induced Ca^{2+} oscillations and (2) that SR101 is not applicable for reliable identification of astrocytes in the brainstem. As a consequence of these findings, the following experiments were performed using transgenic mice with astrocytes that express the fluorescent proteins EGFP or mRFP.

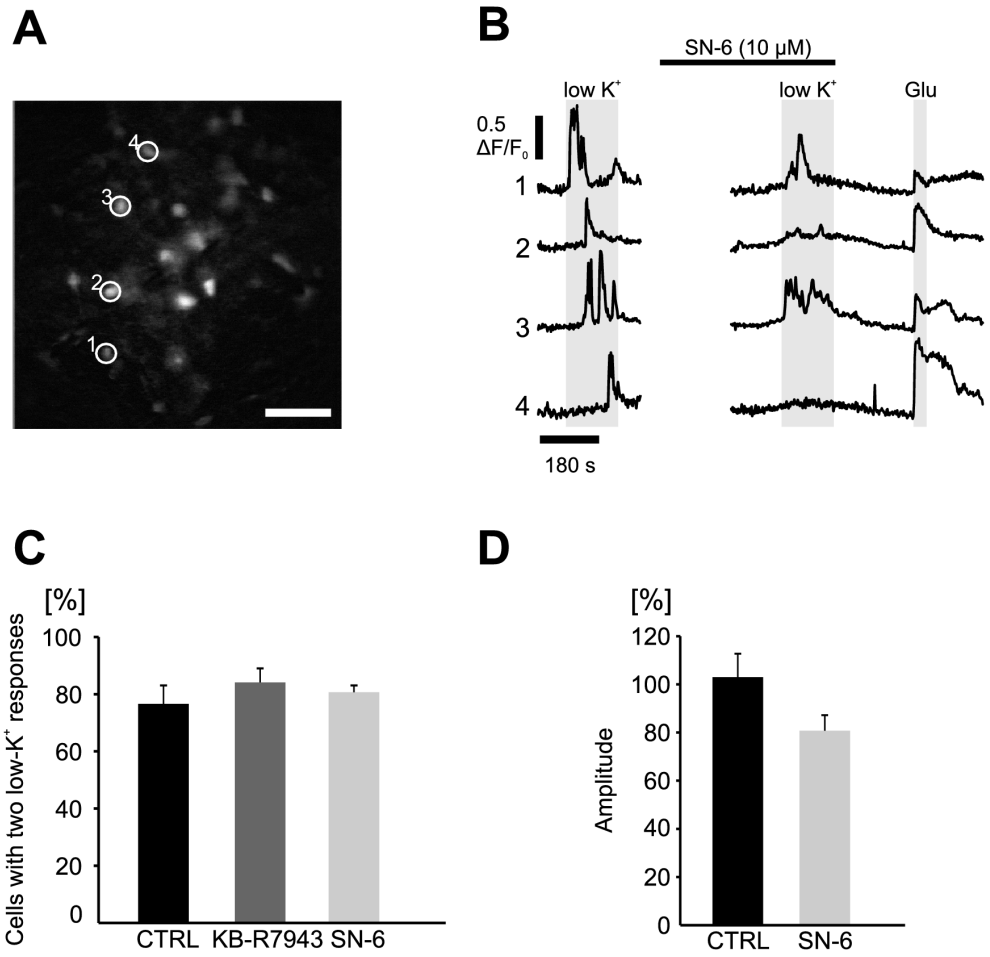

Fig. 3.12: **Inhibition of NCX did not reduce the number of astrocytes with low-K^+ responses.**
A OGB-1 labeling of cells in the preBötC region of a P3 NMRI mouse' 250 µm brainstem slice. Four astrocytes of which Ca^{2+}-imaging traces are shown in (B) are labeled with white arrowheads. Scale bar: 40 µm. **B** Left panel: Responses of the four cells labeled in (A) to superfusion with low-K^+ solution. During incubation of SN-6 (10 µM), recording was stopped to prevent bleaching of OGB-1. Right panel: After two min of recording, superfusion is changed to low K^+ including SN-6. Cells 1 to 3 responded to low K^+, while cell 4 did not response. After washout of low K^+, all four cells responded to 1 mM glutamate. **C** The fraction of cells responding to the second low-K^+ application that also responded to the first low-K^+ application is plotted for three different conditions: Without any blocker (CTRL), 76.6 ± 6.5 % (n=6 slices) responded also to the second low-K^+ application. This fraction remained the same in presence of KB-R7943 (1-20 µM; 84.1 ± 9.7 %; n.s.; t-test; n = 4 slices) or SN-6 (10 µM; 80.7 ± 2.4 %; n.s.; t-test; n = 4 slices). **D** Maximal amplitude of low-K^+ induced Ca^{2+} oscillations was not significantly changed in presence of the NCX blocker SN-6. The second amplitude was 103.0 % of the first one in CTRL conditions, while in presence of SN-6 the amplitude was 80.8 % of the first one (n.s.; t-test; n = 4 slices).

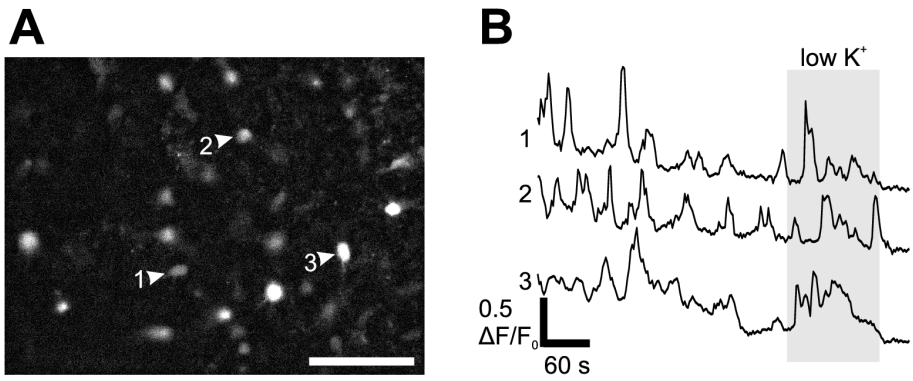

Fig. 3.13: **Hippocampus astrocytes showed spontaneous Ca^{2+} oscillations**
A OGB-1 labeling of cells of a 250 µm hippocampus slice (CA1 region) of a P8 NMRI mouse. Scale bar: 40 µm. **B** Ca^{2+}-imaging traces for three cells labeled by arrowheads in (A) are shown. While it is not clear, if cells one and two responded to low K^+, cell three showed a clear response to low K^+. Scale bar: 40 µm, T = ∼37 °C.

3.2 Respiratory-related signals of astrocytes in the respiratory network

In this section it was tested, whether astrocytes detect the activity of respiratory neurons in the preBötzinger complex (preBötC) and if this activity is translated into astroglial signals that in turn are capable of inducing changes in respiratory activity.

3.2.1 Astrocytes detect neuronal activity in the respiratory network

To test if astrocytes in the preBötC detect neuronal activity resulting in increases of extracellular glutamate and K^+ concentration, whole-cell voltage-clamp recordings of fluorescently labeled astrocytes were performed in rhythmic-slice preparations. Of 569 patched astrocytes, the majority of 510 astrocytes did not show any signal that was correlated to neuronal activity of the preBötC recorded with extracellular field-potential electrodes. Bright EGFP fluorescence (Fig. 3.14 A) and linear current responses to the voltage-step protocol (Fig. 3.14 B) showed that the patched cells belong to the group of passive astrocytes (see also Grass *et al.*, 2004).

In contrast to the astrocytes described above, some astrocytes showed fluctuations of the membrane current that were correlated to respiratory bursts recorded by the extracellular field potential electrode. Fig. 3.15 shows a representative patched passive astrocyte, with membrane-current fluctuations (Fig. 3.15 C, upper trace) that were correlated with respiratory bursts (Fig. 3.15 C, lower trace). Although the fluctuations were very small and almost masked by noise, they could be detected as small inward currents in phase

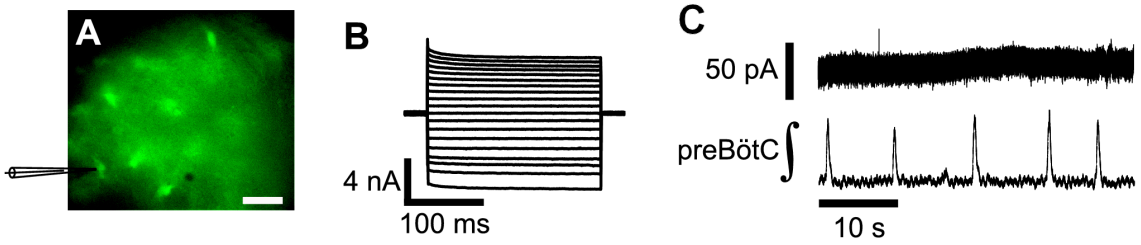

Fig. 3.14: **Example of a patched astrocyte with no respiratory-related signals.** **A** Bright EGFP fluorescence of a patched astrocyte (lower left corner). Scale bar: 40 µm **B** Current responses to a voltage-step protocol confirmed passive character of this astrocyte. **C** Upper trace: membrane current (V_{Hold}=−70 mV) of the patched astrocyte reveals no signals that were correlated to changes of the integrated field potential signal (lower trace). The lower trace was recorded with an extracellular field potential electrode placed on the surface of a rhythmic slice in the region of the preBötC and shows the integrated activity of the respiratory network. Synchroneous firing of respiratory neurons in the network is reflected by the five bursts.

with respiratory bursts. To increase signal-to-noise ratio, cycle-triggered averaging of at least six bursts was performed to analyze duration and amplitude of this current (Fig. 3.15 D), which was termed $I_{Resp,A}$ (I - current, Resp - Respiration, A - Astrocyte).

After recording the membrane current at −70 mV, the astrocytes were clamped to different holding potentials ranging from −90 mV to +20 mV. This was done for at least 2 min for each holding potential to get a minimum of ten bursts as triggers for averaging the membrane current to analyze the voltage dependence of $I_{Resp,A}$ and its composition. The averaged values are listed in Table 3.1. For analysis of voltage dependence only those astrocytes were used, of which $I_{Resp,A}$ was recorded at least at three different holding potentials.

$I_{Resp,A}$ did not reverse its direction and was inwardly directed at all tested holding potentials (Fig. 3.17).

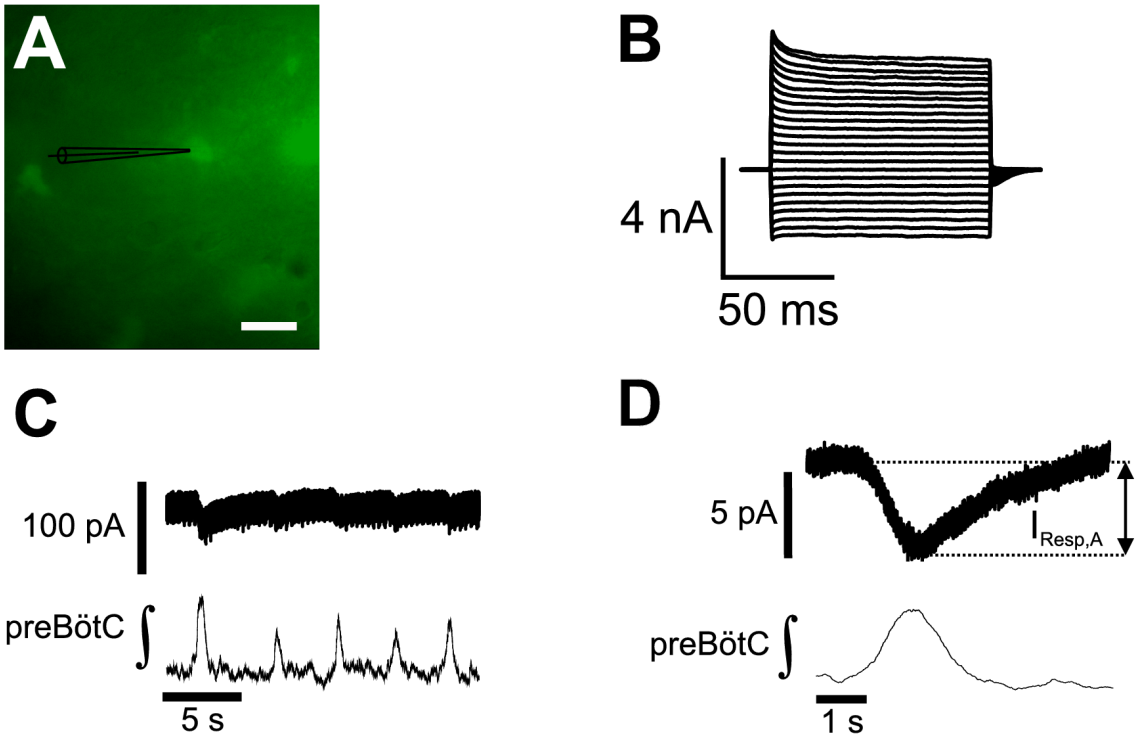

Fig. 3.15: **Patched astrocyte with respiratory-related membrane-current fluctuations.**
A Bright EGFP fluorescence of a patched astrocyte. Scale bar: 40 µm. **B** Passive character of the patched astrocyte is confirmed by its linear responses to the voltage-step protocol. **C** Small current fluctuations of the membrane current (V_{Hold}=−70 mV, upper trace) correlated with respiratory bursts of the integrated field potential (lower trace). **D** After cycle-triggered averaging, signal-to-noise ratio is increased and averaged duration and amplitude of the current fluctuations ($I_{Resp,A}$) as well as of the respiratory bursts can be analyzed.

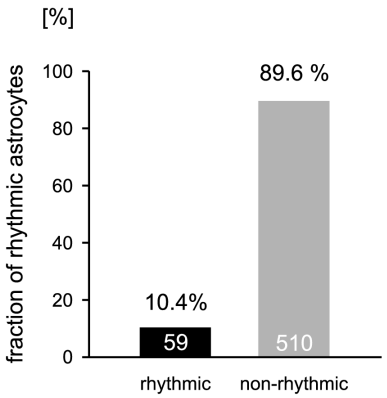

Fig. 3.16: **Fraction of rhythmic astrocytes in comparison to fluorescently-labeled patched astrocytes.**
59 (10.4 %) of the 569 patched astrocytes showed membrane current fluctuations that correlated with respiratory bursts. These astrocytes were named rhythmic astrocytes.

Table 3.1: **Voltage dependence of $I_{Resp,A}$.**
For each tested holding potential, the average amplitude of $I_{Resp,A}$, the normalized amplitude of $I_{Resp,A}$ (calculated by dividing each $I_{Resp,A}$ by the maximal value for each cell), and the number of recorded cells is shown.

$\mathbf{V_{Hold}\ [mV]}$	$\mathbf{I_{Resp,A} \pm SEM\ [pA]}$	$\mathbf{-I_{Resp,A}/I_{max} \pm SEM}$	**n**
-90	-4.26 ± 1.24	-0.63 ± 0.19	3
-80	-6.08 ± 0.76	-0.81 ± 0.06	10
-70	-6.55 ± 0.70	-0.77 ± 0.05	12
-60	-6.56 ± 0.93	-0.79 ± 0.07	10
-40	-6.91 ± 1.51	-0.75 ± 0.07	10
-20	-6.54 ± 1.64	-0.64 ± 0.10	5
0	-5.94 ± 0.96	-0.62 ± 0.11	5
$+20$	-4.76 ± 1.47	-0.43 ± 0.20	3

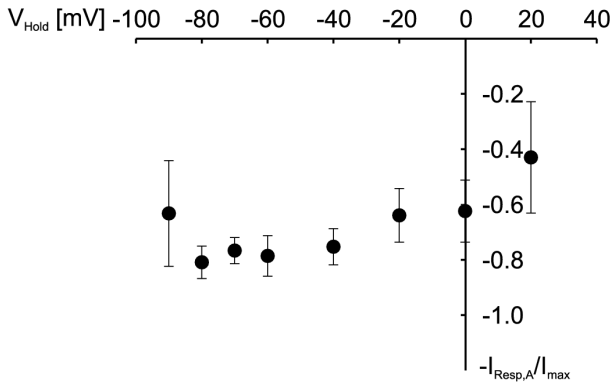

Fig. 3.17: **Voltage dependence of $I_{Resp,A}$.**
The amplitude of $I_{Resp,A}$ was normalized to the maximum value for each cell and is plotted against the tested holding potentials ranging from -90 mV to $+20$ mV. $I_{Resp,A}$ did not change its direction and was always inwardly directed. For number of recorded cells see Table 3.1.

Depolarization of astrocytes did not influence respiratory network activity

Jourdain *et al.* (2007) reported that electrically stimulated astrocytes are capable of influencing synaptic strength. Following the idea that rhythmic astrocytes are located very close to respiratory neurons and are therefore able to be affected by their activity, it was tested if depolarization of rhythmic astrocytes to positive membrane potentials triggers changes of respiratory network activity (Fig. 3.18).

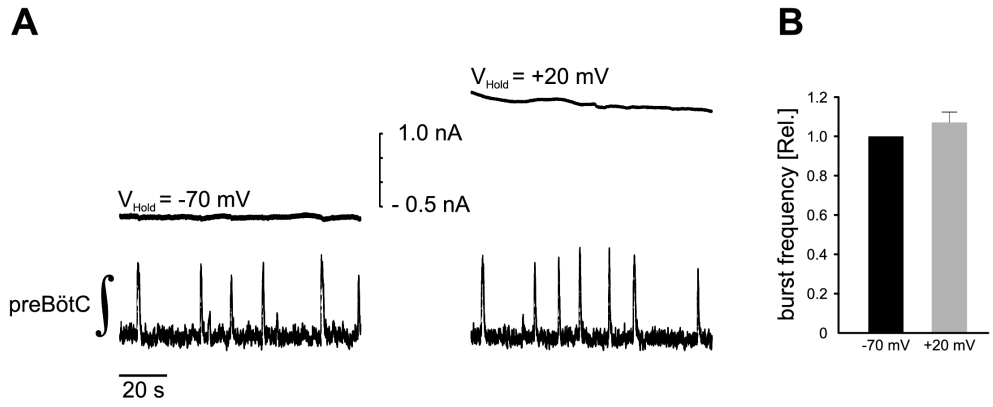

Fig. 3.18: **Depolarization of rhythmic astrocytes did not affect burst frequency of the respiratory network.**
A Left panel: Membrane current at $V_{Hold} = -70$ mV of a rhythmic astrocyte (upper trace) and integrated activity of the respiratory network (lower trace). Right panel: Depolarization of the astrocyte to $V_{Hold} = +20$ mV did not affect burst frequency of the respiratory network. **B**. Summarized data of 5 rhythmic astrocytes, showing that depolarization to $V_{Hold} = +20$ mV does not affect frequency of respiratory bursts in the rhythmic slice preparation.

As it was shown above, a fraction of preBötC astrocytes indeed detects changes of the extracellular milieu caused by synchronized neuronal activity in the respiratory network. Next, we wanted to to clarify the composition of $I_{Resp,A}$.

3.2.2 What is the composition of $I_{Resp,A}$?

Kir channels contribute to $I_{Resp,A}$

Brockhaus *et al.* (1993) have shown that extracellular K^+ activity increases during action potential bursts of inspiratory neurons. Moreover, Neusch *et al.*, 2006 provided evidence that Kir4.1 channels contribute to $[K^+]_{ex}$ regulation in the respiratory network. Furthermore, Kir4.1 channels are the major contributors to potassium conductance in astrocytes of the respiratory network, and Kir4.1$^{-/-}$ mice have reduced inward currents in 50 mM K^+ solution compared to wild-type mice (Neusch *et al.* (2006)). Thus, it was tested here, if blockade of Kir conductance with barium ($BaCl_2$) reduces $I_{Resp,A}$. First, $I_{Resp,A}$ was recorded at different holding potentials in standard ACSF, before $BaCl_2$ was applied. After 10 min of incubation, the same protocol was applied to cell again to measure the effect of $BaCl_2$ on $I_{Resp,A}$.

Application of $BaCl_2$ significantly reduced $I_{Resp,A}$ at $V_{Hold} = -70$ mV from -6.55 ± 0.7 pA in CTRL to -2.91 ± 0.48 pA ($p < 0.05$; t-test; n=12). Significant reductions were also observed at other holding potentials (−90, −80 and −60 mV). For the other holding potentials (−40 mV to +20 mV) the reduction of $I_{Resp,A}$ after application of $BaCl_2$ was not significant (see Table 3.2 for details). $BaCl_2$ application (filled circles) reduced $I_{Resp,A}$ by 50 % compared to CTRL conditions (Fig. 3.19).

Table 3.2: **Kir-conductance blockade with $BaCl_2$ reduced $I_{Resp,A}$** The 2nd column shows $I_{Resp,A}$ under CTRL condition. The third column shows $I_{Resp,A}$ after Kir-channel blockade with $BaCl_2$. Asterisk indicates significant differences of $I_{Resp,A}$ between CTRL and $BaCl_2$.

V_{Hold} [mV]	$I_{Resp,A,CTRL} \pm$ SEM [pA]	-$I_{Resp,A,BaCl_2} \pm$ SEM [pA]	n
−90	-4.26 ± 1.24	-1.65 ± 0.33	3
−80	-6.08 ± 0.76	-2.82 ± 0.67 ⋆	10
−70	-6.55 ± 0.70	-2.91 ± 0.48 ⋆	12
−60	-6.56 ± 0.93	-3.48 ± 0.73 ⋆	10
−40	-6.91 ± 1.51	-3.03 ± 0.52 ⋆	10
−20	-6.54 ± 1.64	-3.92 ± 1.07	5
0	-5.94 ± 0.96	-2.26 ± 0.72	5
+20	-4.76 ± 1.47	-2.33 ± 0.51	3

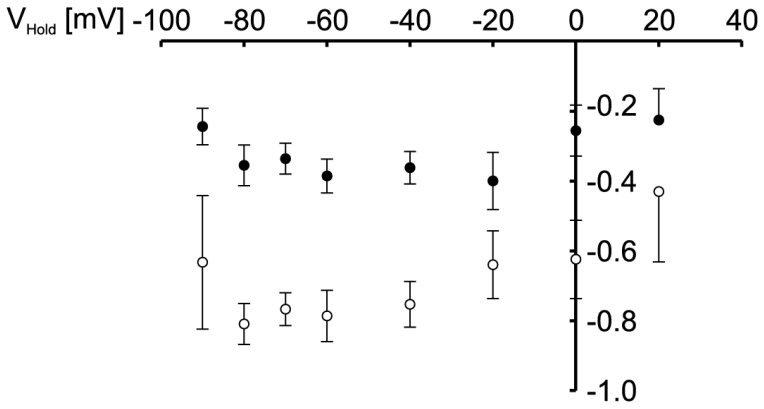

Fig. 3.19: **$I_{Resp,A}$ was reduced after application of $BaCl_2$.** $I_{Resp,A}$ was significantly reduced by ∼50 % after application of $BaCl_2$ at holding potentials of -80, -70, -60 and -40 mV. Reduction at the other tested holding potentials was not significant. For absolute values see Table 3.2.

The $BaCl_2$-induced reduction of $I_{Resp,A}$ might be caused not only by blocking astroglial Kir conductance, but also via $BaCl_2$-mediated effects on respiratory network activity. To test for this, amplitude and frequency of the respiratory bursts as well as their duration at half-maximal amplitude in $BaCl_2$ were compared to CTRL conditions. As shown in Fig. 3.20, the effect of $BaCl_2$ on $I_{Resp,A}$-induced reduction appears not to be caused by effects on respiratory network activity. Amplitude (0.08 ± 0.01 a.u. (CTRL) vs. 0.08 ± 0.01 a.u. ($BaCl_2$), Fig. 3.20 B) and duration at half-maximal amplitude (0.79 ± 0.03 s (CTRL) vs. 0.75 ± 0.04 s ($BaCl_2$), Fig. 3.20 C) of respiratory bursts were not changed compared to CTRL conditions. Only burst frequency was significantly increased by $BaCl_2$ (0.11 ± 0.01 s^{-1} (CTRL) vs. 0.15 ± 0.02 s^{-1} ($BaCl_2$), $p < 0.05$; t-test; $n = 12$; Fig. 3.20 A).

These data indicate that a large part of $I_{Resp,A}$ is caused by K^+ fluxes via Kir channels.

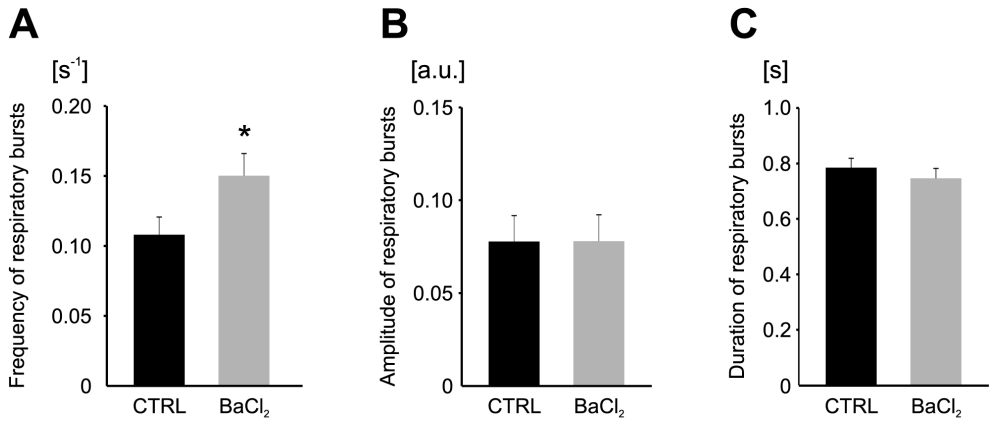

Fig. 3.20: **$BaCl_2$ affected frequency, but not amplitude and duration of respiratory bursts.**
A Application of $BaCl_2$ significantly increased burst frequency from $0.11 \pm 0.01\,s^{-1}$ (CTRL) to $0.15 \pm 0.02\,s^{-1}$ ($p < 0.05$; t-test; $n = 12$). **B** Amplitude of respiratory bursts was not changed by $BaCl_2$ application: 0.08 ± 0.01 a.u. (CTRL) vs. 0.08 ± 0.01 a.u.; n.s.; t-test; $n = 12$. **C** Duration of respiratory bursts at half-maximal amplitude was also not changed by $BaCl_2$: 0.79 ± 0.03 s (CTRL) vs. 0.75 ± 0.04 s ($BaCl_2$); n.s.; t-test; $n = 12$

.

Glutamate transporter currents contribute to $I_{Resp,A}$

Glutamate is the most abundant neurotransmitter within the preBötC and is continuously released by preBötC neurons (Greer *et al.*, 1991). Since $BaCl_2$ did not block $I_{Resp,A}$ completely, it was tested if glutamate uptake also contributes to $I_{Resp,A}$. First, the GABA-receptor blocker bicuculline (10 µM) and the glycine-receptor blocker strychnine (10 µM) were applied to increase activity of the respiratory network. After that, DL-TBOA (100 µM) was added to the bath solution to block glutamate uptake via glutamate transporters. Subsequently, the baseline of the integrated field potential increased and respiratory bursts became smaller and more irregular before respiratory activity was completely inhibited (Fig. 3.21).

On average, the increase of the baseline started at 170 ± 22 s after addition of DL-TBOA to the bath solution. While in two experiments, a final peak occured before complete blockade of respiratory activity (Fig. 3.21, lower trace), in further experiments respiratory bursts became just smaller before they were no longer observable. On average, respiratory activity was completely blocked 382 ± 81 s after adddition of DL-TBOA to the bath solution. In parallel with blockade of respiratory activity, a large inward current could be observed in four of five whole-cell voltage-clamped rhythmic astrocytes. The peak of this current was reached at 481 $\pm$ 100 s and had an average amplitude of -682.5 $\pm$ 293.2 pA ($n = 4$). After washout of DL-TBOA, respiratory activity did not recover within 60 min ($n = 3$).

Having shown the failure of respiratory activity by complete blockade of glutamate uptake, a more selective glutamate uptake inhibitor was used to test the contribution of the glial glutamate transporter currents to $I_{Resp,A}$. DL-TBOA blocks the glial glutamate transporters EAAT1 and EAAT2 (Shimamoto *et al.*, 1998) and also the neuronal EAAT3 glutamate transporter (Jabaudon *et al.*, 1999). Dihydrokainate (DHK) is more specific for GLT-1 (Arriza *et al.*, 1994), which is one of the two glial glutamate transporters.

DHK was applied in a subset of the $BaCl_2$ experiments described above. Five rhythmic astrocytes were whole-cell voltage-clamped to $-70\,\mathrm{mV}$. After recording the membrane current for at least two minutes, DHK (300 µM) was added to the bath solution (Fig. 3.22).

$BaCl_2$ reduced $I_{Resp,A}$ in this set of experiments from $-6.9 \pm 2.8\,\mathrm{pA}$ in CTRL to $-3.8 \pm 1.2\,\mathrm{pA}$. Additional application of DHK further reduced $I_{Resp,A}$ significantly to $\sim$20 % of CTRL amplitude ($-1.4 \pm 0.7\,\mathrm{pA}$ ($p < 0.05$; t-test; $n = 5$), Fig. 3.23).

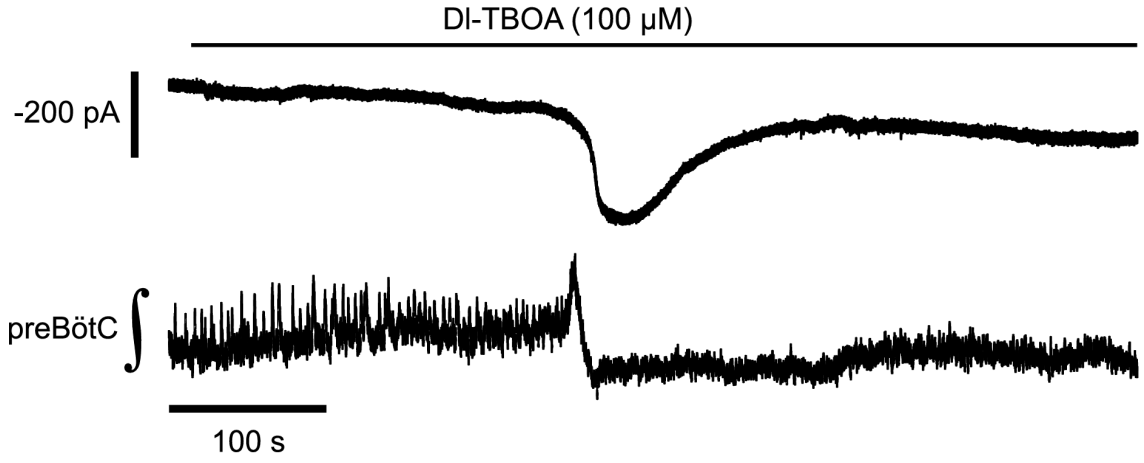

Fig. 3.21: **DL-TBOA induced astroglial inward currents and blockade of respiratory network activity.** The upper trace shows the membrane current of a rhythmic astrocyte voltage-clamped to $V_{Hold} = -70\,\mathrm{mV}$ in presence of bicuculline and strychnine (10 µM each). DL-TBOA induced a small, long-lasting inward-directed current. Around 250 s later, the current increases within a few seconds by more than 200 pA and recovers slowly afterwards. At the level of the respiratory network (lower trace), baseline of the integrated activity increased, while respiratory bursts became smaller and more irregular. Approximately 220 s after baseline increase started, a large peak occured after which no more respiratory bursts were observed.

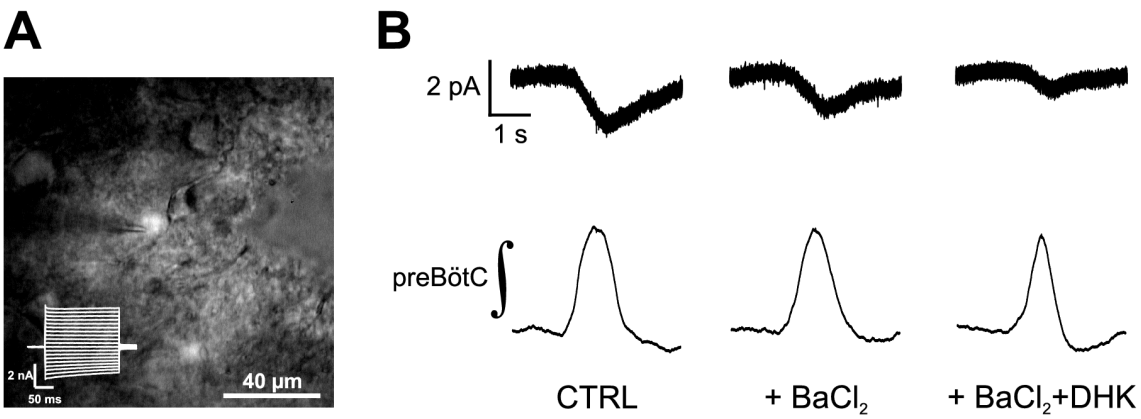

Fig. 3.22: **DHK application reduced $I_{Resp,A}$ in presence of $BaCl_2$.**
A Brightfield image of a EGFP-expressing astrocyte. Scale bar: 40 µm. Inset shows the linear current responses to the voltage-step protocol. **B** The left traces show $I_{Resp,A}$ (upper trace, -1.75 pA) and averaged respiratory bursts under CTRL conditions. Traces in the middle column illustrate reduced amplitude of $I_{Resp,A}$ (upper trace) after $BaCl_2$ application (-1.23 pA). Additional application of DHK (300 µM) further reduced the amplitude of $I_{Resp,A}$ to -0.53 pA at $V_{Hold} = -70$ mV.

It was also tested, if reduction of $I_{Resp,A}$ might be caused by DHK effects on respiratory network activity. While DHK application did not change amplitudes of the respiratory bursts (0.09 ± 0.03 a.u. in $BaCl_2$ compared to 0.07 ± 0.02 a.u.), burst duration at half-maximal amplitude was significantly reduced from 0.77 ± 0.08 s in $BaCl_2$ to 0.56 ± 0.02 s with additional DHK ($p < 0.05$; t-test; $n = 5$). In contrast to this, DHK caused an increase in frequency of respiratory bursts from $0.13 \pm 0.02\,s^{-1}$ in $BaCl_2$ to $0.20 \pm 0.03\,s^{-1}$ with additional DHK.

In conclusion, the DHK effects on respiratory network activity, were not as strong as on $I_{Resp,A}$. This indicates that at least a signficant part of $I_{Resp,A}$ was caused by glutamate transporter currents of GLT-1.

It was shown in this section that major parts of $I_{Resp,A}$ require Kir channels and glutamate transport via the glial glutamate transporter GLT-1. The most likely mechanism of astroglial modulation of neuronal activity involves different pathways, but a common feature of most of these mechanisms is calcium, which could enter the cell from the extracellular space and/or is released from internal calcium stores. Next, it was tested, if rhyhtmic glutamate release from respiratory neurons that cause the current fluctuations of rhythmic astrocytes described above coincide with changes of intracellular astroglial $[Ca^{2+}]$.

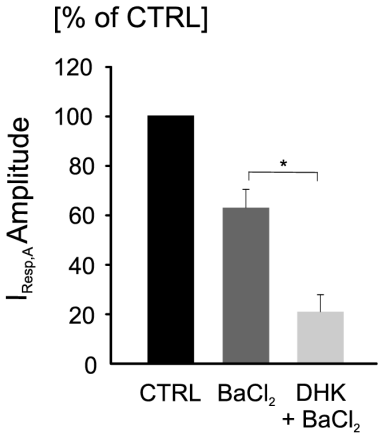

Fig. 3.23: **DHK significantly reduced $I_{Resp,A}$.** First applied $BaCl_2$ reduced averaged $I_{Resp,A}$ from -6.88 ± 2.82 pA to -3.81 ± 1.19 pA (to 55 % of CTRL). Additional application of DHK caused a further significant reduction to -1.42 ± 0.68 pA, corresponding to ~20 % of CTRL $I_{Resp,A}$.

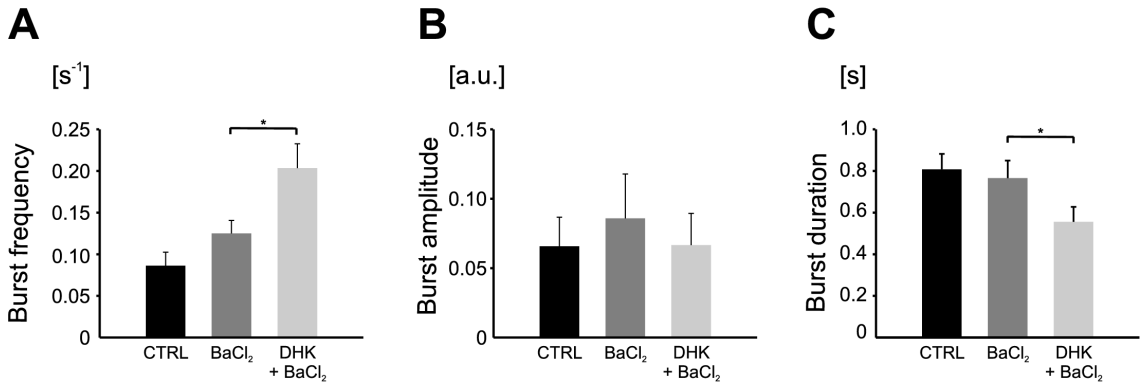

Fig. 3.24: **DHK and $BaCl_2$ affected respiratory network activity.**
A As already shown above, frequency of respiratory bursts was increased by $BaCl_2$ ($0.09 \pm 0.02\ s^{-1}$ in CTRL to $0.13 \pm 0.02\ s^{-1}$ with $BaCl_2$). DHK increased burst frequency even more to $0.20 \pm 0.03\ s^{-1}$ ($p < 0.05$; t-test; $n = 5$). **B** Burst amplitude (0.07 ± 0.02 a.u.) was not changed in presence of $BaCl_2$ (0.09 ± 0.03 a.u.) and DHK (0.07 ± 0.02 a.u.). **C** In contrast to burst frequency, amplitude of respiratory was decreased by addition of DHK to the bath solution. While $BaCl_2$ (0.77 ± 0.08 s) showed no effect compared to CTRL (0.81 ± 0.07), application of DHK significantly decreased burst duration to 0.56 ± 0.07 s.

3.2.3 Are rhythmic current fluctuations translated into astroglial calcium signaling?

Possible mechanisms to increase $[Ca^{2+}]_{in}$ involves unspecific cation conductances via ionotropic glutamate receptors (iGluR) or activation of metabotropic glutamate receptors (mGluR). Contribution of iGluR to $I_{Resp,A}$ has been ruled out by previous experiments in our lab (personal communication, Swen Hülsmann). Thus, the following experiments focussed on mGluR. Of special interest are group I mGluR, because they trigger the release of calcium from internal calcium stores via the Phospholipase C (PLC)/Inositoltriphosphat (IP_3) pathway.

Expression of group I metabotropic glutamate receptors on astrocytes of the preBötC

First, expression of group I mGluRs was tested immunohistochemically in brainstem slices containing the preBötC of TgN(hGFAP-EGFP) mice. Fig. 3.25 B shows broad labeling of mGluR1a antibody via Cy3-conjugated secondary antibodies. The merge in Fig. 3.25 C confirms co-labeling of EGFP and Cy3, indicating mGluR1a expression of preBötC astrocytes. Overall, an average of 22.1 ± 1.8 EGFP-expressing astrocytes per slice were recorded and 63.6 ± 7.1 % of them were labeled by mGluR1a antibodies ($n = 9$ slices, 5 mice).

Single-cell Ca^{2+} imaging of rhythmic astrocytes reveals no respiratory-related fluctuations of $[Ca^{2+}]_{in}$

With the expression of group I mGluR, an important prerequisite for astroglial Ca^{2+} signaling after detection of synaptic activity is fulfilled. Now it was tested with single-cell two-photon Ca^{2+} imaging, if detection of synaptic activity by rhythmic astrocytes is translated into astroglial Ca^{2+} signals.

Astrocytes expressing EGFP or mRFP were patched and filled with calcium indicators via the patch pipette. For astrocytes that showed rhythmic membrane-current fluctuations in phase with respiratory bursts, membrane currents and two-photon Ca^{2+} imaging recordings were performed in parallel. Correlation between current fluctuations and respiratory bursts could be observed (see Fig. 3.26). Obviously, there are fluctuations of $[Ca^{2+}]_{in}$, but there is no correlation between these changes and respiratory bursts. To exclude that fluctuations of $[Ca^{2+}]_{in}$ were masked by noise, cycle-triggered averaging was also performed with the Ca^{2+}-imaging data (Fig. 3.26). While averaged $I_{Resp,A}$ showed an increased signal-to-noise ratio and was easy to detect, the corresponding averaged Ca^{2+} signal of the cell soma showed no fluctuation that was in phase with respiratory bursts. This was also true for dendritic compartments. Next, we increased the number of neurons contributing to respiratory activity and therefore the amount of released glutamate. This

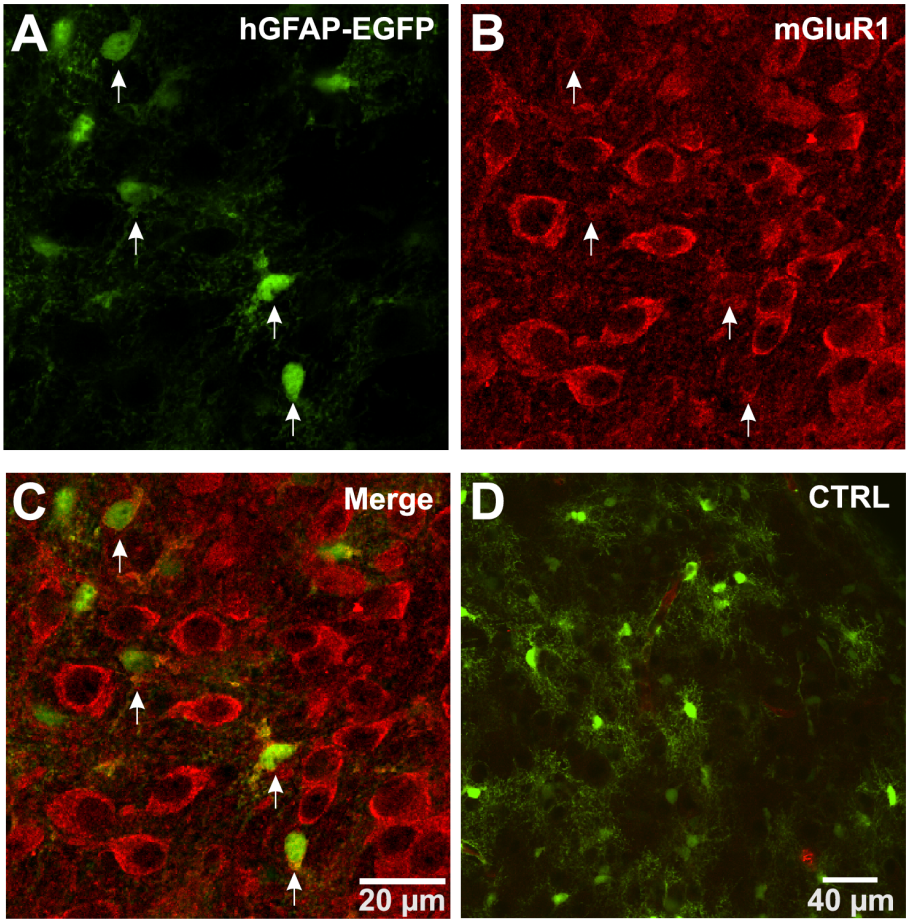

Fig. 3.25: **Astroglial expression of group I mGluR on preBötC astrocytes.** **A** Confocal images of a 50 µm slice from a P5 TgN(hGFAP-EGFP) mouse with EGFP-expressing astrocytes. **B** Immunohistochemical staining with an antibody against mGluR1a is detected via a Cy3-conjugated secondary antibody (red). Several cells are labeled. **C** Merge of (A) and (B) shows co-localisation of mGluR antibody EGFP-expressing astrocytes (arrows), although labeling on non-EGFP cells appears to be stronger. **D** Negative CTRL was performed with the same protocol but without the primary antibody.

was done by blocking synaptic inhibition via application of bicuculline and strychnine to the bath solution. However, even under conditions of increased respiratory network activity, no calcium signal was observed that was correlated to respiratory bursts.

Since at physiological conditions no respiratory-related astroglial Ca^{2+} signals were observed, it was tested if astrocytes show fluctuations of $[Ca^{2+}]_{in}$ after strong stimulation that could be detected using two-photon excitation.

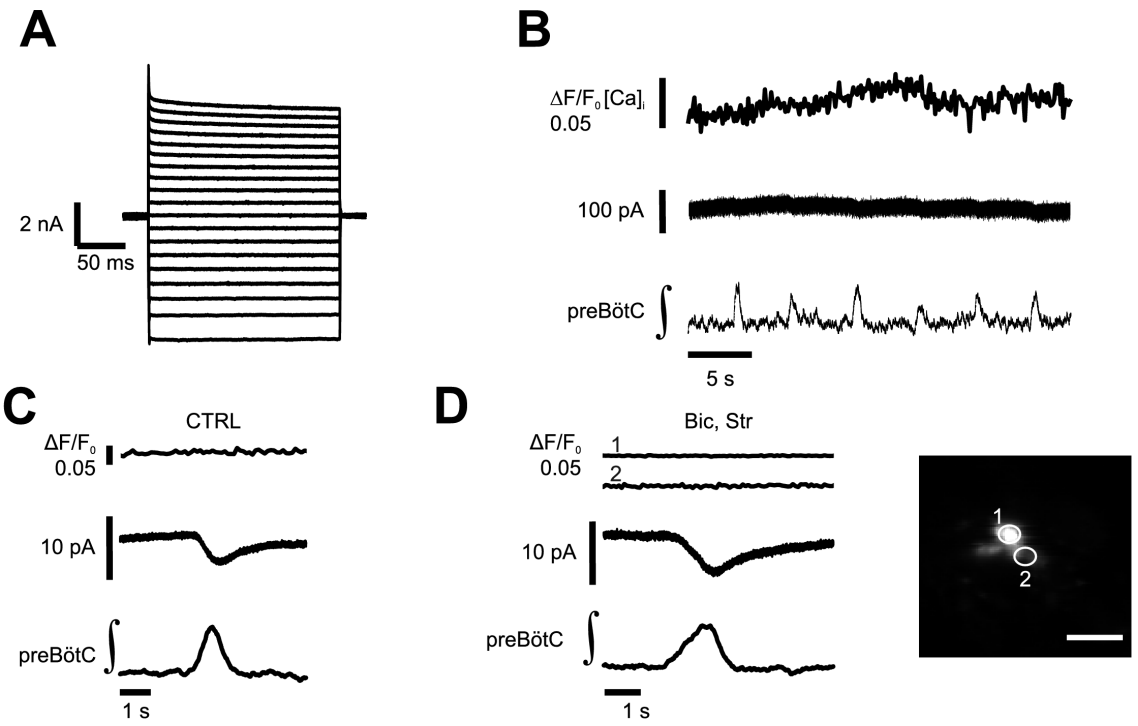

Fig. 3.26: **Single-cell Ca^{2+} imaging of a rhythmic astrocyte revealed no rhythmic Ca^{2+} signal.**
A Current responses of the patched astrocyte to a voltage-step protocol. **B** Lower trace: Integrated field potential recording of the preBötC showing six respiratory bursts. Middle trace: Although very small and almost masked by noise, membrane current fluctuations coincide with respiratory bursts. Upper trace: Ca^{2+} signals of the patched astrocyte. The astrocyte was filled with Calcium Orange via the patch pipette. **C** Cycle-triggerd averaged signals of the same cell. Increased signal-to-noise ratio reveals $I_{Resp,A}$ (middle trace), but no rhyhtmic fluctuation of $[Ca^{2+}]_{in}$ can be detected. **D** After increasing the activity of the respiratory network by application of strychnine (10 µM) and bicuculline (10 µM), $I_{Resp,A}$ is increased (middle trace), but fluctuations of $[Ca^{2+}]_{in}$ coinciding with respiratory bursts were not detected in the cytosol (trace 1) nor in the processes (trace 2).

Electrical stimulation of the respiratory network induced rhythmic astroglial Ca^{2+} transients

250 µm slices of TgN(hGFAP-mRFP) or TgN(hGFAP-EGFP) mice were loaded with calcium indicator dyes and responses to stimulation were recorded using two-photon excitation microscopy. Strong electrical stimulation was performed by placing a patch electrode filled with ACSF on the slice surface at the border of the preBötC. Trains of pulses were applied every 20 s (100 Hz, 200 µs pulse duration) to simulate strong rhythmic neuronal activity. Of the three mRFP-expressing astrocytes shown in green in Fig. 3.27 B, cell

3 shows small Ca^{2+} fluctuations after electrical stimulation, that are hardly exceeding noise. Cells 4 and 5, not expressing mRFP, are presumably neurons and show a strong Ca^{2+} response to electrical stimulation. While there was still no Ca^{2+} response visible in astrocytes 1 and 2 after cycle-triggered averaging, astrocyte 3 and cells 4 and 5 showed a Ca^{2+} signal (Fig. 3.27).

In another recording, astroglial Ca^{2+} transients triggered by electrical stimulation were much stronger, even stronger than the Ca^{2+} transients recorded from neurons (Figure 3.28). Overall, electrical stimulation triggered Ca^{2+} signals in 27 of 272 astrocytes (9.9 %).

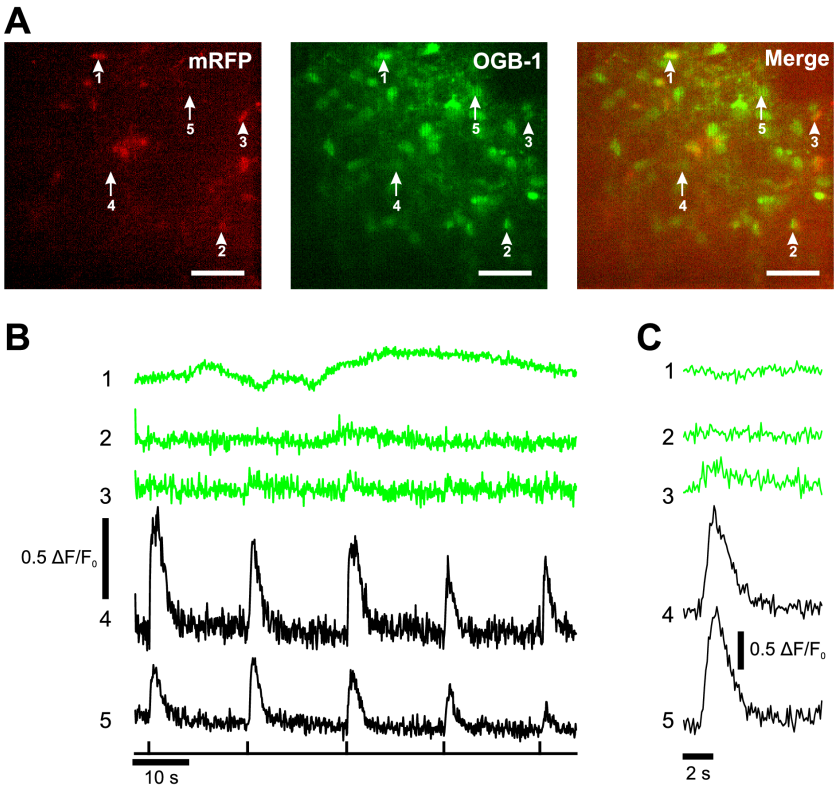

Fig. 3.27: **Strong electrical stimulation of the preBötC area triggered small Ca^{2+} transients in some astrocytes.**
A Left image: Two-photon image of mRFP-expressing astrocytes. Middle image: OGB-1 labeling. Right image: Merge of mRFP and OGB-1 fluorescence. Cells 1-3 labeled as OGB-1 filled astrocytes in yellow (labeled with arrowheads) and cells 4 and 5 as non-astrocytic cells (labeled with arrows). **B** Ca^{2+}-imaging traces of the cells labeled in (A). While astrocytes 1 and 2 show no response to electrical stimulation, cell 3 shows small responses, and non-astrocytic cells 4 and 5 show large responses upon stimulation. Points of stimulation are indicated by vertical bars at the bottom line. **C** Averaged signals of (B) confirm stimulation-triggered Ca^{2+} signals in astrocyte 3 and non-astroglial cells 4 and 5. For astrocytes 1 and 2, averging also does not reveal stimulation-triggered Ca^{2+} signals.

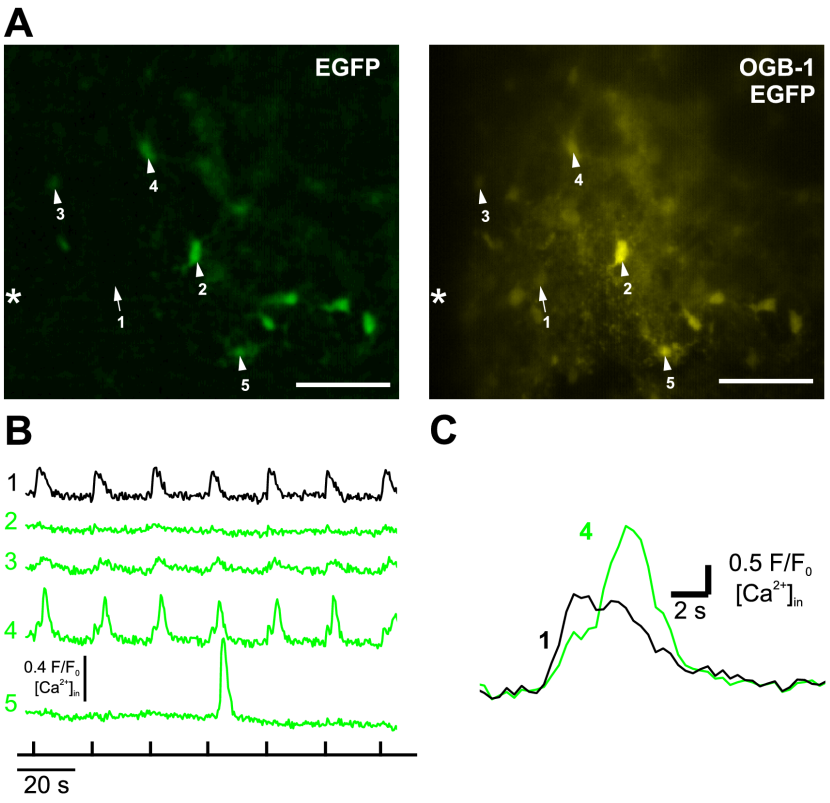

Fig. 3.28: **Strong electrical stimulation of the preBötC area triggered large Ca^{2+} transients in some astrocytes.**
A Left image: Two-photon image of EGFP-expressing astrocytes. Right image: OGB-1 labeling. Cell 1 (white arrow) is labeled with OGB-1 but shows no expression of EGFP. Cells 2-5 are EGFP-expressing astrocytes filled with OGB-1. **B** Ca^{2+}-imaging traces of the cells labeled in (A). While cell 1 (presumably a neuron) and cells 3 and 4 show a strong response to electrical stimulation, cell 2 shows only a small response and cell 5 no response at all upon stimulation. Points of stimulation are indicated by vertical bars at the bottom. **C** Averaged signals of (B) show stimulation-triggered Ca^{2+} signals in astrocyte 4 and non-astroglial cell 1.

Selective blockade of glial glutamate uptake

In the next set of experiments, the effect of TFB-TBOA on astoglial $[Ca^{2+}]_{in}$ was tested. TFB-TBOA is a blocker of glutamate transporters with a significantly higher affinity to the glial glutamate transporters compared to the transporters expressed in neurons (Shimamoto *et al.* (2004)). Since a complete blockade of astroglial glutamate uptake might cause spillover of synaptically released glutamate and therefore activate extrasynaptic receptors, it was hypothesized that astrogial Ca^{2+} signals might occur in this condition. As seen in Fig. 3.29 C, TFB-TBOA application caused an initial baseline increase of the inte-

grated field potential recording and the bursts became smaller and more irregular. Finally, integrated field potential reached a maximum and activity of the respiratory network was completely blocked. This was true for three experiments, while respiratory activity in the remaining two experiments slowly decreased. On average, integrated baseline of the respiratory activity started to increase after 197 ± 32 s and respiratory activity was blocked 320 ± 47 s after TFB-TBOA application. Astroglial Ca^{2+} oscillations always occured after the baseline of the integrated field potential started to increase (38 ± 10 s later, $n = 23$ astrocytes) and before respiratory activity was completely blocked. These oscillations were observed in 89.3 ± 6.6 % of fluorescently labeled astrocytes per slice ($n = 5$ slices, 23 astrocytes). Fig. 3.29 D shows a magnification of the field-potential recording and the Ca^{2+} signals of astrocyte 5 to show that astroglial Ca^{2+} signals and respiratory bursts are not correlated.

In one out of five experiments, respiratory bursts were observed again 19 min after washout of TFB-TBOA was started. In the remaining four experiments, respiratory activity was recorded between 12 and 22 min after washout of TFB-TBOA without respiratory activity being restored.

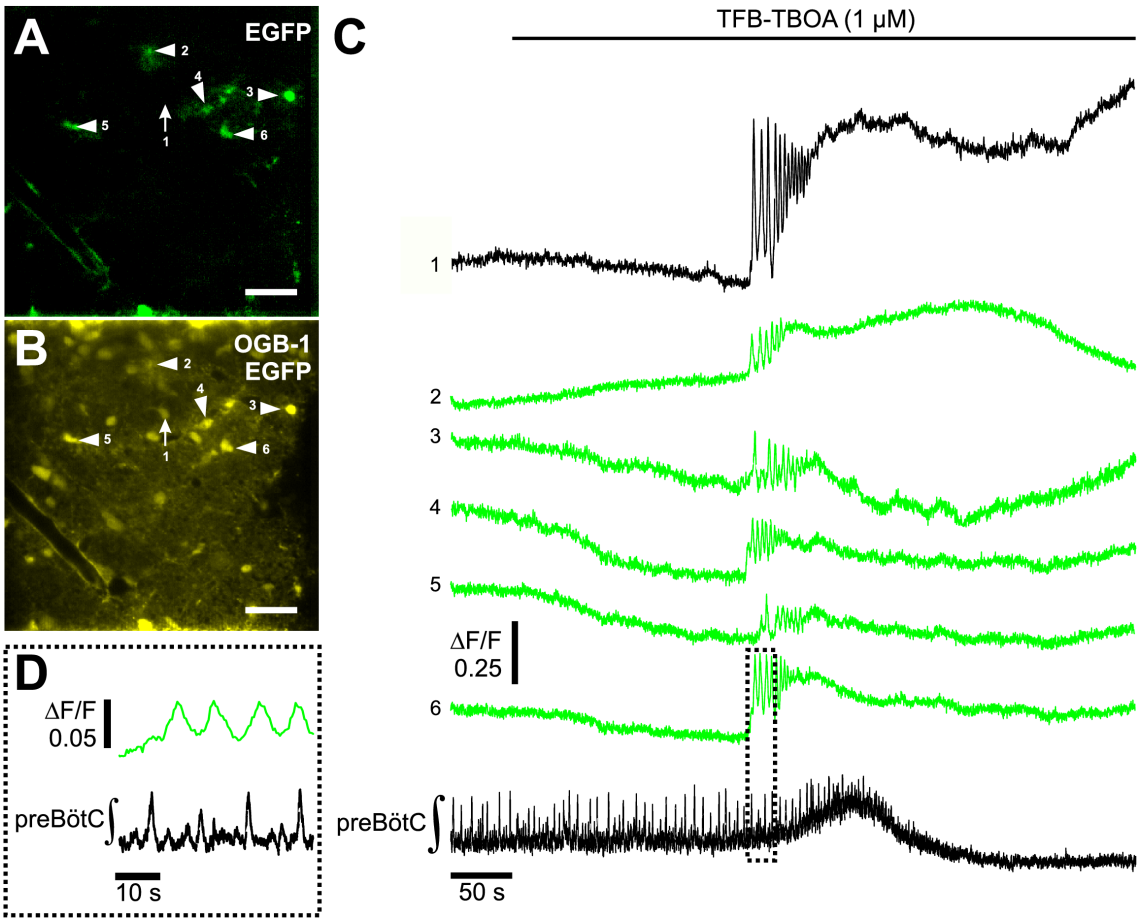

Fig. 3.29: **Blockade of glial glutamate uptake with TFB-TBOA induced astroglial Ca^{2+} oscillations and respiratory network failure.**
A EGFP-expressing astrocytes in a rhythmic slice. Scale bar: 40 µm. **B** The same slice as in (A), OGB-1 and EGFP fluorescence. Scale bar: 40 µm. **C** Ca^{2+}-imaging traces (green) of the astrocytes labeled in (A) and (B). The lower trace in black shows the recording of the integrated field potential of the preBötC. 50 s after start of the recording, TFB-TBOA (1 µM) was added to the bath solution and baseline field potential started to increase with bursts get smaller and less regular. After reaching its maximum, baseline decreases and activity of the respiratory network is completely blocked. In parallel with the increase of the baseline, OGB-1 filled astrocytes showed Ca^{2+} oscillations. **D** Extract of the box from (C) shows that astroglial Ca^{2+} oscillations (upper trace in green) were no correlated to respiratory bursts (lower trace in black).

To test for the involvement of group I mGluR in the astroglial Ca^{2+} oscillations described above, the same experiments were performed in the presence of group I mGluR-blocker CPCCOEt (200 µM). After an incubation of at least 13 min, TFB-TBOA was additionally applied to test for the involvement of mGluR in astroglial Ca^{2+} signaling. In summary of all five independent experiments performed, baseline increase started 319 ± 16 s after

addition of TFB-TBOA (n.s. compared to CTRL without CPCCOEt; Mann-Whitney Rank Sum Test; $n = 5$) and a complete blockade of respiratory network activity was observed at 458 ± 28 s, which was signficantly later compared to TFB-TBOA application without CPCCOEt ($p < 0.05$; Mann-Whitney Rank Sum Test; $n = 5$). Another major effect caused by CPCCOEt was the blockade of TFB-TBOA triggered Ca^{2+} oscillations. While in one experiment, Ca^{2+} oscillations were observed in 90.9 % of astrocytes, in the remaining four experiments, no astroglial Ca^{2+} oscillations were detectable. However, in the experiment shown in Fig. 3.30 C, astrocyte 2 showed a Ca^{2+} transient without oscillatory behaviour. On average, 24.9 ± 17.7 % of astrocytes showed Ca^{2+} oscillations after TFB-TBOA application in presence of CPCCOEt, which is signficantly lower compared to CTRL without CPCCOEt ($p < 0.05$; t-test; $n = 5$). Recovery of respiratory activity was observed more often compared to TFB-TBOA experiments without CPCCOEt. Only in one experiment, respiratory activity did not recover after TFB-TBOA washout within 13.8 min. In the other four experiments, burst activity was restored 12.4 min after washing out TFB-TBOA. Although CPCCOEt did not prevent blockade of respiratory network activity, network failure occured signficantly later and recovery was significantly supported by CPCCOEt.

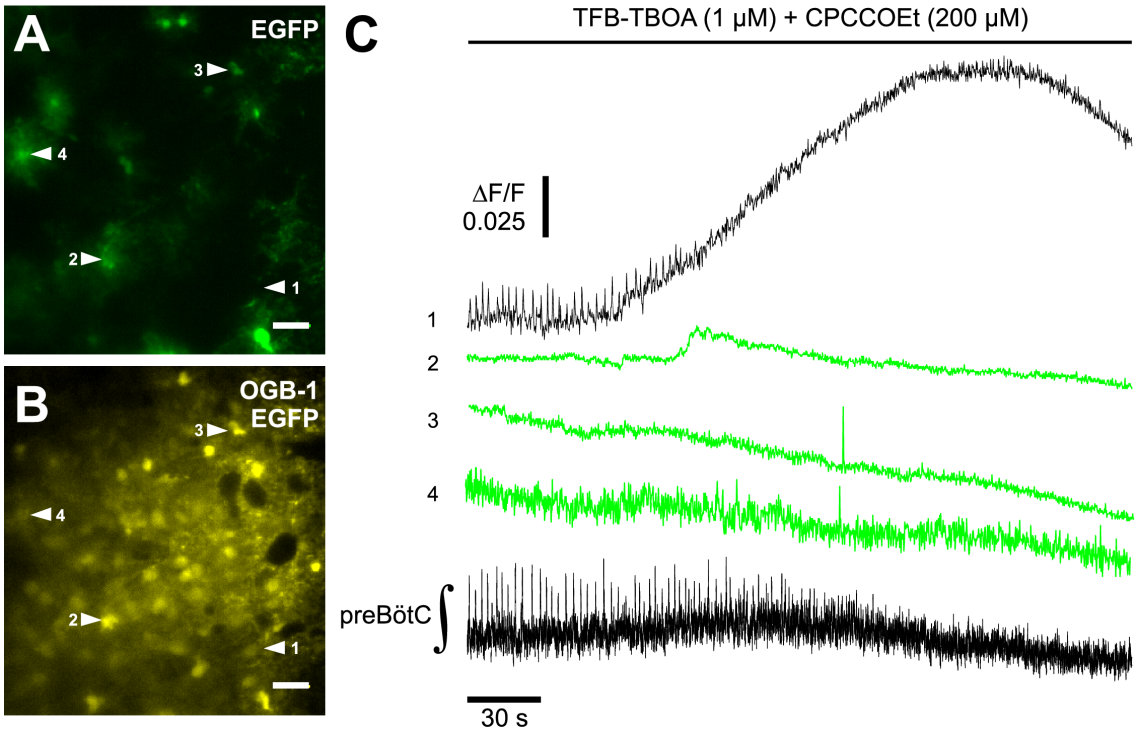

Fig. 3.30: **TFB-TBOA triggered Ca^{2+} signals were blocked by group I mGluR antagonist CPCCOEt**
A EGFP-expressing astrocytes in a rhythmic slice recorded with 900 nm excitation and 475/50 nm bandpass emission filter. Scale bar: 40 µm. **B** The same slice as in (A), but with 800 excitation and 531/40 nm bandpass emission to filter to detect OGB-1 and EGFP fluorescence. Scale bar: 40 µm. **C** Upper trace in black shows the Ca^{2+} trace of a respiratory neuron with Ca^{2+} peaks correlated to respiratory bursts. The green traces (2-4) show Ca^{2+} signals of the respective astrocytes from (A) and (B). Before application of TFB-TBOA, this slice was preincubated for 15 min in CPCCOEt (200 µM) to block group I mGluR. In the presence of CPCCOEt, TFB-TBOA no longer elicits Ca^{2+} oscillations in astrocytes. Only astrocyte 2 shows a small increase of $[Ca^{2+}]_{in}$, but without oscillations seen in Fig. 3.29.

Is increased inhibition the cause for respiratory network failure after blockade of glial glutamate transporters?

Lee *et al.* (2010) reported tonic GABA release from astroglial cells via an anion channel. To test if astroglial release of GABA or glycine is the reason for the failure of the respiratory network, bicuculline or strychnine was added before TFB-TBOA application. In two preliminary experiments with bicuculline and three experiments with strychnine, network failure was not prevented. This indicates that network failure is not due to increased GABA or glycine-mediated inhibition.

It was shown in this chapter that astrocytes indeed detect activity of respiratory neurons in the preBötC by rhythmic fluctuations of the membrane current. However, under physiological conditions, these fluctuations are not translated into changes of $[Ca^{2+}]_{in}$, indicating that preBötC astrocytes do not modulate respiratory activity by release of gliotransmitters in a Ca^{2+}-dependent manner. Under conditions of strong electrical stimulation, $[Ca^{2+}]_{in}$ was increased, proving that astrocytes are able to show activity-correlated Ca^{2+} signals. This is in line with the results that indicate that blockade of glial glutamate uptake elicits mGluR-mediated calcium signals in astrocytes.

4 Discussion

4.1 Identification of astrocytes

4.1.1 Identification of astrocytes via SR101 labeling

Sulforhodamine 101 (SR101) was orignally used as a marker for neuronal activity, since it was supposed to be taken up via endocytosis of synaptically activated neurons (Lichtman *et al.*, 1985; Anderson, 2001). Therefore it was quite suprising, when Nimmerjahn *et al.* (2004) showed that SR101 is a selective marker for astrocytes in the *in vivo* cortex of rodents. The use of animals expressing EGFP or mRFP in astrocytes is not always possible and has its own drawbacks, such as overlap of EGFP fluorescence with Ca^{2+} indicator fluorescence. Another drawback is the need for time-consuming crossbreeding, if the focus is on astrocytes in mouse models for diseases. Therefore, the SR101-staining protocol published by Langer & Rose (2009) was used here to stain astrocytes in the brainstem. But in contrast to the studies in the hippocampus and neocortex, SR101 labeled brainstem astrocytes only very weak and not sufficient for reliable identification (Fig. 3.1). The fraction of SR101+ EGFP-expressing astrocytes did not differ between hippocampus and brainstem, but the SR101 fluorescence intensity was significantly lower in the brainstem compared to the hippocampus (Fig. 3.2). In both regions, SR101 labeled cells that did not express EGFP. In the hippocampus, these cells had a similar shape to EGFP-expressing astrocytes. In contrast, SR101+ cells in the brainstem that were not labeled by EGFP, had often a large soma and did not resemble astrocytes.

In conclusion, SR101 was not suitable for reliable identification of astrocytes in the brainstem.

It was already hypothesized by Nimmerjahn *et al.* (2004), that SR101 staining may differ between various brain regions, since in the retina exclusively oligodendrocytes were labeled by SR101 (Ehinger *et al.*, 1994). Notably, SR101 staining in the retina took much more time (12-16 h) compared to SR101 staining in the hippocampus. In our hands, two-photon time-lapse imaging of SR101 uptake revealed the first SR101-labeled astrocytes already after 2 min of incubation in SR101.

We decided to elucidate the cause of the heterogeneity of SR101 labeling in the hippocampus and the brainstem, since it might help to identify the reasons for other differ-

ences between hippocampal and brainstem astrocytes (for example frequent spontaneous Ca^{2+} oscillations (see next section) or Ca^{2+} waves (Haas *et al.*, 2006), both in hippocampal astrocytes).

The differences of SR101 labeling in the brainstem and the hippocampus could be caused by two principal components: Either brainstem astrocytes do not take up SR101 or the dye is rapidly removed after uptake. The presented results do not completely answer the question of the underlying differences, but they give hints to the cause of the differences in SR101 labeling.

Possible uptake mechanisms of SR101

Different mechanisms were suggested to be responsible for the uptake of SR101 into cells. Initially, SR101 was used to label active nerve terminals because it was selectively taken up via endocytosis by the nerve terminals of stimulated axons (Lichtman *et al.*, 1985; Teng *et al.*, 1999). In contrast, because of the rapid uptake and homogenous cytoplasmic staining of neocortical astrocytes, a transporter system for the dye uptake was suggested by Nimmerjahn *et al.* (2004). Since it was reported that Carbenoxolone (CBX) inhibited staining of SR101 in the neocortex (Nimmerjahn *et al.*, 2004), we tested the effect of CBX in the hippocampus. We confirmed blockade of SR101 staining in hippocampal astrocytes when CBX was present during SR101 incubation (Fig. 3.3). CBX-sensitive Pannexin1 (Panx1) hemichannels have been shown to be expressed by astrocytes (Bruzzone *et al.*, 2003; Huang *et al.*, 2007) and are not blocked by $[Ca^{2+}]_{ex}$, but their expression on brainstem astrocytes was not tested yet. We performed immunohistochemical detection of Panx1 expression in brainstem and hippocampal astrocytes and did not reveal significant differences in Panx1 expression between brainstem and hippocampus (Fig. 3.4). Furthermore, pharmacological blockade of Panx1 with Mefloquine (MFQ, 0.1-1.0 µM) did not affect SR101 labeling, neither in the hippocampus nor in the brainstem (Fig. 3.5). Since the MFQ diastereomer used here (QU024 from Bioblocks) has been shown to reduce currents via Panx1 (Iglesias *et al.*, 2009) to less than 30 %, a significant change of SR101 would have been expected, if Panx1 hemichannels account for SR101 influx into or removal from hippocampal astrocytes.

Astroglial expression of gap junction proteins, especially Connexin 30 (Cx30) and Connexin (Cx43), has been shown for many brain regions. (for review see Nagy & Rash, 2000). SR101 has a molecular size of approximately 0.6 kDa. Thus, it should easily pass gap junctions. Connexin proteins are not only present as gap junction proteins, but can also occur as unpaired hemichannels, connecting the cytosol with the extracellular medium. Since functional hemichannel opening was shown for cultured astrocytes (Ye *et al.*, 2003) and gap junction hemichannels are also blocked by CBX (Ye *et al.*, 2003), it was tested here,

if different opening states of these hemichannels do account for the SR101-labeling differences. To open hemichannels, $[Ca^{2+}]_{ex}$ and $[Mg^{2+}]_{ex}$ are removed from the bath solution (Ye *et al.*, 2003). When the SR101-staining protocol was applied in DCFS, SR101 labeling of EGFP-expressing astrocytes was not improved (Fig. 3.6). Moreover, SR101 intensity tended to be lower in hippocampal astrocytes, reflecting maybe leak-out of SR101 from the astrocytes via open hemichannels. However, addition of CBX to the washout solution did not rescue SR101 intensity, probably because hemichannels are already closed in regular ACSF by extracellular Ca^{2+} and Mg^{2+} (Fig. 3.7).

The results presented here do not point to SR101 uptake via gap junction or pannexin hemichannels, but rather to an active uptake mechanism, because of three reasons: (i) Panx1 hemichannels are expressed to a similar degree in the hippocampus and the brainstem and pharmacological blockade did not affect the SR101 labeling. (ii) Opening of hemichannels in the brainstem with DCFS did not improve SR101 labeling. (iii) Opening of gap junction hemichannels in the hippocampus tended to reduce SR101 intensity. Further experiments, e.g. comparison of astroglial expression of connexins and staining experiments with Lucifer Yellow, are required to provide further insights into functional hemichannel expression in brainstem and hippocampal astrocytes. However, passive diffusion of SR101 via gap junction or Panx1 hemichannels into cells seems rather unlikely, since SR101 fluorescence in the cells is brighter than the fluorescence of the extracelluar medium. The mechanism of active SR101 in hippocampal astrocytes remains unclear. Endocytotic, activity dependent uptake is rather improbable (Lichtman *et al.*, 1985; Teng *et al.*, 1999), since we did not observe vesicle-like structures filled with SR101 during two-photon time-lapse staining. Ischemia-induced SR101 fluxes via open Panx1 hemichannels (Thompson *et al.*, 2006) also seems to be unlikely, since blockade of Panx1 with MFQ did not change the SR101 labeling, neither in the brainstem (excluding SR101 efflux via open hemichannels) nor in the hippocampus (excluding SR101 influx via open hemichannels). In some slices, superficial neurons of the pyramidal cell layer were also filled with SR101, probably due to the effect described by Thompson *et al.* (2006).

Altogether, these results lead to the conclusion, that the higher SR101 uptake of hippocampal astrocytes might be caused by active transport of SR101 into hippocampal astrocytes.

MRP1 is not involved in removal of SR101 from brainstem astrocytes

Two-photon time-lapse imaging of SR101 staining revealed, that the decay of SR101 fluorescence intensity after removal of SR101 is quite fast in neurons and brainstem astrocytes compared to hippocampal astrocytes (Figs. 3.8, 3.9). Passive diffusion via open hemichannels has been ruled out to account for the SR101-labeling differences. Possible candidates

for active remove of xenobiotics from cells are ATP-binding cassette (ABC) transporters. Inhibitors of these transporters have been used to improve dye-loading of neurons in brain tissue (Manzini *et al.*, 2008). SR101 was shown to be a subtrate for the ABC transporter subtypes MRP1 (Gong *et al.*, 2003) and MRP2 (Miller *et al.*, 2000). Of these two, only mRNA for MRP1 has been found in mouse brain astrocytes (Hirrlinger *et al.*, 2005a), therefore MK-571 was used to inhibit MRP1-mediated drug remove.
When applied in the brainstem, there was no increase of astroglial SR101 staining when incubated with MK-571 (50-200 µM, Fig. 3.10). Contrary, non-EGFP-expressing cells were stronger labeled with SR101, similar to the timepoint of maximum SR101 labeling from the two-photon time-lapse imaging experiments. It appears that MRP1 transporters account for removal of SR101 from non-EGFP-expressing cells, but not in brainstem astrocytes.
In the hippocampus, neuronal cells in the pyramidal cell layer were often filled with SR101 when staining was performed in presence of MK-571. Even more interesting, astroglial SR101 labeling was very weak and hard to discriminate from the background, when SR101 staining was performed with MK-571 in the bath solution (Fig. 3.11). Thus, MK-571 (i) decreased astroglial SR101 uptake and (ii) increased background fluorescence maybe due to neuronal uptake of SR101. When MK-571 was only applied during washout, three effects were observed: (i) astroglial SR101 fluorescence was not obviously decreased, (ii) neuronal staining was still more often observed and (iii) background fluorescence was higher compared to CTRL stainings without MK-571.
In conclusion, MK-571 increased neuronal staining in the hippocampus and the brainstem, suggesting export of intracellular SR101 after removal of SR101 from the bath. In contrast, MK-571 did not improve SR101 labeling of astrocytes in the brainstem, indicating that MRP1 transporters do not account for removal of SR101 from brainstem astrocytes. In the hippocampus, almost no astroglial SR101 labeling was observed anymore after staining in presence of MK-571. Since MRP1 transporters are only reported to account for transport out of cells and not into cells, the most likely explanation is, that MK-571 affects another uptake mechanism. Possible candidates for this are Na^+ dependent transporters of the SLC13 family (for review see Pajor, 2006). Members of this family have been reported to be expressed in the brain (Inoue *et al.*, 2002), but astroglial expression has not been investigated until now.

Altogether, the results presented here, show that SR101 is not applicable for reliable identification of astrocytes in the brainstem. Passive diffusion via hemichannels plays no role for the strong SR101 uptake in hippocampal astrocytes. A not yet identified, MK-571-sensitive transporter is more likely to explain the differences in SR101 labeling. Non-EGFP-expressing cells were also initially labeled by SR101, but SR101 was removed

from these cells via a MK-571-sensitive transporter, which is likely the ABC-transporter MRP1.

Meanwhile, a major drawback of labeling astrocytes with SR101 was discovered. It was reported, that SR101 affects also neurons via induction of long-term potentiation of intrinsic excitability and synaptic efficacy. Kang *et al.* (2010) even suggested to use SR101 for the induction of epileptic seizures. This does not completely rule out the use of SR101, since it can be applied after the experiment for cell identification, but this study reveals the limitation of SR101 application for identification of astrocytes.

4.1.2 Astroglia specific calcium signals in low-K^+ solution

Identification of astrocytes via low-K^+ induced Ca^{2+} oscillations (low-K^+ method) makes use of Ca^{2+} oscillations that occur selectively in astrocytes after lowering $[K^+]_{ex}$ (Dallwig *et al.*, 2000; Härtel *et al.*, 2007). It is already known, that Ca^{2+} entry from the extracellular space is necessary for the Ca^{2+} oscillations, since depletion of intracellular Ca^{2+} stores do not block low K^+-induced Ca^{2+} oscillations. Furthermore, Ca^{2+}-channel blockers do not reduce the Ca^{2+} oscillations (Dallwig *et al.*, 2000). However, the source of Ca^{2+} might be other channels, e.g. Kir4.1 channels. Currently, it is thought that Kir4.1 channels lose their selectivity for K^+ and become permeable for divalent cations such as Ca^{2+} (Dallwig *et al.*, 2000; Härtel *et al.*, 2007). However, it was not ruled out, that the proposed anomalous gating occurs for Na^+ instead of Ca^{2+}.

Here, it was tested for a different mechanism that involves Na^+/Ca^{2+} exchangers (NCX). NCX expresssion was reported for astrocytes in culture (Goldman *et al.*, 1994) or in hippocampus and cortex (Minelli *et al.*, 2007). In physiological conditions, NCX operates using the Na^+ gradient across the membrane to remove intracellular Ca^{2+} (for review see Blaustein & Lederer, 1999). In conditions of low $[K^+]_{ex}$, Kir4.1 channels might become permeabel for Na^+ (such anomalous gating was reported for the K^+ channel Kv2.1 Korn & Ikeda, 1995), although the permeability for Na^+ versus K^+ is around 1:1000 under normal conditions (for review see Choe, 2002). Subsequent increase of $[Na^+]_{in}$ reverses the operating modus of the NCX. Thus, Ca^{2+} is transported into the cell and Na^+ is removed from the cell (Fig. 4.1). A similar mechanism of NCX action has been described in microglia (Newell *et al.*, 2007).

From the results presented in this study, there is no hint for contribution of reversed mode action of NCX to the low-K^+ induced Ca^{2+} oscillations in astrocytes. Both NCX blockers tested here, SN-6 and KB-R7943, did not reduce the fraction of astrocytes with Ca^{2+} oscillations in low-K^+ solution (Fig. 3.12). Another test of this hypothesis would be to peform Na^+ imaging with SBFI, a fluorescent Na^+ dye, that was reported to indicate increase of $[Na^+]_{in}$, followed by reversed mode action of the NCX (Newell *et al.*, 2007).

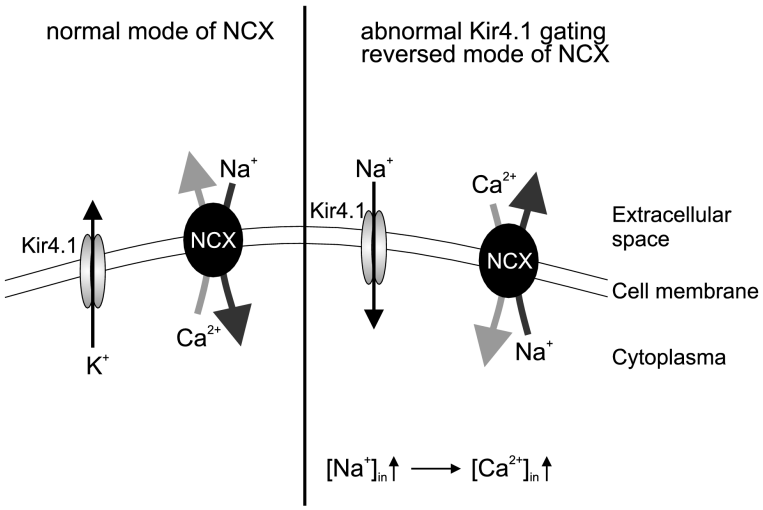

Fig. 4.1: **Hypothesized mechanism of low-K^+-induced Ca^{2+} oscillations via reversed-mode action of NCX.**
In regular $[K^+]_{ex}$, Kir4.1 is permeable for K^+ and NCX works in normal mode (left side). In conditions of decreased $[K^+]_{ex}$, abnormal gating of Kir4.1 was suggested. Kir4.1 becomes permeable for Na^+, which causes an increase of $[Na^+]_{in}$. Since NCX use the Na^+ gradient across the membrane, they operate in reversed mode, when $[Na^+]_{in}$ increases. Then, instead of being removed from the cell, Ca^{2+} is transported into the cell. This transport would reflect the low-K^+-induced Ca^{2+} oscillations observed in astrocytes.

But from the results presented here, it appears unlikely that the major effect of anomalous gating of Kir4.1 is Na^+ dependent.

Spontaneous Ca^{2+} transients in hippocampal astrocytes are not inhibited by higher temperatures

The high frequency and amplitude of spontaneous Ca^{2+} transients in hippocampal astrocytes were in strong contrast to the observations made in the brainstem. Spontaneous Ca^{2+} transients in brainstem astrocytes occur very infrequently and do not interfere with identification of low-K^+ induced Ca^{2+} oscillations. Occurence of spontaneous Ca^{2+} oscillations was also reported for cortical astrocytes of mice. Frequency and duration of cortical Ca^{2+} oscillations were higher at room temperature compared to 37 °C (Schipke *et al.*, 2008a). Our experiments are usually carried out at 30 °C and increase of the temperature to 37 °C did not reduce the frequency of the spontaneous Ca^{2+} oscillations. Nieden & Deitmer (2006) reported spontaneous Ca^{2+} oscillations in acute slice preparations from rat hippocampus. The authors did not report the temperature at which recordings were performed, but they were able to block spontaneous Ca^{2+} oscillations by application of mGluR blockers. Both studies showed, that Ca^{2+} from intracellular stores is necessary for

the spontaneous Ca^{2+} oscillations (Nieden & Deitmer, 2006; Schipke *et al.*, 2008a). Since our experiment ruled out that the Ca^{2+} oscillations are caused by temperatures below 37 °C, it is likely, that astroglial mGluR do account for the observed spontaneous Ca^{2+} oscillations. Although brainstem astrocytes also express mGluR, we only rarely observe spontaneous Ca^{2+} oscillations. This indicates, that extracellular glutamate levels are lower in the brainstem or that glutamate in the brainstem does not escape the synapse because it is rapidly taken up by glutamate transporters.

4.2 Respiratory-related signals of astrocytes in the respiratory network

In the second part of this thesis it was investigated, if astrocytes in the preBötC detect the rhythmic bursting activity of respiratory neurons. Furthermore it was tested, if this activity is translated into astroglial Ca^{2+} signals. This would provide a mechanism for astroglial modulation of respiratory activity, since most mechanisms of astrocyte-to-neuron communication involve astroglial Ca^{2+} signals.

4.2.1 Composition of $I_{Resp,A}$

Elevations of extracellular K^+ contribute to $I_{Resp,A}$

Since rhythmic bursting activity of respiratory neurons causes changes of $[K^+]_{ex}$ (Brockhaus *et al.*, 1993) and astrocytes in the preBötC show large K^+ conductances (Grass *et al.*, 2004), it is likely that the respiratory-related current fluctuations that were observed in approximately 10 % of the patched astrocytes are due to shifts of $[K^+]_{ex}$ (Fig. 3.15). Between respiratory bursts, the astroglial membrane potential is close to the electrochemical equlibrium potential of $[K^+]$ (E_K) across the membrane. In our experiments, E_K at rest was -72 mV (assuming $[K^+]_{in} = 125$ mM, $[K^+]_{ex} = 8$ mM, and T = 30 °C). During respiratory bursts, $[K^+]_{ex}$ has been reported to increase only between 0.1 mM (Richter *et al.*, 1978) and 0.6 mM (Brockhaus *et al.*, 1993), the latter would change E_K to -70 mV. This shift can be recorded as an inward current (Fig. 3.19, Somjen *et al.*, 2008). Since the membrane potential of preBötC astrocytes is largely determined by the weakly inward rectifying K^+ channel Kir4.1 (Neusch *et al.*, 2006), astroglial Kir4.1 channels (the major K^+ conductance) were blocked with $BaCl_2$. According to Ohm's law, the increase of the membrane resistance by $BaCl_2$ application (Neusch *et al.*, 2006) resulted in reduced amplitudes of the astrocytic respiratory-related current $I_{Resp,A}$.

The effect of $BaCl_2$ on the respiratory network was tested by analysis of frequency, amplitude, and duration of respiratory bursts. The only parameter significantly changed

by $BaCl_2$ was the frequency of respiratory bursts (Fig. 3.20). This is in contrast to published data obtained from Kir4.1$^{-/-}$ mice (Neusch *et al.*, 2006). The authors of that study found no significant increase of respiratory burst frequency in Kir4.1$^{-/-}$ mice compared to wildtype mice. This discrepancy might be explained by compensatory effects in Kir4.1$^{-/-}$ mutant mice. Another reason for this difference could be, that $BaCl_2$ is a non-selective blocker for Kir4.1 channels (for example see Töpert *et al.*, 1998). Because Ba^{2+} at 100 µM is selective for Kir channels (Kettenmann & Ransom, 2005) and Kir4.1 channels represent the major K^+ conductance of preBötC astrocytes (Neusch *et al.*, 2006), it is likely that major parts of the K^+ conductance are due to astroglial expression of Kir4.1 channels.

Glial glutamate-transporter currents contribute to $I_{Resp,A}$

Astrocytes express two glutamate transporter types to remove released glutamate from the extracellular space: GLAST and GLT-1. Expression of both transporters on preBötC astrocytes has been shown previously (Grass *et al.*, 2004). We applied the GLT-1 blocker dihydrokainate (DHK) to test if glutamate uptake currents contribute to $I_{Resp,A}$. Glutamate is transported into cells together with three Na^+ and one H^+ against one K^+. This results in a net uptake of two positive charges and can be measured as an inward current (Levy *et al.*, 1998). Indeed, blocking of GLT-1 with DHK in presence of $BaCl_2$, significantly reduced $I_{Resp,A}$ (Fig. 3.22).

By analysis of burst frequency, amplitude, and duration, it was tested for DHK effects on the respiratory network. Burst amplitude was not significantly changed, but burst frequency was increased (Fig. 3.24, see also Greer *et al.*, 1991; Funk *et al.*, 1993) and duration was decreased. One can assume, that the amount of released neurotransmitter during a burst is best reflected by the amplitude and duration of the respiratory bursts, since changes of burst frequency would only affect basal level. Furthermore, the DHK-induced reduction of burst duration is about 69 % of $BaCl_2$, while $I_{Resp,A}$ was reduced to approximately 20 %. Therefore the reduction of the burst duration alone is not sufficient to explain the reduction of $I_{Resp,A}$. Since glutamate uptake via GLT-1 is dependent on the electrochemical gradients of K^+ and Na^+ across the cell membrane, the contribution of GLT-1-mediated currents to $I_{Resp,A}$ might even be underestimated in these experiments. By blocking the Kir channels with $BaCl_2$, basal level of $[K^+]_{ex}$ is increased (Neusch *et al.*, 2006), E_K is smaller and thus the driving force for glutamate uptake is reduced.

In conclusion, we have found that a subpopulation of preBötC astrocytes closely monitors activity of respiratory neurons and detects rhythmic fluctuations of the extracellular environment. These changes, reflected by respiratory-related membrane current fluctuations, indicate that astrocytes closely monitor activity of respiratory neurons and might in turn be able to modulate their activity.

4.2.2 No neuron-to-astrocyte coupling via rhythmic glutamate release in the preBötC

Most of the possible ways for intercellular communication between astrocytes and astrocytes and between astrocytes and neurons require the intracellular release of the second messenger Ca^{2+} in astrocytes. Transmission of information between astrocytes can work via the direct spread of small signaling molecules like IP_3 or Ca^{2+} via gap junctions (Loewenstein, 1981). This signaling can cause traveling Ca^{2+} waves (Cornell-Bell *et al.*, 1990) and can also include the release of ATP (Guthrie *et al.*, 1999; Cotrina *et al.*, 1998) or other neurotransmitters like glutamate (Parpura *et al.*, 1994). Both compounds are capable to trigger signals in neighbouring astrocytes and neurons. The excitatory neurotransmitter glutamate has been shown to activate intracellular Ca^{2+} increases in astrocytes (Cornell-Bell *et al.*, 1990; Porter & McCarthy, 1996), including the preBötC region (Härtel *et al.*, 2007, 2009).
Since glutamate is rhythmically released during bursting activity of respiratory neurons in the preBötC and it was shown here that preBötC astrocytes detect the rhythmic fluctuations of extracellular glutamate (see above), it was tested using two-photon Ca^{2+} imaging, if rhythmically released glutamate triggers astroglial Ca^{2+} signals. In this thesis, Ca^{2+} imaging was performed on rhythmic, whole-cell voltage-clamped astrocytes that were filled with fluorescent Ca^{2+} indicator dyes via the patch pipette. None of the patched astrocytes showed intracellular Ca^{2+} fluctuations that were correlated to respiratory activity (Fig. 3.26).

Thus, although the extracellular glutamate concentration is rhythmically increased, no astroglial glutamate receptors that cause increase of $[Ca^{2+}]_{in}$ are activated. This indicates, that under physiological conditions, glutamate does not escape from the synapse but is rapidly taken up by glial glutamate transporters. Coupling of increased extracellular glutamate to intracellular Ca^{2+} signals was also tested after blocking inhibitory transmission with GABA receptor and glycine receptor blockers, bicuculline and strychnine, respectively. By this measure, the number of neurons contributing to respiratory activity is increased (see also below). But again, no intracellular Ca^{2+} signals correlated to respiratory activity were detected.

In a parallel medical thesis performed in the lab, Jens Fresemann tested for respiratory-related Ca^{2+} signals in preBötC astrocytes using membrane-permeable Ca^{2+} indicator dyes. From 300 fluorescent-protein expressing astrocytes that were in close vicinity to respiratory neurons ($<50\,\mu m$), 38 (12.7 %) astrocytes showed occasionally spontaneous Ca^{2+} transients, but these were not correlated to respiratory activity. Cycle-triggered averaging did also not reveal astroglial respiratory-related Ca^{2+} transients. Application of strychnine and bicuculline increased the number of rhythmically active neurons from 103 in

CTRL to 323 (n = 13 slices). The number of astrocytes with spontaneous Ca^{2+} transients was also increased to 19.9 % of astrocytes identified by expression of fluorescent proteins. 99 % of astrocytes identified by expression of fluorescent proteins showed no respiratory-related Ca^{2+} transients at all, but in three cells, rhythmic fluctuations of $[Ca^{2+}]_{in}$ were partly overlapping with EGFP fluorescence. However, it remains debatable, if these signals orginated from neuronal processes nearby, since the activity maps of OGB-1 and EGFP fluorescence did not completely overlap. Furthemore, the kinetics of the recorded signal were indistinguishable from the signal of the neighbouring neuron. Since Kerr *et al.* (2005) reported detection of Ca^{2+} transients in the neuropil of brain tissue and not only on cell bodies, we conclude, that neuronal activity does not induce respiratory-related Ca^{2+} signaling in astrocytes. Even under conditions of increased excitation (by addition of bicuculline and strychnine), glutamate is taken up by glutamate transporters before it can escape the synaptic cleft and activate glial glutamate receptors.

4.2.3 Glial glutamate uptake is essential for maintenance of respiratory activity

Rapid removal of glutamate is essential for normal brain function (for review see Danbolt, 2001). Greer *et al.* (1991) and Funk *et al.* (1993) observed increased respiratory burst frequencies after application of GLT-1 blocker DHK in preBötC preparations from rat. Both groups observed irregular respiratory bursts if DHK concentration was raised above 400 µM (Greer *et al.*, 1991) or 500 µM (Funk *et al.*, 1993). In the study from Greer *et al.* (1991), respiratory activity ceased completely. The observed effects of DHK on burst amplitude are not confirmed by the results of this thesis. However, increase of frequency was also observed. The differences may be due to the different preparations (rat vs. mouse) and prior blockade of astroglial K^+ conductance with $BaCl_2$ which might further reduce the amount of glutamate that is taken up by GLT-1, since glutamate uptake depends also on the K^+ gradient across the membrane. This is partly reflected by the fact, that two out of seven experiments had to be excluded from analysis. Because respiratory activity was completely blocked by DHK (300 µM), because $I_{Resp,A}$ could not be analyzed anymore.

Two other glutamate uptake blockers were tested in this thesis. DL-TBOA (Shimamoto *et al.*, 1998) selectively blocks all five glutamate uptake transporters with similar affinities (Shimamoto *et al.*, 1998, 2000; Shigeri *et al.*, 2001), while TFB-TBOA is more selective for the glial glutamate transporters GLAST and GLT-1 (Shimamoto *et al.*, 2004; Bozzo & Chatton, 2010).
DL-TBOA caused an increase of the baseline of the integrated field potential (Fig. 3.21). Furthermore, the respiratory bursts became smaller and irregular. Eventually, respiratory activity was completely blocked, which is in line with the assumption that the blockade of glutamate transporters increases extracellular glutamate levels which might cause in-

creased excitability (Campbell & Hablitz, 2004), spillover of glutamate to extrasynaptic receptors and potential excitotoxic effects (for review see Lau & Tymianski, 2010). In patched astrocytes DL-TBOA application induced a slow and large inward current after the peak of the baseline of the integrated field potential was reached. The composition of this current has not been analyzed here, but other groups reported involvement of K^+ currents (Bellamy & Ogden, 2005; Bernardinelli & Chatton, 2008).
Similar to DL-TBOA, TFB-TBOA blocked respiratory activity after increasing baseline activity of the respiratory network (Fig. 3.29). This indicates the importance of glial glutamate uptake in the preBötC for maintenance of respiratory activity. Similar results have been reported for the hippocampus and the striatum (Rothstein *et al.*, 1996), where the glial glutamate transporters account for 40 % and 60 % of overall glutamate uptake, respectively. Silencing only one of the glial glutamate transporters was already sufficient to increase extracellular glutamate levels with subsequent degeneration and cytotoxic effects, while silencing of the neuronal glutamate transporter EAAC caused milder effects and no increase of extracellular glutamate (Rothstein *et al.*, 1996).

Here it was also investigated, if TFB-TBOA affects astroglial $[Ca^{2+}]_{in}$ after blockade of glial glutamate uptake. In this conditions of massive elevation of extracellular glutamate, glutamate might escape from the synaptic cleft, activate astroglial mGluRs and trigger the release of Ca^{2+} from intracellular Ca^{2+} stores. Indeed, in 89 % of EGFP-expressing astrocytes, TFB-TBOA triggered Ca^{2+} oscillations, which started shortly after the baseline increase of respiratory activity began and lasted for several seconds. These Ca^{2+} oscillations were not phase-locked to the respiratory bursts (Fig. 3.29). Since astroglial expression of group I mGluR was also confirmed immunohistochemically (Fig. 3.25), TFB-TBOA was also applied in presence of the group I mGluR antagonist CPCCOEt (Schoepp *et al.*, 1999). CPCCOEt significantly reduced the fraction of EGFP-expressing astrocytes that showed Ca^{2+} oscillations after TFB-TBOA application (Fig. 3.30). Furthermore, recovery of respiratory activity after washout of TFB-TBOA was improved.

In a parallel thesis in the lab, Mahmoud Rashad tested if the group I mGluR agonist DHPG is capable to induce Ca^{2+} signals in astrocytes. He showed, that almost all astrocytes responded to DHPG with Ca^{2+} oscillations, that were similar to the TFB-TBOA-triggered Ca^{2+} oscillation observed here.

To conclude, blockade of glial glutamate uptake is sufficient to increase the extracellular glutamate concentration to an extend that respiratory activity is blocked. Under this conditions of increased extracellular glutamate concentration, glutamate activates astroglial group I mGluR and induces astroglial Ca^{2+} signaling. It remains to be clarified, if this signal is of any physiological consequence, like release of gliotransmitters, enhanced expression or surface transport of glutamate transporters, or transmission of the signal to distant neurons or astrocytes.

4.2.4 Strong electrical stimulation triggers Ca^{2+} transients in some astrocytes

It was shown that mechanical stimulation of a whisker induces Ca^{2+} transients in astrocytes of the barrel cortex. The Ca^{2+} transients depended on the stimulation frequency and were inhibited by group I mGluR antagonists MPEP and LY367385 (Wang *et al.*, 2006). Another group elicited Ca^{2+} transients also in barrel cortex astrocytes with an electrial stimulation protocol. Astroglial Ca^{2+} transients were mostly larger than neuronal Ca^{2+} transients and also mediated via group I mGluR (Schipke *et al.*, 2008a).
Since we were not able to detect rhythmic changes of $[Ca^{2+}]_{in}$ during physiological activity of the respiratory network, we applied an electrical stimulation protocol to OGB-1 loaded brainstem slices. Although the protocol (100 Hz, 2 s, 20-150 V) produced a very strong neuronal stimulation, the number of responding astrocytes was rather small (10 %). Furthermore, the responses were heterogeneous. In a single experiment (Fig. 3.27), the astroglial Ca^{2+} response was larger than the neuronal Ca^{2+} signal (similar to the observations of Schipke *et al.*, 2008a), while in the other experiments the astroglial Ca^{2+} responses were rather small and sometimes not distinguishable from signals of the neuropil around the soma (Fig. 3.28, see also Kerr *et al.*, 2005). It was also reported, that the astroglial Ca^{2+} transients are caused by neuronal activation and not by direct stimulation of the astrocytes, since blockade of action potentials with TTX also blocked astroglial Ca^{2+} transients (Schipke *et al.*, 2008a). In the respiratory network, inhibitory transmission is an important feature (Winter *et al.*, 2009). Electrical stimulation in the brainstem probably activates also inhibitory neurons, which might reduce the effect of released glutamate that is available to activate astroglial mGluR. Since GABA can also elicit astroglial Ca^{2+} signaling (Meier *et al.*, 2008; Doengi *et al.*, 2009), further experiments are required to elucidate, why strong stimulation causes only weak astroglial Ca^{2+} signaling. Such an experiment would be to perform the electrical stimulation experiments in presence of GABA and glycine receptor blocker bicuculline and strychnine, respectively, to block inhibitory transmission.

4.2.5 Depolarization of astrocytes does not affect burst frequency of the respiratory network

Depolarization of rat hippocampal astrocytes by electrical stimulation induced reversible, intracellular Ca^{2+} elevations, that were followed by astroglial glutamate release (Jourdain *et al.*, 2007). The released glutamate increased the frequency of spontaneous excitatory postsynaptic currents (sEPSC) in neighbouring granule cells (Jourdain *et al.*, 2007). To test for such a mechanism in the brainstem, it was analyzed here, if depolarization of astrocytes to +20 mV increases the frequency of the respiratory bursts. However, no correlation between depolarization and respiratory burst frequency was found in our preparation

(Fig. 3.18). Since we did not record simultaneously from a neighbouring neuron, we cannot exclude from this experiment, that depolarization of astrocytes affects neighbouring neurons. Rather, the influence of a single astrocyte might be too small to the change activity of the whole respiratory network. To test for this, it would be necessary to perform dual patch-clamp experiments of a respiratory neuron and a coupled astrocyte nearby. Since we ruled out Ca^{2+} dependent astrocyte-to-neuron communication, it could be analyzed with these experiments in detail, if selective stimulation of the astrocyte affects sEPSC, sIPSC or slow-inward currents (Bardoni *et al.*, 2010) of the nearby respiratory neuron. Possible ways for such a Ca^{2+} independent astrocyte-to-neuron communication include reversal of glutamate transporters (Rossi *et al.*, 2000), release of gliotransmitters via hemichannels (Ye *et al.*, 2003), $P2X_7$ receptors (Hamilton *et al.*, 2008) or volume-regulated anion channels (Seki *et al.*, 1999).

5 Summary

Astrocytes are the major type of glial cells in the brain and were already described in the 19th century by Rudolf Virchow. The physiological investigation of astrocytes has long been hampered by difficulties to identify astrocytes during physiological experiments. Apart from using transgenic mice with astrocytes expressing fluorescent proteins, the method of selectively labeling astrocytes with the fluorescent dye Sulforhodamine 101 (SR101) emerged in recent years. SR101 was reported to label astrocytes in the hippocampus and the neocortex of rodents. However, here it was shown that SR101 labeling was not sufficient to reliably identify astrocytes in the brainstem. Investigations of the cause of this discrepancy revealed that passive diffusion of SR101 via gap junction or pannexin hemichannels does not account for the labeling differences. Since the inhibitor of ATP-binding cassette transporters, MK-571 blocked astroglial SR101 labeling in the hippocampus but did not improve SR101 labeling of brainstem astrocytes, active transport of SR101 into hippocampal astrocytes via a not yet identified, MK-571 sensitive transporter is more probable.

During rhythmic bursting activity of respiratory neurons in the pre-Bötzinger Complex (preBötC), extracellular concentrations of K^+ and neurotransmitters increase rhythmically. It was found in this study, that around 10 % of the patched astrocytes detected these rhythmic changes of the extracellular milieu and showed respiratory-related current fluctuations that based on Kir4.1 channels and glutamate transporters. It was further tested under different conditions for Ca^{2+}-dependent coupling of astrocytes to neurons in the preBötC. Astrocyte-to-neuron communication is mostly dependent on intracellular Ca^{2+} signals in astrocytes. Though, during normal respiratory activity and in conditions of increased activity after blockade of inhibitory transmission, we found no correlation between respiratory bursts and $[Ca^{2+}]_{in}$ in preBötC astrocytes. Only after blocking the glial glutamate uptake and subsequent increase of extracellular glutamate levels, astroglial Ca^{2+} oscillations were induced. Furthermore, depolarization of single astrocytes during normal respiratory activity did not affect respiratory bursts. Thus, we conlude that during normal respiratory activity, coupling between astrocytes and neurons in the preBötC is low. However, the astroglial glutamate uptake is essential for maintenance of respiratory network activity and adds further data for the importance of astrocytes in the preBötC.

6 Bibliography

Agulhon, C., **Petravicz, J.**, **McMullen, A.B.**, **Sweger, E.J.**, **Minton, S.K.**, **Taves, S.R.**, **Casper, K.B.**, **Fiacco, T.A.** & **McCarthy, K.D.** What is the role of astrocyte calcium in neurophysiology? *Neuron*, volume 59(6):932–946 [2008].

Anderson, C.W. Anatomical evidence for brainstem circuits mediating feeding motor programs in the leopard frog, rana pipiens. *Exp Brain Res*, volume 140(1):12–19 [2001].

Araque, A., **Parpura, V.**, **Sanzgiri, R.P.** & **Haydon, P.G.** Tripartite synapses: glia, the unacknowledged partner. *Trends Neurosci*, volume 22(5):208–215 [1999].

Arriza, J.L., **Fairman, W.A.**, **Wadiche, J.I.**, **Murdoch, G.H.**, **Kavanaugh, M.P.** & **Amara, S.G.** Functional comparisons of three glutamate transporter subtypes cloned from human motor cortex. *J Neurosci*, volume 14(9):5559–5569 [1994].

Bardoni, R., **Ghirri, A.**, **Zonta, M.**, **Betelli, C.**, **Vitale, G.**, **Ruggieri, V.**, **Sandrini, M.** & **Carmignoto, G.** Glutamate-mediated astrocyte-to-neuron signalling in the rat dorsal horn. *J Physiol*, volume 588(Pt 5):831–846 [2010].

Bellamy, T.C. & **Ogden, D.** Short-term plasticity of bergmann glial cell extrasynaptic currents during parallel fiber stimulation in rat cerebellum. *Glia*, volume 52(4):325–335 [2005].

Bernardinelli, Y. & **Chatton, J.Y.** Differential effects of glutamate transporter inhibitors on the global electrophysiological response of astrocytes to neuronal stimulation. *Brain Res*, volume 1240:47–53 [2008].

Bezzi, P., **Carmignoto, G.**, **Pasti, L.**, **Vesce, S.**, **Rossi, D.**, **Rizzini, B.L.**, **Pozzan, T.** & **Volterra, A.** Prostaglandins stimulate calcium-dependent glutamate release in astrocytes. *Nature*, volume 391(6664):281–285 [1998].

Blaustein, M.P. & **Lederer, W.J.** Sodium/calcium exchange: its physiological implications. *Physiol Rev*, volume 79(3):763–854 [1999].

Bowman, C.L. & **Kimelberg, H.K.** Excitatory amino acids directly depolarize rat brain astrocytes in primary culture. *Nature*, volume 311(5987):656–659 [1984].

Bozzo, L. & **Chatton, J.Y.** Inhibitory effects of (2s, 3s)-3-[3-[4-(trifluoromethyl)benzoylamino]benzyloxy]aspartate (tfb-tboa) on the astrocytic sodium responses to glutamate. *Brain Res*, volume 1316:27–34 [2010].

Brockhaus, J., **Ballanyi, K.**, **Smith, J.C.** & **Richter, D.W.** Microenvironment of respiratory neurons in the in vitro brainstem-spinal cord of neonatal rats. *J Physiol*, volume 462:421–445 [1993].

Bruzzone, R., **Hormuzdi, S.G.**, **Barbe, M.T.**, **Herb, A.** & **Monyer, H.** Pannexins, a family of gap junction proteins expressed in brain. *Proc Natl Acad Sci U S A*, volume 100(23):13644–13649 [2003].

Campbell, S.L. & **Hablitz, J.J.** Glutamate transporters regulate excitability in local networks in rat neocortex. *Neuroscience*, volume 127(3):625–635 [2004].

Chever, O., **Djukic, B.**, **McCarthy, K.D.** & **Amzica, F.** Implication of kir4.1 channel in excess potassium clearance: an in vivo study on anesthetized glial-conditional kir4.1 knock-out mice. *J Neurosci*, volume 30(47):15769–15777 [2010].

Choe, S. Potassium channel structures. *Nat Rev Neurosci*, volume 3(2):115–121 [2002].

Coco, S., **Calegari, F.**, **Pravettoni, E.**, **Pozzi, D.**, **Taverna, E.**, **Rosa, P.**, **Matteoli, M.** & **Verderio, C.** Storage and release of atp from astrocytes in culture. *J Biol Chem*, volume 278(2):1354–1362 [2003].

Cornell-Bell, A.H., **Finkbeiner, S.M.**, **Cooper, M.S.** & **Smith, S.J.** Glutamate induces calcium waves in cultured astrocytes: long-range glial signaling. *Science*, volume 247(4941):470–473 [1990].

Cotrina, M.L., **Lin, J.H.**, **Alves-Rodrigues, A.**, **Liu, S.**, **Li, J.**, **Azmi-Ghadimi, H.**, **Kang, J.**, **Naus, C.C.** & **Nedergaard, M.** Connexins regulate calcium signaling by controlling atp release. *Proc Natl Acad Sci U S A*, volume 95(26):15735–15740 [1998].

Dallwig, R., **Vitten, H.** & **Deitmer, J.W.** A novel barium-sensitive calcium influx into rat astrocytes at low external potassium. *Cell Calcium*, volume 28(4):247–259 [2000].

D'Ambrosio, R., **Gordon, D.S.** & **Winn, H.R.** Differential role of kir channel and na(+)/k(+)-pump in the regulation of extracellular k(+) in rat hippocampus. *J Neurophysiol*, volume 87(1):87–102 [2002].

Danbolt, N.C. Glutamate uptake. *Prog Neurobiol*, volume 65(1):1–105 [2001].

Davidson, J.S., **Baumgarten, I.M.** & **Harley, E.H.** Reversible inhibition of intercellular junctional communication by glycyrrhetinic acid. *Biochem Biophys Res Commun*, volume 134(1):29–36 [1986].

Denk, W., **Strickler, J.H.** & **Webb, W.W.** Two-photon laser scanning fluorescence microscopy. *Science*, volume 248(4951):73–76 [1990].

Dermietzel, R., **Traub, O.**, **Hwang, T.K.**, **Beyer, E.**, **Bennett, M.V.**, **Spray, D.C.** & **Willecke, K.** Differential expression of three gap junction proteins in developing and mature brain tissues. *Proc Natl Acad Sci U S A*, volume 86(24):10148–10152 [1989].

DeVries, S.H. & **Schwartz, E.A.** Hemi-gap-junction channels in solitary horizontal cells of the catfish retina. *J Physiol*, volume 445:201–230 [1992].

Doengi, M., **Hirnet, D.**, **Coulon, P.**, **Pape, H.C.**, **Deitmer, J.W.** & **Lohr, C.** Gaba uptake-dependent ca(2+) signaling in developing olfactory bulb astrocytes. *Proc Natl Acad Sci U S A*, volume 106(41):17570–17575 [2009].

Edwards, F.A., **Konnerth, A.**, **Sakmann, B.** & **Takahashi, T.** A thin slice preparation for patch clamp recordings from neurones of the mammalian central nervous system. *Pflugers Arch*, volume 414(5):600–612 [1989].

Ehinger, B., **Zucker, C.L.**, **Bruun, A.** & **Adolph, A.** In vivo staining of oligodendroglia in the rabbit retina. *Glia*, volume 10(1):40–48 [1994].

Feldman, J.L., **Mitchell, G.S.** & **Nattie, E.E.** Breathing: rhythmicity, plasticity, chemosensitivity. *Annu Rev Neurosci*, volume 26:239–266 [2003].

Funk, G.D., **Smith, J.C.** & **Feldman, J.L.** Generation and transmission of respiratory oscillations in medullary slices: role of excitatory amino acids. *J Neurophysiol*, volume 70(4):1497–1515 [1993].

Goldman, W.F., **Yarowsky, P.J.**, **Juhaszova, M.**, **Krueger, B.K.** & **Blaustein, M.P.** Sodium/calcium exchange in rat cortical astrocytes. *J Neurosci*, volume 14(10):5834–5843 [1994].

Gomeza, J., **Ohno, K.**, **Hülsmann, S.**, **Armsen, W.**, **Eulenburg, V.**, **Richter, D.W.**, **Laube, B.** & **Betz, H.** Deletion of the mouse glycine transporter 2 results in a hyperekplexia phenotype and postnatal lethality. *Neuron*, volume 40(4):797–806 [2003a].

Gomeza, J., **Hülsmann, S.**, **Ohno, K.**, **Eulenburg, V.**, **Szöke, K.**, **Richter, D.** & **Betz, H.** Inactivation of the glycine transporter 1 gene discloses vital role of glial glycine uptake in glycinergic inhibition. *Neuron*, volume 40(4):785–796 [2003b].

Gong, Y., **Duvvuri, M.** & **Krise, J.P.** Separate roles for the golgi apparatus and lysosomes in the sequestration of drugs in the multidrug-resistant human leukemic cell line hl-60. *J Biol Chem*, volume 278(50):50234–50239 [2003].

Grass, D., **Pawlowski, P.G.**, **Hirrlinger, J.**, **Papadopoulos, N.**, **Richter, D.W.**, **Kirchhoff, F.** & **Hülsmann, S.** Diversity of functional astroglial properties in the respiratory network. *The Journal of neuroscience : the official journal of the Society for Neuroscience*, volume 24(6):1358–1365 [2004]. ISSN 1529-2401.

Greer, J.J., **Smith, J.C.** & **Feldman, J.L.** Role of excitatory amino acids in the generation and transmission of respiratory drive in neonatal rat. *J Physiol*, volume 437:727–749 [1991].

Grisar, T., **Franck, G.** & **Schoffeniels, E.** Glial control of neuronal excitability in mammals: Ii. enzymatic evidence : Two molecular forms of the (na(+),k(+))-atpase in brain. *Neurochem Int*, volume 2C:311–320 [1980].

Guthrie, P.B., **Knappenberger, J.**, **Segal, M.**, **Bennett, M.V.**, **Charles, A.C.** & **Kater, S.B.** Atp released from astrocytes mediates glial calcium waves. *J Neurosci*, volume 19(2):520–528 [1999].

Haas, B., **Schipke, C.G.**, **Peters, O.**, **Söhl, G.**, **Willecke, K.** & **Kettenmann, H.** Activity-dependent atp-waves in the mouse neocortex are independent from astrocytic calcium waves. *Cereb Cortex*, volume 16(2):237–246 [2006].

Hamilton, N., **Vayro, S.**, **Kirchhoff, F.**, **Verkhratsky, A.**, **Robbins, J.**, **Gorecki, D.C.** & **Butt, A.M.** Mechanisms of atp- and glutamate-mediated calcium signaling in white matter astrocytes. *Glia*, volume 56(7):734–749 [2008].

Härtel, K., **Singaravelu, K.**, **Kaiser, M.**, **Neusch, C.**, **Hülsmann, S.** & **Deitmer, J.W.** Calcium influx mediated by the inwardly rectifying K^+ channel Kir4.1 (KCNJ10) at low external K^+ concentration. *Cell calcium*, volume 42(3):271–280 [2007].

Härtel, K., **Schnell, C.** & **Hülsmann, S.** Astrocytic calcium signals induced by neuromodulators via functional metabotropic receptors in the ventral respiratory group of neonatal mice. *Glia*, volume 57(8):815–827 [2009].

Hirrlinger, J., **König, J.**, **Keppler, D.**, **Lindenau, J.**, **Schulz, J.B.** & **Dringen, R.** The multidrug resistance protein mrp1 mediates the release of glutathione disulfide from rat astrocytes during oxidative stress. *J Neurochem*, volume 76(2):627–636 [2001].

Hirrlinger, J., **Moeller, H.**, **Kirchhoff, F.** & **Dringen, R.** Expression of multidrug resistance proteins (mrps) in astrocytes of the mouse brain: a single cell rt-pcr study. *Neurochem Res*, volume 30(10):1237–1244 [2005a].

Hirrlinger, P.G., **Scheller, A.**, **Braun, C.**, **Quintela-Schneider, M.**, **Fuss, B.**, **Hirrlinger, J.** & **Kirchhoff, F.** Expression of reef coral fluorescent proteins in the

central nervous system of transgenic mice. *Mol Cell Neurosci*, volume 30(3):291–303 [2005b].

Hoogland, T.M. & **Kuhn, B.** Recent developments in the understanding of astrocyte function in the cerebellum in vivo. *Cerebellum*, volume 9(3):264–271 [2010].

Huang, Y., **Grinspan, J.B.**, **Abrams, C.K.** & **Scherer, S.S.** Pannexin1 is expressed by neurons and glia but does not form functional gap junctions. *Glia*, volume 55(1):46–56 [2007].

Hülsmann, S., **Oku, Y.**, **Zhang, W.** & **Richter, D.W.** Metabolic coupling between glia and neurons is necessary for maintaining respiratory activity in transverse medullary slices of neonatal mouse. *Eur J Neurosci*, volume 12(3):856–862 [2000].

Huxtable, A.G., **Zwicker, J.D.**, **Poon, B.Y.**, **Pagliardini, S.**, **Vrouwe, S.Q.**, **Greer, J.J.** & **Funk, G.D.** Tripartite purinergic modulation of central respiratory networks during perinatal development: the influence of atp, ectonucleotidases, and atp metabolites. *J Neurosci*, volume 29(47):14713–14725 [2009].

Iglesias, R., **Locovei, S.**, **Roque, A.**, **Alberto, A.P.**, **Dahl, G.**, **Spray, D.C.** & **Scemes, E.** P2x7 receptor-pannexin1 complex: pharmacology and signaling. *Am J Physiol Cell Physiol*, volume 295(3):C752–C760 [2008].

Iglesias, R., **Spray, D.C.** & **Scemes, E.** Mefloquine blockade of pannexin1 currents: resolution of a conflict. *Cell Commun Adhes*, volume 16(5-6):131–137 [2009].

Inoue, K., **Zhuang, L.** & **Ganapathy, V.** Human na+ -coupled citrate transporter: primary structure, genomic organization, and transport function. *Biochem Biophys Res Commun*, volume 299(3):465–471 [2002].

Jabaudon, D., **Shimamoto, K.**, **Yasuda-Kamatani, Y.**, **Scanziani, M.**, **Gähwiler, B.H.** & **Gerber, U.** Inhibition of uptake unmasks rapid extracellular turnover of glutamate of nonvesicular origin. *Proc Natl Acad Sci U S A*, volume 96(15):8733–8738 [1999].

Jabs, R., **Kirchhoff, F.**, **Kettenmann, H.** & **Steinhäuser, C.** Kainate activates ca(2+)-permeable glutamate receptors and blocks voltage-gated k+ currents in glial cells of mouse hippocampal slices. *Pflugers Arch*, volume 426(3-4):310–319 [1994].

Jourdain, P., **Bergersen, L.H.**, **Bhaukaurally, K.**, **Bezzi, P.**, **Santello, M.**, **Domercq, M.**, **Matute, C.**, **Tonello, F.**, **Gundersen, V.** & **Volterra, A.** Glutamate exocytosis from astrocytes controls synaptic strength. *Nat Neurosci*, volume 10(3):331–339 [2007].

Kang, J., **Kang, N.**, **Yu, Y.**, **Zhang, J.**, **Petersen, N.**, **Tian, G.F.** & **Nedergaard, M.** Sulforhodamine 101 induces long-term potentiation of intrinsic excitability and synaptic efficacy in hippocampal ca1 pyramidal neurons. *Neuroscience*, volume 169(4):1601–1609 [2010].

Kerr, J.N.D., **Greenberg, D.** & **Helmchen, F.** Imaging input and output of neocortical networks in vivo. *Proc Natl Acad Sci U S A*, volume 102(39):14063–14068 [2005].

Kettenmann, H., **Backus, K.H.** & **Schachner, M.** Aspartate, glutamate and gamma-aminobutyric acid depolarize cultured astrocytes. *Neurosci Lett*, volume 52(1-2):25–29 [1984].

Kettenmann, H. & **Ransom, B.R.** *Neuroglia*. Oxford University Press [2005].

Kofuji, P. & **Newman, E.A.** Potassium buffering in the central nervous system. *Neuroscience*, volume 129(4):1045–1056 [2004].

Korn, S.J. & **Ikeda, S.R.** Permeation selectivity by competition in a delayed rectifier potassium channel. *Science*, volume 269(5222):410–412 [1995].

Langer, J. & **Rose, C.R.** Synaptically induced sodium signals in hippocampal astrocytes in situ. *J Physiol*, volume 587(Pt 24):5859–5877 [2009].

Lau, A. & **Tymianski, M.** Glutamate receptors, neurotoxicity and neurodegeneration. *Pflugers Arch*, volume 460(2):525–542 [2010].

Lee, S., **Yoon, B.E.**, **Berglund, K.**, **Oh, S.J.**, **Park, H.**, **Shin, H.S.**, **Augustine, G.J.** & **Lee, C.J.** Channel-mediated tonic gaba release from glia. *Science*, volume 330(6005):790–796 [2010].

Levy, L.M., **Warr, O.** & **Attwell, D.** Stoichiometry of the glial glutamate transporter glt-1 expressed inducibly in a chinese hamster ovary cell line selected for low endogenous na+-dependent glutamate uptake. *J Neurosci*, volume 18(23):9620–9628 [1998].

Li, D., **Ropert, N.**, **Koulakoff, A.**, **Giaume, C.** & **Oheim, M.** Lysosomes are the major vesicular compartment undergoing ca2+-regulated exocytosis from cortical astrocytes. *J Neurosci*, volume 28(30):7648–7658 [2008].

Lichtman, J.W., **Wilkinson, R.S.** & **Rich, M.M.** Multiple innervation of tonic endplates revealed by activity-dependent uptake of fluorescent probes. *Nature*, volume 314(6009):357–359 [1985].

Liu, Q.R., **López-Corcuera, B.**, **Mandiyan, S.**, **Nelson, H.** & **Nelson, N.** Cloning and expression of a spinal cord- and brain-specific glycine transporter with novel structural features. *J Biol Chem*, volume 268(30):22802–22808 [1993].

Locovei, S., **Bao, L.** & **Dahl, G.** Pannexin 1 in erythrocytes: function without a gap. *Proc Natl Acad Sci U S A*, volume 103(20):7655–7659 [2006].

Loewenstein, W.R. Junctional intercellular communication: the cell-to-cell membrane channel. *Physiol Rev*, volume 61(4):829–913 [1981].

Manzini, I., **Schweer, T.S.** & **Schild, D.** Improved fluorescent (calcium indicator) dye uptake in brain slices by blocking multidrug resistance transporters. *J Neurosci Methods*, volume 167(2):140–147 [2008].

Manzke, T., **Preusse, S.**, **Hülsmann, S.** & **Richter, D.W.** Developmental changes of serotonin 4(a) receptor expression in the rat pre-bötzinger complex. *J Comp Neurol*, volume 506(5):775–790 [2008].

Martinez-Hernandez, A., **Bell, K.P.** & **Norenberg, M.D.** Glutamine synthetase: glial localization in brain. *Science*, volume 195(4284):1356–1358 [1977].

Meier, S.D., **Kafitz, K.W.** & **Rose, C.R.** Developmental profile and mechanisms of gaba-induced calcium signaling in hippocampal astrocytes. *Glia*, volume 56(10):1127–1137 [2008].

Miller, D.S., **Nobmann, S.N.**, **Gutmann, H.**, **Toeroek, M.**, **Drewe, J.** & **Fricker, G.** Xenobiotic transport across isolated brain microvessels studied by confocal microscopy. *Mol Pharmacol*, volume 58(6):1357–1367 [2000].

Minelli, A., **Castaldo, P.**, **Gobbi, P.**, **Salucci, S.**, **Magi, S.** & **Amoroso, S.** Cellular and subcellular localization of na+-ca2+ exchanger protein isoforms, ncx1, ncx2, and ncx3 in cerebral cortex and hippocampus of adult rat. *Cell Calcium*, volume 41(3):221–234 [2007].

Mothet, J.P., **Pollegioni, L.**, **Ouanounou, G.**, **Martineau, M.**, **Fossier, P.** & **Baux, G.** Glutamate receptor activation triggers a calcium-dependent and snare protein-dependent release of the gliotransmitter d-serine. *Proc Natl Acad Sci U S A*, volume 102(15):5606–5611 [2005].

Nagy, J.I. & **Rash, J.E.** Connexins and gap junctions of astrocytes and oligodendrocytes in the cns. *Brain Res Brain Res Rev*, volume 32(1):29–44 [2000].

Neusch, C., **Papadopoulos, N.**, **Müller, M.**, **Maletzki, I.**, **Winter, S.M.**, **Hirrlinger, J.**, **Handschuh, M.**, **Bähr, M.**, **Richter, D.W.**, **Kirchhoff, F.** & **Hülsmann, S.** Lack of the kir4.1 channel subunit abolishes k+ buffering properties of astrocytes in the ventral respiratory group: impact on extracellular k+ regulation. *J Neurophysiol*, volume 95(3):1843–1852 [2006].

Newell, E.W., **Stanley, E.F.** & **Schlichter, L.C.** Reversed na+/ca2+ exchange contributes to ca2+ influx and respiratory burst in microglia. *Channels (Austin)*, volume 1(5):366–376 [2007].

Newman, E. & **Reichenbach, A.** The müller cell: a functional element of the retina. *Trends Neurosci*, volume 19(8):307–312 [1996].

Nieden, R.Z. & **Deitmer, J.W.** The role of metabotropic glutamate receptors for the generation of calcium oscillations in rat hippocampal astrocytes in situ. *Cereb Cortex*, volume 16(5):676–687 [2006].

Nielsen, T., **Fricke, M.**, **Hellweg, D.** & **Andresen, P.** High efficiency beam splitter for multifocal multiphoton microscopy. *J Microsc*, volume 201:368–376 [2001].

Nimmerjahn, A., **Kirchhoff, F.**, **Kerr, J.N.D.** & **Helmchen, F.** Sulforhodamine 101 as a specific marker of astroglia in the neocortex in vivo. *Nat Methods*, volume 1(1):31–37 [2004].

Nolte, C., **Matyash, M.**, **Pivneva, T.**, **Schipke, C.G.**, **Ohlemeyer, C.**, **Hanisch, U.K.**, **Kirchhoff, F.** & **Kettenmann, H.** Gfap promoter-controlled egfp-expressing transgenic mice: a tool to visualize astrocytes and astrogliosis in living brain tissue. *Glia*, volume 33(1):72–86 [2001].

Orkand, R.K., **Nicholls, J.G.** & **Kuffler, S.W.** Effect of nerve impulses on the membrane potential of glial cells in the central nervous system of amphibia. *J Neurophysiol*, volume 29(4):788–806 [1966].

Owe, S.G., **Marcaggi, P.** & **Attwell, D.** The ionic stoichiometry of the glast glutamate transporter in salamander retinal glia. *J Physiol*, volume 577(Pt 2):591–599 [2006].

Pace, R.W., **Mackay, D.D.**, **Feldman, J.L.** & **Negro, C.A.D.** Inspiratory bursts in the prebötzinger complex depend on a calcium-activated non-specific cation current linked to glutamate receptors in neonatal mice. *J Physiol*, volume 582(Pt 1):113–125 [2007].

Pajor, A.M. Molecular properties of the slc13 family of dicarboxylate and sulfate transporters. *Pflugers Arch*, volume 451(5):597–605 [2006].

Panchin, Y., **Kelmanson, I.**, **Matz, M.**, **Lukyanov, K.**, **Usman, N.** & **Lukyanov, S.** A ubiquitous family of putative gap junction molecules. *Curr Biol*, volume 10(13):R473–R474 [2000].

Parpura, V., **Basarsky, T.A.**, **Liu, F.**, **Jeftinija, K.**, **Jeftinija, S.** & **Haydon, P.G.** Glutamate-mediated astrocyte-neuron signalling. *Nature*, volume 369(6483):744–747 [1994].

Parpura, V. & **Zorec, R.** Gliotransmission: Exocytotic release from astrocytes. *Brain Res Rev*, volume 63(1-2):83–92 [2010].

Pellerin, L. & **Magistretti, P.J.** Neuroenergetics: calling upon astrocytes to satisfy hungry neurons. *Neuroscientist*, volume 10(1):53–62 [2004].

Petralia, R.S., **Wang, Y.X.**, **Niedzielski, A.S.** & **Wenthold, R.J.** The metabotropic glutamate receptors, mglur2 and mglur3, show unique postsynaptic, presynaptic and glial localizations. *Neuroscience*, volume 71(4):949–976 [1996].

Porter, J.T. & **McCarthy, K.D.** Hippocampal astrocytes in situ respond to glutamate released from synaptic terminals. *J Neurosci*, volume 16(16):5073–5081 [1996].

Ramirez, J.M., **Quellmalz, U.J.** & **Richter, D.W.** Postnatal changes in the mammalian respiratory network as revealed by the transverse brainstem slice of mice. *The Journal of physiology*, volume 491 (Pt 3):799–812 [1996].

Richter, D.W., **Camerer, H.** & **Sonnhof, U.** Changes in extracellular potassium during the spontaneous activity of medullary respiratory neurones. *Pflugers Arch*, volume 376(2):139–149 [1978].

Richter, D.W. & **Spyer, K.M.** Studying rhythmogenesis of breathing: comparison of in vivo and in vitro models. *Trends Neurosci*, volume 24(8):464–472 [2001].

Richter, D.W., **Manzke, T.**, **Wilken, B.** & **Ponimaskin, E.** Serotonin receptors: guardians of stable breathing. *Trends Mol Med*, volume 9(12):542–548 [2003].

Rossi, D.J., **Oshima, T.** & **Attwell, D.** Glutamate release in severe brain ischaemia is mainly by reversed uptake. *Nature*, volume 403(6767):316–321 [2000].

Rothstein, J.D., **Dykes-Hoberg, M.**, **Pardo, C.A.**, **Bristol, L.A.**, **Jin, L.**, **Kuncl, R.W.**, **Kanai, Y.**, **Hediger, M.A.**, **Wang, Y.**, **Schielke, J.P.** & **Welty, D.F.** Knockout of glutamate transporters reveals a major role for astroglial transport in excitotoxicity and clearance of glutamate. *Neuron*, volume 16(3):675–686 [1996].

Schipke, C.G., **Haas, B.** & **Kettenmann, H.** Astrocytes discriminate and selectively respond to the activity of a subpopulation of neurons within the barrel cortex. *Cereb Cortex*, volume 18(10):2450–2459 [2008a].

Schipke, C.G., **Heidemann, A.**, **Skupin, A.**, **Peters, O.**, **Falcke, M.** & **Kettenmann, H.** Temperature and nitric oxide control spontaneous calcium transients in astrocytes. *Cell Calcium*, volume 43(3):285–295 [2008b].

Schoepp, D.D., **Jane, D.E.** & **Monn, J.A.** Pharmacological agents acting at subtypes of metabotropic glutamate receptors. *Neuropharmacology*, volume 38(10):1431–1476 [1999].

Schousboe, A. Pharmacological and functional characterization of astrocytic gaba transport: a short review. *Neurochem Res*, volume 25(9-10):1241–1244 [2000].

Seki, Y., **Feustel, P.J.**, **Keller, R.W.**, **Tranmer, B.I.** & **Kimelberg, H.K.** Inhibition of ischemia-induced glutamate release in rat striatum by dihydrokinate and an anion channel blocker. *Stroke*, volume 30(2):433–440 [1999].

Shao, X.M. & **Feldman, J.L.** Respiratory rhythm generation and synaptic inhibition of expiratory neurons in pre-bötzinger complex: differential roles of glycinergic and gabaergic neural transmission. *J Neurophysiol*, volume 77(4):1853–1860 [1997].

Shigeri, Y., **Shimamoto, K.**, **Yasuda-Kamatani, Y.**, **Seal, R.P.**, **Yumoto, N.**, **Nakajima, T.** & **Amara, S.G.** Effects of threo-beta-hydroxyaspartate derivatives on excitatory amino acid transporters (eaat4 and eaat5). *J Neurochem*, volume 79(2):297–302 [2001].

Shimamoto, K., **Lebrun, B.**, **Yasuda-Kamatani, Y.**, **Sakaitani, M.**, **Shigeri, Y.**, **Yumoto, N.** & **Nakajima, T.** Dl-threo-beta-benzyloxyaspartate, a potent blocker of excitatory amino acid transporters. *Mol Pharmacol*, volume 53(2):195–201 [1998].

Shimamoto, K., **Shigeri, Y.**, **Yasuda-Kamatani, Y.**, **Lebrun, B.**, **Yumoto, N.** & **Nakajima, T.** Syntheses of optically pure beta-hydroxyaspartate derivatives as glutamate transporter blockers. *Bioorg Med Chem Lett*, volume 10(21):2407–2410 [2000].

Shimamoto, K., **Sakai, R.**, **Takaoka, K.**, **Yumoto, N.**, **Nakajima, T.**, **Amara, S.G.** & **Shigeri, Y.** Characterization of novel l-threo-beta-benzyloxyaspartate derivatives, potent blockers of the glutamate transporters. *Mol Pharmacol*, volume 65(4):1008–1015 [2004].

Silverman, W., **Locovei, S.** & **Dahl, G.** Probenecid, a gout remedy, inhibits pannexin 1 channels. *Am J Physiol Cell Physiol*, volume 295(3):C761–C767 [2008].

Smith, J.C., **Ellenberger, H.H.**, **Ballanyi, K.**, **Richter, D.W.** & **Feldman, J.L.** Pre-bötzinger complex: a brainstem region that may generate respiratory rhythm in mammals. *Science*, volume 254:726–729 [1991].

Somjen, G.G., **Kager, H.** & **Wadman, W.J.** Computer simulations of neuron-glia interactions mediated by ion flux. *J Comput Neurosci*, volume 25(2):349–365 [2008].

Steinhäuser, C., **Jabs, R.** & **Kettenmann, H.** Properties of gaba and glutamate responses in identified glial cells of the mouse hippocampal slice. *Hippocampus*, volume 4(1):19–35 [1994].

Stosiek, C., **Garaschuk, O.**, **Holthoff, K.** & **Konnerth, A.** In vivo two-photon calcium imaging of neuronal networks. *Proceedings of the National Academy of Sciences of the United States of America*, volume 100(12):7319–7324 [2003].

Szatkowski, M., **Barbour, B.** & **Attwell, D.** Non-vesicular release of glutamate from glial cells by reversed electrogenic glutamate uptake. *Nature*, volume 348(6300):443–446 [1990].

Szoke, K., **Härtel, K.**, **Grass, D.**, **Hirrlinger, P.G.**, **Hirrlinger, J.** & **Hülsmann, S.** Glycine transporter 1 expression in the ventral respiratory group is restricted to protoplasmic astrocytes. *Brain Res*, volume 1119:182–189 [2006].

Tanaka, K., **Watase, K.**, **Manabe, T.**, **Yamada, K.**, **Watanabe, M.**, **Takahashi, K.**, **Iwama, H.**, **Nishikawa, T.**, **Ichihara, N.**, **Kikuchi, T.**, **Okuyama, S.**, **Kawashima, N.**, **Hori, S.**, **Takimoto, M.** & **Wada, K.** Epilepsy and exacerbation of brain injury in mice lacking the glutamate transporter glt-1. *Science*, volume 276(5319):1699–1702 [1997].

Teng, H., **Cole, J.C.**, **Roberts, R.L.** & **Wilkinson, R.S.** Endocytic active zones: hot spots for endocytosis in vertebrate neuromuscular terminals. *J Neurosci*, volume 19(12):4855–4866 [1999].

Thompson, R.J., **Zhou, N.** & **MacVicar, B.A.** Ischemia opens neuronal gap junction hemichannels. *Science*, volume 312(5775):924–927 [2006].

Töpert, C., **Döring, F.**, **Wischmeyer, E.**, **Karschin, C.**, **Brockhaus, J.**, **Ballanyi, K.**, **Derst, C.** & **Karschin, A.** Kir2.4: a novel k+ inward rectifier channel associated with motoneurons of cranial nerve nuclei. *J Neurosci*, volume 18(11):4096–4105 [1998].

Trotter, J., **Karram, K.** & **Nishiyama, A.** Ng2 cells: Properties, progeny and origin. *Brain Res Rev*, volume 63(1-2):72–82 [2010].

Valiunas, V. Biophysical properties of connexin-45 gap junction hemichannels studied in vertebrate cells. *J Gen Physiol*, volume 119:147–164 [2002].

van Lenhossék, M. *Der feinere Bau des Nervensystems im Lichte neuester Forschung*. Berlin: Fischer's Medicinische Buchhandlung [1893].

Viemari, J.C. & **Ramirez, J.M.** Norepinephrine differentially modulates different types of respiratory pacemaker and nonpacemaker neurons. *J Neurophysiol*, volume 95(4):2070–2082 [2006].

Virchow, R. über das granulierte ansehen der wandungen der gehirnventrikel. *All. Z. Psychiatr*, pages 242–250 [1846].

Vyskocil, F., **Kritz, N.** & **Bures, J.** Potassium-selective microelectrodes used for measuring the extracellular brain potassium during spreading depression and anoxic depolarization in rats. *Brain Res*, (1):255–259 [1972].

Wang, X., **Lou, N.**, **Xu, Q.**, **Tian, G.F.**, **Peng, W.G.**, **Han, X.**, **Kang, J.**, **Takano, T.** & **Nedergaard, M.** Astrocytic ca2+ signaling evoked by sensory stimulation in vivo. *Nat Neurosci*, volume 9(6):816–823 [2006].

Watase, K., **Hashimoto, K.**, **Kano, M.**, **Yamada, K.**, **Watanabe, M.**, **Inoue, Y.**, **Okuyama, S.**, **Sakagawa, T.**, **Ogawa, S.**, **Kawashima, N.**, **Hori, S.**, **Takimoto, M.**, **Wada, K.** & **Tanaka, K.** Motor discoordination and increased susceptibility to cerebellar injury in glast mutant mice. *Eur J Neurosci*, (3):976–988 [1998].

Winter, S.M., **Fresemann, J.**, **Schnell, C.**, **Oku, Y.**, **Hirrlinger, J.** & **Hülsmann, S.** Glycinergic interneurons are functionally integrated into the inspiratory network of mouse medullary slices. *Pflugers Arch*, volume 458(3):459–469 [2009].

Ye, Z.C., **Wyeth, M.S.**, **Baltan-Tekkok, S.** & **Ransom, B.R.** Functional hemichannels in astrocytes: a novel mechanism of glutamate release. *J Neurosci*, volume 23(9):3588–3596 [2003].

Zafra, F., **Aragón, C.**, **Olivares, L.**, **Danbolt, N.C.**, **Giménez, C.** & **Storm-Mathisen, J.** Glycine transporters are differentially expressed among cns cells. *J Neurosci*, volume 15(5 Pt 2):3952–3969 [1995].

Zeilhofer, H.U., **Studler, B.**, **Arabadzisz, D.**, **Schweizer, C.**, **Ahmadi, S.**, **Layh, B.**, **Bösl, M.R.** & **Fritschy, J.M.** Glycinergic neurons expressing enhanced green fluorescent protein in bacterial artificial chromosome transgenic mice. *J Comp Neurol*, volume 482(2):123–141 [2005].

Zhuo, L., **Sun, B.**, **Zhang, C.L.**, **Fine, A.**, **Chiu, S.Y.** & **Messing, A.** Live astrocytes visualized by green fluorescent protein in transgenic mice. *Dev Biol*, volume 187(1):36–42 [1997].

Acknowledgements

First I would like to thank my supervisor, Prof. Swen Hülsmann, for giving me the opportunity to work in this group and on this project. I am thankful for all the techniques, I learned in the lab and for broadening my scientific horizon in a lot of discussions and the support to develop own ideas and approaches.

I would also like to thank the members of my thesis committee: Prof. Gabriele Flügge and Prof. Tobias Moser for their support, and helpful and critical advice. Furthermore, I want to thank Prof. Richter for hosting me in the institute.

I want to thank Prof. Yoshitaka Oku for providing the MATLAB routine for cycle-triggered averging and help with MATLAB and Mihai Alevra for help to correct for movement artifacts in time-lapse SR101 recordings.

Many thanks go to Anja for great technical assistance and support, and for being the *good soul* of the lab.

I also want to thank all the people from the mechanical, electronic workshop and our animal facility.

Many thanks go also to the current and former lab members Jamil, Jens, Kai, Kirsten, Mahmoud, Michal, and Tobias for lots of discussion, advice and the the good atmosphere in the lab.

For comments and typo corrections, I thank Christiane, Dirk, Jamil, Jessica, Katja, and Ramya.

Furthermore, I want to thank the colleagues from the group of Prof. Müller for discussions, support, the nice atmosphere in the *U-Boot* and of course the soccer matches on monday evenings!

Many thanks for funding go to the DFG and the CMPB.

I am extremely grateful for my parents for their encouragement and support in every sense throughout my life.

And finally, I want to thank my wonderful girlfriend Katja for your love and support and for being there for me whenever I needed you!